Paleoceanography and Paleoclimatology

RESEARCH ARTICLE
10.1029/2020PA003953

Special Section:
The Miocene: The Future of the Past

Effects of CO_2 and Ocean Mixing on Miocene and Pliocene Temperature Gradients

Gerrit Lohmann[1,2], Gregor Knorr[1], Akil Hossain[1], and Christian Stepanek[1]

[1]Alfred Wegener Institute (AWI) Helmholtz Center for Polar and Marine Research, Bremerhaven, Germany, [2]Department of Environmental Physics and MARUM, University of Bremen, Bremen, Germany

Key Points:

- Miocene experiment with standard mixing and atmospheric CO_2 of 600 ppm captures large-scale temperature characteristics of the mid-Miocene
- With enhanced ocean mixing the temperature characteristics and meridional temperature gradient can be reproduced with a CO_2 level of 450 ppm
- Miocene shows a strong warming at polar latitudes and reduced seasonality, vertical mixing, and CO_2 are less important for the Pliocene

Supporting Information:

Supporting Information may be found in the online version of this article.

Correspondence to:

G. Lohmann,
Gerrit.Lohmann@awi.de

Citation:

Lohmann, G., Knorr, G., Hossain, A., & Stepanek, C. (2022). Effects of CO_2 and ocean mixing on Miocene and Pliocene temperature gradients. *Paleoceanography and Paleoclimatology*, *37*, e2020PA003953. https://doi.org/10.1029/2020PA003953

Received 27 MAR 2020
Accepted 1 NOV 2021

Author Contributions:

Conceptualization: Gerrit Lohmann, Gregor Knorr
Data curation: Christian Stepanek
Formal analysis: Gerrit Lohmann, Gregor Knorr, Christian Stepanek
Funding acquisition: Gerrit Lohmann

Abstract Cenozoic climate changes have been linked to tectonic activity and variations in atmospheric CO_2 concentrations. Here, we present Miocene and Pliocene sensitivity experiments performed with the climate model COSMOS. The experiments contain changes with respect to paleogeography, ocean gateway configuration, and atmospheric CO_2 concentrations, as well as a range of vertical mixing coefficients in the ocean. For the mid-Miocene, we show that the impact of ocean mixing on surface temperature is comparable to the effect of the possible range in reconstructed CO_2 concentrations. In combination with stronger vertical mixing, relatively moderate CO_2 concentrations of 450 ppmv enable global-mean surface, deep-water, and meridional temperature characteristics representative of mid-Miocene Climatic Optimum (MMCO) reconstructions. The Miocene climate shows a reduced meridional temperature gradient and reduced seasonality. In the case of enhanced mixing, surface and deep ocean temperatures show significant warming of up to 5–10°C and an Arctic temperature anomaly of >12°C. In the Pliocene simulations, the impact of vertical mixing and CO_2 is less important for the deep ocean, which we interpret as a different sensitivity dependence on the background state and mixed layer dynamics. We find a significant reduction in surface albedo and effective emissivity for either a high level of atmospheric CO_2 or increased vertical mixing. Our mixing sensitivity experiments provide a warm deep ocean via ocean heat uptake. We propose that the mixing hypothesis can be tested by reconstructions of the thermocline and seasonal paleoclimate data indicating a lower seasonality relative to today.

Plain Language Summary Cenozoic climate changes have been associated with tectonic changes and altered atmospheric CO_2 concentrations. Here, we present Miocene and Pliocene computer simulations where we changed paleogeography, ocean gateways, and atmospheric CO_2 concentrations as well as vertical mixing in the ocean. We show that the effect of ocean mixing on temperature is comparable to the respective effect of a possible range of CO_2 concentrations. In combination with stronger vertical mixing, relatively moderate CO_2 concentrations of 450 ppmv allow surface and deep-water temperatures representative for reconstructions of the climate optimum of the mid-Miocene. In the Pliocene simulations, the influence of vertical mixing and CO_2 is less important than in the Miocene. We provide a possible mechanism of ocean heat absorption, albedo, and emissivity changes including a deeper oceanic mixing layer and a lower seasonality in the Miocene compared to today.

1. Introduction

Despite crucial progress in our understanding of the processes driving climate change, there is still a great need for knowledge about uncertainties in modeling future climate change (Forest et al., 2002; IPCC, 2013; Knutti & Sedláček, 2012). Paleoclimate studies offer a unique opportunity to study feedbacks potentially relevant for future climate warming (Steinthorsdottir, Coxall, et al., 2021), to evaluate the quality of climate models in reproducing large-scale climate changes that have occurred in the past (e.g., Braconnot & Kageyama, 2015; de Nooijer et al., 2020; Haywood et al., 2013, 2020; Lohmann et al., 2013), and this continues to provide valuable out-of-sample tests for the tools used to simulate future climate and environmental changes (Hay et al., 1997; Haywood et al., 2019). Over the last decades, enhanced ocean warming emerges over the subtropical and high-latitude regions (Yang et al., 2020). These warming patterns expand the tropical warm water zones and drive the tropical expansion which weakens meridional temperature gradients.

Current hypotheses to explain past warm climates during the Cenozoic are related to classical approaches that are based on tectonic changes and declining atmospheric carbon dioxide (CO_2) concentrations, or on extreme Earth

Investigation: Gerrit Lohmann, Gregor Knorr
Methodology: Gerrit Lohmann, Akil Hossain, Christian Stepanek
Project Administration: Gerrit Lohmann
Resources: Gerrit Lohmann
Software: Akil Hossain, Christian Stepanek
Validation: Christian Stepanek
Visualization: Akil Hossain, Christian Stepanek
Writing – original draft: Gerrit Lohmann
Writing – review & editing: Gerrit Lohmann, Gregor Knorr, Christian Stepanek

orbital variations around the Sun (Mikolajewicz et al., 1993; Nong et al., 2000; Toggweiler & Bjornsson, 2000; Toggweiler & Samuels, 1995). These factors are likely to have played a key role as suggested by different model studies of the ocean, atmosphere, and ice sheet components (Cristini et al., 2012; Huber & Nof, 2006; Knorr et al., 2011; Stap et al., 2019). Furthermore, ocean gateway evolution is thought to have impacted on the climate of the Miocene and Pliocene (e.g., Brierley & Fedorov, 2016; Otto-Bliesner, Jahn, et al., 2017), inducing global scale changes in meridional oceanic transport. Associated changes in the mode of the Atlantic Ocean circulation are likely to influence the interhemispheric heat balance (Bice et al., 2000; Butzin et al., 2011; Lohmann et al., 2015; Mikolajewicz et al., 1993; Sijp et al., 2009; Von der Heydt & Dijkstra, 2006).

Although there are controversial issues, e.g., the necessity of CO_2 concentrations beyond levels supported by reconstructions (Steinthorsdottir, Jardine, & Rember, 2021; Super et al., 2018) for models to reproduce Miocene warmth, and concerns regarding the magnitude and timing of CO_2 variations at key transitions such as the Eocene/Oligocene and the mid-Miocene climate transition (Coxall et al., 2005; Royer, 2008; Ruddiman, 2010; Sosdian et al., 2020; Stoll et al., 2019), the decline in CO_2 is likely to be a critical factor (Berner, 1992; Crowley, 2000; Raymo, 1991). It has been speculated that the CO_2 drawdown is related to enhanced carbon burial at the midlatitude continental margins or enhanced silicate weathering rates (Raymo, 1994). Alternatively, the drawdown in atmospheric CO_2 might stem from the development of the Southern Ocean gateway changes. Analogies based on late Quaternary climate dynamics suggest that CO_2 variations can be related to the strength of the Antarctic Circumpolar Current (Skinner et al., 2010) with potential global impact (Barker & Knorr, 2007). Modeling studies indicate that a gradual decrease in CO_2, in combination with Milankovitch and ice-albedo feedbacks, could cause a cooling, sufficient to trigger Antarctic glaciation below a critical threshold (DeConto & Pollard, 2003; Stap et al., 2019; Zachos & Kump, 2005).

For the Pliocene, Miocene, and Eocene periods, pronounced warming at high latitudes is reconstructed relative to today (Greenwood & Wing, 1995; Huber et al., 2000; Markwick, 1994; Mosbrugger et al., 2005; Shellito et al., 2003; Sloan & Rea, 1996; Tripati et al., 2003; Utescher & Mosbrugger, 2007; Utescher et al., 2017; Wolfe, 1994). As a general feature, numerical simulations indicate higher tropical (e.g., Huber & Caballero, 2011) and lower high-latitudes temperatures than the proxies (e.g., Barron, 1987; Dowsett, Foley et al., 2013; Huber & Sloan, 2001; Huber et al., 2000; Knorr et al., 2011; Mosbrugger et al., 2005; Sloan & Rea, 1996). On the one hand, models are not able to capture warming in upwelling regions as suggested by the paleo data, on the other hand, a low-latitude warming that is outside upwelling regions is not supported by the data (Dowsett, Foley et al., 2013). The question of past temperatures is furthermore related to the heat uptake by the ocean, which currently represents >90% of the excess energy gained by the Earth (IPCC, 2013). As a result of manmade emissions, climate is currently in a transient phase. In equilibrium the response of dynamics and mean characteristics of climate may look quite different (Heede et al., 2020), highlighting the importance of paleoclimate research on quasi-equilibrated climate states.

For the Pliocene, increased temperatures in midlatitude to high latitude are not matched by warming of a similar degree in regions closer to the equator (e.g., Dowsett et al., 1996; Dowsett, Foley et al., 2013; Dowsett, Robinson et al., 2013). The Arctic warming in mid-Pliocene climate simulations is underestimated compared to paleoclimate data (de Nooijer et al., 2020). For the late Pliocene, however, Tierney et al. (2019) argue that the models capture to a large degree the meridional gradient changes seen in the proxies. For the early Pliocene, models do not seem to be able to capture the full extent of gradient weakening seen in the data without ad-hoc changes to clouds or ocean mixing (Burls & Fedorov, 2014; Fedorov et al., 2010, 2013, 2015), although the upper ocean mixing changes imposed in Fedorov et al. (2010, 2013) weaken the zonal gradient and strengthen the meridional temperature gradient. Ad-hoc cloud and ocean mixing mechanisms for the Pliocene have also been suggested to resolve the high-latitude warming problem (Abbot & Tziperman, 2008; Cronin & Tziperman, 2015). For the Cretaceous which is a completely different time with different land-sea distribution, similar ad-hoc solutions for the temperature problem have been proposed through changes in cloudiness and the type of clouds (Upchurch et al., 2015), changes in paleogeography (Donnadieu et al., 2006), and imposing a more well mixed ocean through tuning of the vertical diffusivity, which is a strategic parameter in climate models (Prange et al., 2003; Thomas et al., 2014). Other suggestions are related to the type of vegetation to favor a lower albedo (Knorr et al., 2011; Micheels et al., 2011) and to a related lower sensitivity to snow fall (Otto-Bliesner & Upchurch, 1997).

The Miocene had a higher global-mean temperature and a weaker equator-to-pole temperature gradient (Pound et al., 2012; Utescher et al., 2017). However, climate models have difficulties to capture the reconstructed

decrease of the meridional temperature gradient (e.g., Micheels et al., 2011). Compared to reconstructions, this predominantly reflects too cold high-latitude temperatures which echoes the principle model challenge to simulate the magnitude of high-latitude warming in a warmer than modern climate (e.g., Goldner et al., 2014; Stein et al., 2017). Potential mechanisms that could explain the mismatch between models and reconstructions are related to elevated climate sensitivity (Steinthorsdottir, Jardine, & Rember, 2021) and to the Arctic amplification (Pithan & Mauritsen, 2014), where lapse rate and surface albedo provide a feedback to climate warming, which sensitively depends on the vertical structure in the atmosphere. Another effect might be related to major reorganizations of the global ocean circulation (e.g., Butzin et al., 2011), potentially in combination with feedbacks including the hydrological cycle and vegetation (Lohmann et al., 2015). Gateways were suggested to have redirected meridional heat transport in the ocean toward the Northern Hemisphere (NH) during the period from the Eocene to mid-Miocene (Bice et al., 2000).

The oxygen isotope records of benthic foraminifera show peak warmth occurring in the early to mid-Miocene (Mudelsee et al., 2014; Shevenell et al., 2004, and references therein). It has been proposed that the subsequent cooling took place after this interval at relatively low atmospheric CO_2. This suggests involvement of additional feedback mechanisms, or other than those related to global carbon cycling in this major Cenozoic climate transition (Shevenell et al., 2004). The expansion of the Antarctic ice sheet led to nonheterogeneous oceanic/atmospheric cooling and warming pattern in the Southern Ocean (Knorr & Lohmann, 2014; Lear et al., 2000; Shevenell et al., 2008), suggesting that the climate response and feedback can be complex providing heterogenous trends (Goldner et al., 2014; Mudelsee et al., 2014).

The question arises how we can combine these building blocks into a consistent picture of the Earth system and where are the great uncertainties regarding the energy input. A small fraction of the total generated power by the planet is transferred to ocean to generate waves and maintain the wind-driven circulation (Ferrari & Wunsch, 2009; Kleidon, 2012; Lorenz, 1960). Atmospheric convection and circulation are about 2 orders of magnitude larger than the energy transfer to the ocean (Kleidon, 2012, and references therein). The potential importance of tropical cyclones for mixing of the upper ocean has been proposed (Fedorov et al., 2010; Sriver, 2013; Sriver & Huber, 2010; Sriver et al., 2010). It could be that in a warmer climate the energy input and ocean mixing were enhanced (Korty et al., 2017; Sriver, 2013; Vincent et al., 2013). Lyle (1997) was the first to really explore some of these ramifications. He used a box model to show that a mixing scheme that depends inversely on stratification might imply a strong heat flux in warmer climates. With smaller changes in stratification between the warm upper ocean and colder interior, the amount of energy available to mixing processes could be used more efficiently since less work against gravity would be necessary at weaker stratification. Nilsson et al. (2003) further develops this idea in a more sophisticated climate model.

Marine reconstructions suggest the possibility of an ocean with a deeper thermocline, higher surface temperatures, and reduced vertical temperature gradients (Ford et al., 2015; La Riviere et al., 2012). Here, we explore this effect by performing a series of climate model sensitivity experiments with changed CO_2 and background mixing in the ocean for paleogeographic settings that are characteristic for the Miocene and Pliocene. Thomas et al. (2014) applied higher mixing rates to an ocean model, driven by a coupled climate model, to explain neodymium (Nd) tracer distributions in the Pacific Ocean. Their Nd isotope data indicate a vigorous and separate overturning circulation in each basin and South Pacific and North Pacific deep convection until ~40 Ma. Cases using a strong deep ocean vertical mixing with 4.7 cm^2/s vertical diffusivity produced the best data-model match. The vertical mixing coefficients are among the most uncertain properties that control the climate system's response to radiative forcing (Forest et al., 2002; Gregory, 2000; Raper et al., 2002). Here, we quantify the effect of different magnitudes of increased vertical mixing on temperatures of atmosphere and ocean in the context of varying CO_2 and paleogeography.

2. Model and Experimental Setup

We use the COmmunity Earth System MOdels (COSMOS; Jungclaus et al., 2010). COSMOS comprises the standardized IPCC4 model configuration which incorporates the ocean-sea ice model MPIOM (Marsland et al., 2003), the ECHAM5 atmosphere model at T31 spherical resolution (~3.75° × 3.75°) with 19 vertical levels (Roeckner et al., 2003, 2006) and the land surface model JSBACH (Raddatz et al., 2007) including vegetation dynamics (Brovkin et al., 2009). The ocean model is resolved at 40 unevenly spaced vertical z-layers, employs

partial vertical cells for a better representation of bathymetry on model levels, and takes advantage of a bipolar curve-linear grid with poles over Greenland and Antarctica at a formal resolution of 3° × 1.8° on the horizontal dimension. Grid resolution increases toward the grid poles at Greenland and Antarctica (~30 km). Consequently, high resolution in the realm of the grid poles advances the representation of detailed physical processes at locations of deep-water formation, such as in Weddell, Labrador, and Greenland and Norwegian Seas. The ocean model includes a dynamic-thermodynamic sea ice model (Hibler, 1979). The coupled climate model has a river routing scheme to close the global water cycle (Hagemann & Dümenil, 1997; Hagemann & Gates, 2003). The reference setup of COSMOS, that serves as the starting point for implementation of Miocene and Pliocene paleogeography, is based on high-resolution modern data sets derived from satellites (Hagemann, 2002; Hagemann et al., 1999).

COSMOS (version: COSMOS-landveg r2413, 2009) has been successfully applied to various paleoclimates, ranging from the Cretaceous (Klages et al., 2020; Niezgodzki et al., 2017, 2019), Eocene (Vahlenkamp, Niezgodzki, De Vleeschouwer, Bickert, et al., 2018; Vahlenkamp, Niezgodzki, De Vleeschouwer, Lohmann, et al., 2018), Oligocene (Walliser et al., 2016, 2017), Miocene (Hossain et al., 2020; Knorr & Lohmann, 2014; Knorr et al., 2011; Stärz et al., 2017; Stein et al., 2016), the Pliocene (Stepanek & Lohmann, 2012; Stepanek et al., 2020), interglacials (Lohmann et al., 2013, 2020; Pfeiffer & Lohmann, 2016; Wei & Lohmann, 2012), as well as future climates (Gierz et al., 2015; Lohmann et al., 2008). The model has been recently evaluated in comparison to other models for both the Pliocene (Haywood et al., 2020) and Miocene (Burls et al., 2021). Here, we present results obtained from model setups encompassing a time period ~20–15 Million years (Ma) Before Present (BP) within the mid-Miocene (Herold et al., 2008; Stärz et al., 2017), and the mid-Pliocene (3.29-2.97 Ma BP; Dowsett et al., 2016; Haywood et al., 2016). Vegetation reconstructions are available for mid-Pliocene (Dowsett & Caballero Gill, 2010; Salzmann et al., 2008, 2013) and some subdivisions of the Miocene (e.g., Micheels et al., 2007, and references therein), but sparse. We resolve climate-vegetation feedbacks by using our dynamical vegetation model setup.

For the preindustrial (PI) simulations, ocean bathymetry and land-sea mask have been taken from the standard modern setup of the COSMOS. The generation of paleoclimate setups is described in detail by Stepanek and Lohmann (2012). The geographic setup of the COSMOS is modified from recent global distributions of ice sheet distribution, bathymetry, land elevation, as well as the corresponding land-sea mask (Figure 1). In particular, bathymetry and land-sea masks of model setups of Miocene and Pliocene are designed to represent past ocean gateways to the best of our knowledge.

Model setups that refer to the Pliocene are developed in the framework of PlioMIP2 (Haywood et al., 2016) by Stepanek et al. (2020) and are based on updated boundary conditions (Dowsett et al., 2016). The implemented setup refers to the mid-Pliocene (~3.3-3.0 Ma BP), more precisely the KM5C time slice (Haywood et al., 2016). Distribution of bathymetry and land elevation is generated by Stepanek et al. (2020) based on the enhanced set of mid-Pliocene boundary conditions employed in PlioMIP2 (Haywood et al., 2016). Implementation of soil types, bathymetry, land elevation, and ice sheet distribution is based on the PRISM4 reconstruction for the mid-Piacenzian by Dowsett et al. (2016), and references therein. Dowsett et al. (2016) state that direct evidence for the size and extent of ice sheets during the mid-Pliocene is sparse. They employ inference from the geologic record and ice sheet simulations to provide a reconstruction of extent and elevation of Antarctic Ice Sheets and Greenland Ice Sheet. The mid-Pliocene West Antarctic Ice Sheet and Greenland Ice Sheet were much smaller than today, a characteristic that is reflected in our mid-Pliocene model setup.

Simulations relating to Miocene geography are based on a model setup by Stärz et al. (2017) and Hossain et al. (2020) that implements boundary conditions indicative of the early to mid-Miocene time period (~23-15 Ma BP). The setup includes reconstructions of land elevation, ocean bathymetry, gateway states, ice sheets, as well as land-sea mask derived from the work by Herold et al. (2008) and Ehlers and Jokat (2013). Elevation of the Miocene land surface is in many regions lower than today related to a reduced Antarctic Ice Sheet and lower altitude of Rocky Mountains, Tibetan Plateau, Andes, and East Africa. Furthermore, we employ improved Weddell Sea bathymetry based on the work by Huang et al. (2017). North Atlantic and Arctic Ocean bathymetry are based on a regional high-resolution reconstruction by Ehlers and Jokat (2013). A modification in our model setup relative to Stärz et al. (2017) and Huang et al. (2017) is described in Hossain et al. (2020) where ocean grid cells representing the Barents Sea region have been transferred to land cells, as indicated by geological data for the Miocene (Butt et al., 2002).

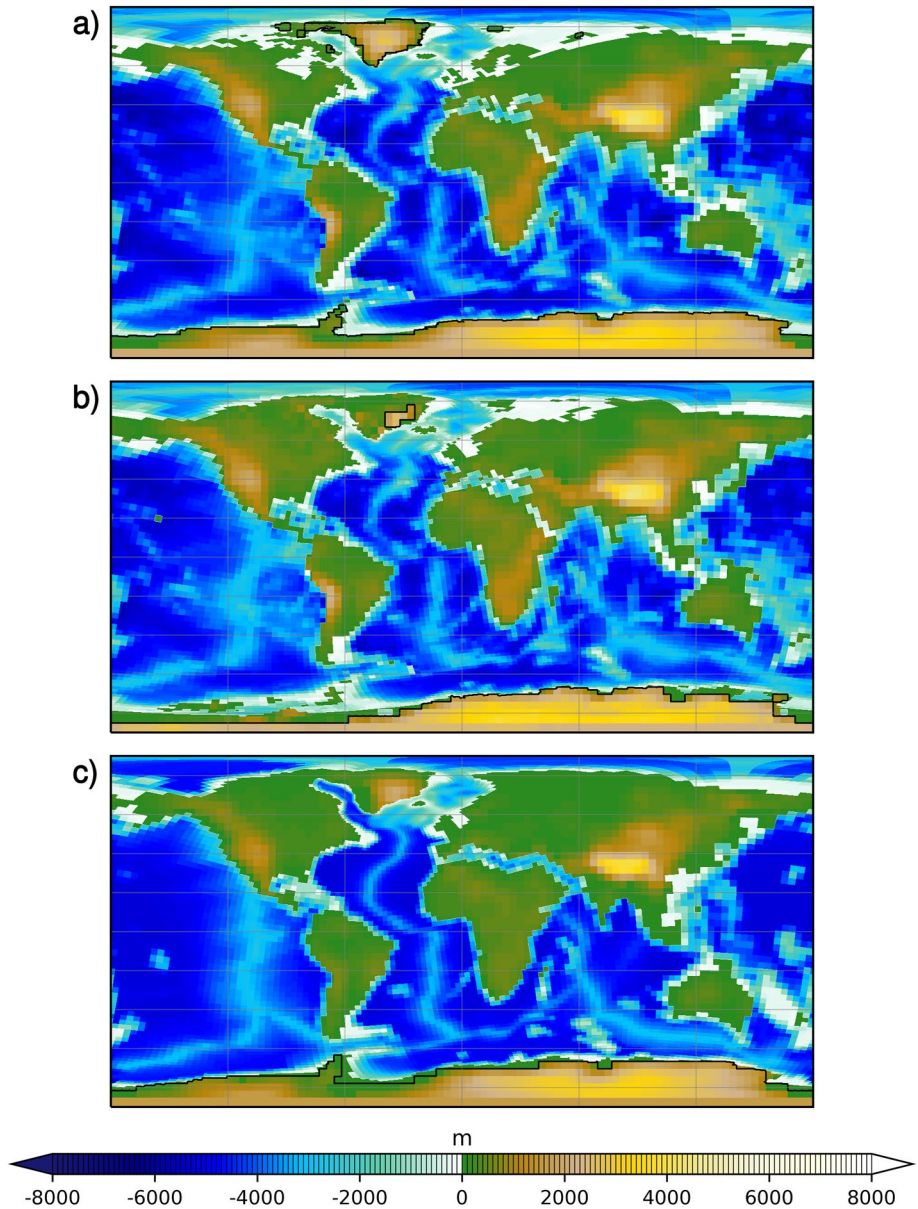

Figure 1. Paleogeographic model setup for simulations of preindustrial (a), Pliocene (b), and Miocene (c) climates based on adjustments of land-sea mask, bathymetry (left side of the color scale), land surface elevation including ice sheet thickness (right side of the color scale), and spatial distribution of prescribed ice sheets (illustrated by black contours). See text for details.

Study of the relative contributions of vertical mixing, CO_2, and paleogeography at tectonic time scales necessitates a realistic representation of past ocean gateway states. The representation of the Bering Strait in the model setup is of relevance. It has been suggested by Molnar (2008), based on the work by Marincovich (2000) and Marincovich and Gladenkov (1999, 2001), that the Bering Strait has been certainly absent during the Miocene. There are suggestions that after the opening of the gateway, intermittent closure of the Bering Strait may have occurred since the early Miocene and during the Pliocene (Matthiessen et al., 2009). A closed Bering Strait affects the Atlantic Ocean circulation (Hu et al., 2010, 2015). Otto-Bliesner, Jahn, et al. (2017) have shown for the Pliocene that as a result of ocean circulation rearrangement due to closure of the Bering Strait surface temperatures of the North Atlantic Ocean increase. As a direct result, closing the Bering Strait reduces the mismatch that is evident between mid-Pliocene sea surface temperatures (SSTs; Dowsett, Robinson, et al., 2013) and PlioMIP1 simulations (Dowsett, Foley, et al., 2013). Both the Bering Strait and the Canadian Arctic Archipelago

Table 1

Configuration of Preindustrial (PI), Pliocene (Plio), and Miocene (Mio) Simulations for Model Setups With Standard Vertical Mixing Parameters ($A_{V0,\,min}$ = 5 × 10^{-5} m^2 s^{-1}, $D_{V0,\,min}$ = 1.05 × 10^{-5} m^2 s^{-1}), and for Setups With Enhanced Vertical Mixing, the Latter Parameterized by an Increase of the Minimum Setting of Vertical Momentum ($A_{V0,\,min}$) and Tracer ($D_{V0,\,min}$) Diffusion

	Trace gas forcing			Orbital forcing			Vertical mixing (10^{-5} m^2 s^{-1})			
Simulation	CO_2 (ppmv)	CH_4 (ppbv)	N_2O (ppbv)	ecc	obl (°)	lonp (°)	$A_{V0,\,min}$	$D_{V0,\,min}$	Spin-up	Analysis
PI	280	808	273	0.0167643	23.459277	280.32687	5	1.05	1,850	100
Plio400	400	808	273	0.0167643	23.459277	280.32687	5	1.05	1,850	100
Plio450	450	808	273	0.0167643	23.459277	280.32687	5	1.05	1,850	100
$Plio450_{Mio}$	450	650	270	0.016724	23.4468	282.157	5	1.05	1,850	100
Plio560	560	808	273	0.0167643	23.459277	280.32687	5	1.05	1,850	100
$Plio400_{Mix5}$	400	808	273	0.0167643	23.459277	280.32687	25	5.25	1,850	100
$Plio450_{Mix5}$	450	650	270	0.016724	23.4468	282.157	25	5.25	1,850	100
$Plio400_{Mix10}$	400	808	273	0.0167643	23.459277	280.32687	50	10.25	1,850	100
$Plio450_{Mix10}$	450	650	270	0.016724	23.4468	282.157	50	10.25	1,850	100
$Plio400_{Mix25}$	400	808	273	0.0167643	23.459277	280.32687	125	26.25	1,850	100
$Plio450_{Mix25}$	450	650	270	0.016724	23.4468	282.157	125	26.25	1,850	100
Mio450	450	650	270	0.016724	23.4468	282.157	5	1.05	1,850	100
Mio600	600	650	270	0.016724	23.4468	282.157	5	1.05	1,850	100
Mio840	840	650	270	0.016724	23.4468	282.157	5	1.05	1,850	100
$Mio450_{Mix5}$	450	650	270	0.016724	23.4468	282.157	25	5.25	1,850	100
$Mio450_{Mix10}$	450	650	270	0.016724	23.4468	282.157	50	10.25	1,850	100
$Mio450_{Mix25}$	450	650	270	0.016724	23.4468	282.157	125	26.25	1,850	100

Note. We consider 5 times ($A_{V0,\,min}$ = 25 × 10^{-5} m^2 s^{-1}, $D_{V0,\,min}$ = 5.25 × 10^{-5} m^2 s^{-1}), 10 times ($A_{V0,\,min}$ = 50 × 10^{-5} m^2 s^{-1}, $D_{V0,\,min}$ = 10.25 × 10^{-5} m^2 s^{-1}), and 25 times ($A_{V0,\,min}$ = 125 × 10^{-5} m^2 s^{-1}, $D_{V0,\,min}$ = 26.25 × 10^{-5} m^2 s^{-1}) enhanced vertical mixing, indicated by subscripts Mix5, Mix10, and Mix25, respectively. Numbers indicate the prescribed concentration of CO_2. Reference setups for Pliocene (Plio400) and Miocene (Mio450), as well as the derived setups with modified CO_2 and mixing parameters, differ slightly in orbital forcing and concentrations of CH_4 and N_2O. Simulation $Plio450_{Mio}$ tests the impact of these differences on comparability of the various simulations from the Miocene and Pliocene framework. A setting that is common to all simulations is the solar constant at a value of 1,367 W/m^2. All simulations have been spun up for 1,850 model years. Analyses presented in this study are derived over a time period of 100 years after the spin-up. ppmv: parts per million by volume; ppbv: parts per billion by volume; ecc: eccentricity of the Earth's orbit around the sun; obl: tilt of the Earth's rotational axis in reference to the ecliptic in degrees; lonp: longitude of the perihelion in reference to the spring equinox in degrees; $A_{V0,\,min}$: minimum setting for vertical momentum diffusion; $D_{V0,\,min}$: minimum setting for vertical tracer diffusion; Plio: setup for the mid-Piacenzian (3.3-3.0 Ma BP); see Stepanek et al. (2020); Mio: setup for the early to middle Miocene (23-15 Ma BP); Hossain et al. (2020); spin-up: integration time before analysis of the derived climate states in model years; and analysis: time period after spin-up over which the model state has been analyzed.

are assumed to have been absent during the mid-Pliocene (Haywood et al., 2016) and are hence also absent in our Pliocene model setup.

Important differences between gateway states of Miocene and modern reference setups include Bering Strait, Canadian Arctic Archipelago, Central American Seaway, and the Tethys Ocean. While the Central American Seaway leads to a direct low-latitude connection between Atlantic Ocean and Pacific Ocean, the Tethys Ocean provides a link between Indian Ocean and North Atlantic Ocean. The implemented gateway changes are supported by geologic evidence. Bering Strait and Canadian Arctic Archipelago developed after the mid-Miocene (Molnar, 2008; and references therein), while Central American Seaway and Tethys Ocean closed after the early to mid-Miocene (Molnar, 2008; Rögl, 1999).

Details of the model setup for each of the simulations are outlined in Table 1. Generally, our modeling methodology follows for the Pliocene and PI simulations the protocol of the Paleoclimate Model Intercomparison Project

(PMIP4; Otto-Bliesner, Braconnot, et al., 2017). Miocene simulations follow an earlier reference setup with slightly different values of modern orbit and PI greenhouse gas concentrations (Table 1). The solar constant is in all simulations set to 1367.0 W/m^2, orbital configuration is always as modern. Slight differences between PI/Pliocene and Miocene reference orbit and greenhouse gas level stem from updates of the COSMOS PI/Pliocene model setups to PMIP4. For the PI simulation and the Pliocene model setup, the concentrations of nitrous oxide (N_2O) and methane (CH_4) are 273 and 808 ppmv, respectively. For Miocene simulations, the respective values are 650 ppmv of CH_4 and 270 ppmv of N_2O. The impact of variations in radiative forcing within a specific time period is parameterized via the prescribed concentration of CO_2. Model simulation names employed here identify the geologic epoch ("Plio" for Pliocene, "Mio" for Miocene) and the prescribed concentration of CO_2.

For the Pliocene, we define a reference simulation with 400 ppmv of CO_2 and standard parameters of vertical mixing (Plio400). The concentration of atmospheric CO_2 is in line with the range of current estimates for that time slice (Haywood et al., 2016). To test the impact of variations of CO_2, we apply in our Pliocene sensitivity experiments furthermore 450 and 560 ppmv. The model setup with 450 ppmv is still within the range of uncertainty in reconstructions of CO_2 for the KM5c time slice (Haywood et al., 2016). For our Miocene experiments, we define a reference simulation with 450 ppmv of CO_2 and standard parameters of vertical mixing (Mio450). In addition, we consider two further CO_2 concentrations in the atmosphere: 600 and 840 ppmv. All three values are in the range of CO_2 estimates for the Miocene (Kürschner et al., 2008; Pagani et al., 1999; Pearson & Palmer, 2000).

A second set of sensitivity experiments is motivated by Klotz et al. (2006) indicating a seasonality intensification and long-term winter cooling as a part of the late Pliocene climate development. Along the consecutive "interglacials" there is a trend toward a reduction in annual and winter temperatures, by >2.3°C, and toward a higher seasonality. It is conceivable that Pliocene and Miocene conditions were associated to a deeper mixed layer with lower seasonality. Ocean mixing parameterizations use a background value additional to a mixing which is influenced by the shear of the mean current (Nilsson et al., 2003). COSMOS uses the standard Pacanowski and Philander (1981) scheme for vertical eddy viscosity and diffusion. Here, the minimum settings for background values are increased by a factor of 5, 10, and 25. Changes in vertical mixing coefficients are ad hoc and not physically motivated. Our approach is inspired by Forest et al. (2002) who evaluate the uncertainty range in decadal climate variability by varying the mixing coefficient by 1 order of magnitude. Prange et al. (2003) performed ocean circulation experiments where vertical mixing coefficients have been varied up to a factor of 13, and explored the resulting stability of the large-scale Atlantic meridional overturning. Thomas et al. (2014) varied the vertical diffusivity profiles in their coupled model up to 4.7 cm^2/s in vertical diffusivity to evaluate the signature of the deep ocean circulation. Here, we concentrate on the surface temperature response for the Pliocene and Miocene conditions. Details of ocean dynamics and deep-sea conditions are provided where necessary to support conclusions on the mechanisms behind observed climate anomalies.

In cases where vertical mixing is changed from the reference setup (simulations with the subscript "Mix"), the increment factor is given as a subscript. Absolute values of the two mixing parameters modified by us are given in Table 1. The mixing parameters are also constrained by numerics and to compensate gaps of unresolved physics (e.g., Griffies et al., 2005). They are linked to tidal dissipation, abyssal stratification, turbulence, and wave braking (e.g., Green & Huber, 2013; Kagan & Sündermann, 1996; St. Laurent et al., 2002; Thomas et al., 2014; Wang et al., 2019).

The length of model integrations is 1,850 model years of model spin-up in order to create a climate state in quasi-equilibrium. After model spin-up, 100 years of model output are produced for each simulation and are employed to calculate the mean of the climate states and to perform a significance test of anomalies of paleoclimate simulations with the reference state PI.

3. Results

3.1. Meridional Temperature Gradient and Climate Characteristics

When applying paleogeography, adjustments of CO_2, and modifications of vertical mixing, we find a profound impact on the modeled meridional temperature distribution (Figure 2). A reduced surface air temperature (SAT) gradient relative to PI emerges between polar regions and low latitudes when increasing CO_2 concentrations and the intensity of vertical mixing in the ocean (Figure 2). Independently of the employed paleogeography, in both Pliocene (Figure 2a) and Miocene (Figure 2b), an increase in CO_2 reduces the meridional range of SAT because

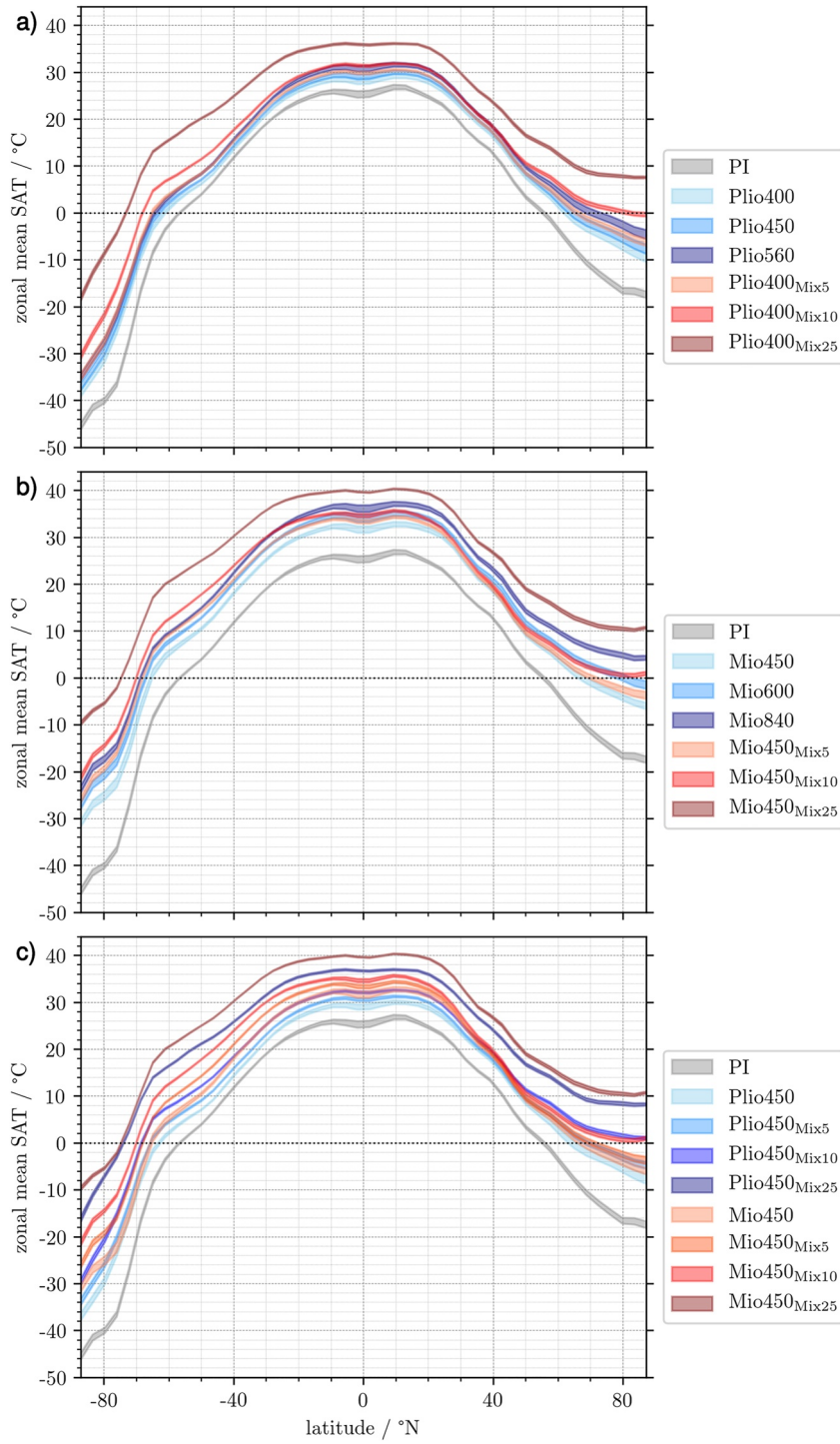

Figure 2. Zonal mean annual mean absolute surface air temperature (SAT) for the Pliocene (Plio) with various concentrations of greenhouse gases (a), for the Miocene (Mio) with various concentrations of greenhouse gases (b), as well as for the Pliocene and Miocene with identical concentrations of greenhouse gases (in particular, 450 ppmv carbon dioxide; c). Levels of carbon dioxide indicated by numbers after the time period. In each panel, we show results of a reference simulation (Plio400 and Mio450, respectively), of the preindustrial (PI)—all of these with standard vertical mixing parameters—as well as three simulations with 5, 10, and 25 times increased vertical mixing (indicated by subscripts Mix5, Mix10, and Mix25, respectively). For the Pliocene, we show in (a) also simulations with standard mixing and increased carbon dioxide (450 and 560 ppmv, Plio450 and Plio560). For the Miocene, we show in (b) also simulations with standard mixing and increased carbon dioxide (600 and 840 ppmv, Mio600 and Mio840). The temperature range of interannual variability (±1 standard deviation) is illustrated via shading.

the high-latitude warming is stronger than the simulated low-latitude warming. Differences between modern orbital forcing and PI levels of CH_4 and N_2O between Miocene and Pliocene modeling frameworks have only a minor impact on the meridional temperature range in comparison to applied changes in paleogeography, CO_2, and vertical mixing parameters (cf. Figure S1 in Supporting Information S1).

In Table 2, we list various climate indices for both hemispheres for annual mean, summer, and winter. For the Pliocene, the meridional range of SAT drops by 2.3°C in the annual NH mean by means of CO_2 control from simulation $Plio_{400}$ to $Plio_{560}$. In the Southern Hemisphere (SH), there is a similar CO_2-dependency of the equator-to-pole temperature range, at a smaller magnitude of 0.8°C from simulation $Plio_{400}$ to $Plio_{560}$. For the Miocene, where we consider a larger range of CO_2 concentrations in our simulation ensemble, the change in the meridional temperature gradient due to CO_2 is larger, with a drop by 5.9°C in the NH annual mean from simulation Mio450 to Mio840, and a respective drop by 2.8°C for SH.

While our results show that, overall, increased CO_2 reduces the meridional range of SAT in both the NH and SH, our simulation ensemble also shows that increased vertical mixing has a similar effect, albeit at a much larger amplitude and with appreciable seasonal bias (Figure 2 and Table 2). The parameterized increase of vertical mixing by a factor of 25 (simulation $Plio400_{Mix25}$ relative to Plio400) causes a drop in the Pliocene NH temperature gradient by 9.4°C in the annual mean, 18.0°C in boreal winter, and 2.2°C in boreal summer, again highlighting a substantial seasonal modulation of the change in meridional temperature range. In the SH, changes by 12.5, 12.8, and 12.2°C occur in annual mean, DJF, and JJA, respectively. Similar results are found for enhanced vertical mixing in the Miocene ($Mio450_{Mix25}$ relative to Mio450).

Comparing simulations with enhanced vertical mixing for Pliocene and Miocene with identical orbital and greenhouse forcing, in particular with 450 ppmv of CO_2 ($Plio450_{Mix5}$, $Plio450_{Mix10}$, $Plio450_{Mix25}$; $Mio450_{Mix5}$, $Mio450_{Mix10}$, $Mio450_{Mix25}$), allows a separation of the impact of enhanced vertical mixing from that of differences in other nongeographic boundary conditions between Pliocene and Miocene setups on the meridional SAT gradient (Figure 2c and Table 2). We find that in the high latitudes of the NH enhanced vertical mixing by a factor of 10 or 25 causes annual mean zonal mean SAT to be above the freezing point of water for both Pliocene and Miocene. This effect is not reproduced by any Pliocene simulation with standard mixing parameters, and necessitates high to very high levels of CO_2 in the Miocene setup (Table 2). For 5 and 10 times enhanced vertical mixing, zonal mean temperatures of the NH are in large parts similar, independently of the applied paleogeography (Pliocene versus Miocene). In low latitudes, as well as in the SH, there is a clear separation of temperature curves between Pliocene and Miocene setups with 5 and 10 times enhanced vertical mixing (Figure 2c). Similarity of SAT is lower for the upper endmembers of mixing simulations ($Plio450_{Mix25}$ and $Mio450_{Mix25}$), that both represent extreme climate states where even at the North Pole temperatures are at around +10°C in the annual mean in the Miocene, and only slightly below that in the Pliocene. Nonetheless, this result suggests that enhanced vertical mixing may have a relatively strong control on the meridional temperature gradient in the NH. Depending on the intensity of mixing enhancement this may mitigate the effect of differences in the paleogeography of the Pliocene and Miocene (cf. Plio450 and Mio450 in Figure 2c). It is also evident that enhanced vertical mixing strongly reduces the interannual variability of temperature (shading in Figures 2a–2c), an effect that is not reproduced by increased levels of CO_2.

The impacts of CO_2 and vertical mixing on the simulated climate states are also shown in the simulated sea ice extent (Table 2). While for high CO_2 concentrations in the Pliocene we find nearly sea ice-free NH and SH summer conditions, increasing vertical mixing by a factor of 25 causes a climate state that is quasi-free of sea ice year-round ($Plio400_{Mix25}$ and $Plio450_{Mix25}$). This is despite the fact that in the respective simulation with strongly enhanced vertical mixing the prescribed concentration of CO_2 is identical to the relatively low reference value (400 ppmv) or only slightly increased (450 ppmv). Consequently, with regard to the simulated sea ice extent, increasing vertical mixing in the ocean by a factor of 25 has an effect that exceeds that of increasing CO_2 from 400 to 560 ppmv in the framework of a Pliocene paleogeography. For the Miocene, where considered concentrations of CO_2 are much higher, we still fail to produce a year-round completely ice-free climate state with standard mixing parameters even for high CO_2 (840 ppmv), while, again, strongly enhanced vertical mixing at low Miocene greenhouse forcing (450 ppmv) manages to accomplish this effect.

Paleoceanography and Paleoclimatology

10.1029/2020PA003953

Table 2

Climate Indices of the Preindustrial (PI), Pliocene (Plio), and Miocene (Mio) Experiments Listed in Table 1 for the Global Domain (Glob) and Separately for NH and SH: Sea Ice Extent (SIE) for Annual Mean (Ann), Boreal Sea Ice Maximum (February/March/April = FMA), and Boreal Sea Ice Minimum (August/September/October = ASO), Values With an Asterisk Indicate That Sea Ice Cover is Completely Absent; Mean Surface Air Temperature (SAT) in NH and SH for Ann, Boreal Winter (December/January/February = DJF), and Boreal Summer (June/July/August = JJA); Meridional Range (or Meridional Gradient) of SAT Between Pole and Equator (ΔSAT) in NH and SH for Ann, DJF, and JJA; ΔSAT Refers to the Temperature Difference Between the Pole and the Lowest Latitude in Any Hemisphere, it Does Not Necessarily Refer to the Highest Overall Temperature Difference That is Present Within a Specific Hemisphere

	SIE (10^6 km^2)									SAT (°C)									ΔSAT (°C)					
	Glob			NH			SH			glob			NH			SH			NH			SH		
Simulation	Ann	FMA	ASO	Ann	FMA	ASO	Ann	FMA	ASO	Ann	DJF	JJA	Ann	DJF	JJA	Ann	DJF	JJA	Ann	DJF	JJA	Ann	DJF	JJA
PI	26.29	25.41	27.44	12.95	17.86	7.78	13.34	7.55	19.66	13.5	11.5	15.4	14.3	8.1	20.3	12.7	15.0	10.4	42.8	55.6	26.9	70.8	59.7	77.4
Plio400	13.45	11.47	13.94	5.45	9.14	0.70	7.99	2.33	13.24	16.9	14.9	18.7	18.1	12.2	24.0	15.6	17.7	13.5	37.7	47.5	28.4	66.6	57.0	71.8
$Plio400_{Mix5}$	7.40	8.41	7.29	3.79	8.08	0.01	3.61	0.34	7.28	18.5	16.8	20.3	19.5	14.0	25.1	17.6	19.6	15.6	36.0	41.8	29.6	64.8	55.7	69.8
$Plio400_{Mix10}$	1.06	1.81	1.21	0.57	1.79	0*	0.49	0.02	1.21	20.6	19.1	22.3	21.3	16.2	26.6	19.9	22.0	18.0	31.7	33.1	29.0	62.0	52.8	67.4
$Plio400_{Mix25}$	0.00	0.01	0*	0.00	0.01	0*	0*	0*	0*	26.5	25.1	28.1	26.5	21.8	31.4	26.6	28.5	24.7	28.3	29.5	26.2	54.1	44.2	59.6
Plio450	10.87	9.94	10.93	4.68	8.63	0.15	6.19	1.30	10.78	17.8	15.9	19.7	19.1	13.2	24.9	16.5	18.6	14.5	36.8	44.9	29.0	66.0	56.5	71.1
$Plio450_{MIO}$	11.76	10.48	11.95	4.87	8.76	0.23	6.89	1.72	11.71	17.6	15.7	19.5	18.9	13.0	24.7	16.3	18.4	14.2	37.2	45.9	29.0	66.1	56.5	71.3
$Plio450_{Mix5}$	6.19	7.53	6.38	3.11	7.28	0.00	3.07	0.25	6.38	19.3	17.6	21.1	20.3	15.0	25.8	18.3	20.3	16.3	35.3	38.9	30.0	64.5	55.3	69.6
$Plio450_{Mix10}$	0.61	0.75	0.99	0.22	0.74	0*	0.39	0.01	0.99	21.4	19.9	23.1	22.1	17.1	27.4	20.7	22.7	18.7	31.0	32.4	28.4	61.8	52.3	67.2
$Plio450_{Mix25}$	0.00	0.01	0*	0.00	0.01	0*	0*	0*	0*	27.3	25.9	28.9	27.1	22.4	32.1	27.5	29.4	25.7	28.4	29.6	26.4	53.0	42.3	58.7
Plio560	8.34	8.47	9.04	3.38	7.70	0.00	4.96	0.77	9.03	19.4	17.6	21.2	20.8	15.2	26.4	18.0	20.1	15.9	35.4	39.7	29.9	65.8	56.4	71.1
Mio450	6.04	8.08	4.64	3.60	7.55	0.01	2.44	0.53	4.63	20.4	18.5	22.4	21.1	15.0	27.3	19.7	22.0	17.5	37.7	44.5	30.9	62.7	52.3	68.7
$Mio450_{Mix5}$	2.19	4.98	0.55	1.98	4.98	0.00	0.21	0.01	0.55	22.3	20.6	24.2	22.1	16.5	28.1	22.5	24.8	20.3	37.0	40.2	31.8	59.4	49.1	65.3
$Mio450_{Mix10}$	0.16	0.54	0.03	0.15	0.54	0*	0.01	0.00	0.03	24.1	22.5	26.0	23.3	17.8	29.1	24.9	27.2	22.8	33.6	35.5	30.5	55.9	46.1	61.5
$Mio450_{Mix25}$	0*	0*	0*	0*	0*	0*	0*	0*	0*	30.5	29.0	32.1	29.9	25.0	35.2	31.0	33.0	29.1	28.8	30.1	26.5	49.3	39.8	54.8
Mio600	2.38	4.30	1.75	1.61	4.26	0.00	0.77	0.04	1.75	22.9	21.1	24.9	23.7	17.8	29.8	22.1	24.4	19.9	35.5	37.6	31.3	61.3	51.0	67.2
Mio840	0.24	0.17	0.52	0.04	0.16	0*	0.20	0.00	0.52	25.2	23.5	27.1	26.1	20.3	32.2	24.3	26.6	22.1	31.8	34.0	28.6	59.9	49.5	65.8

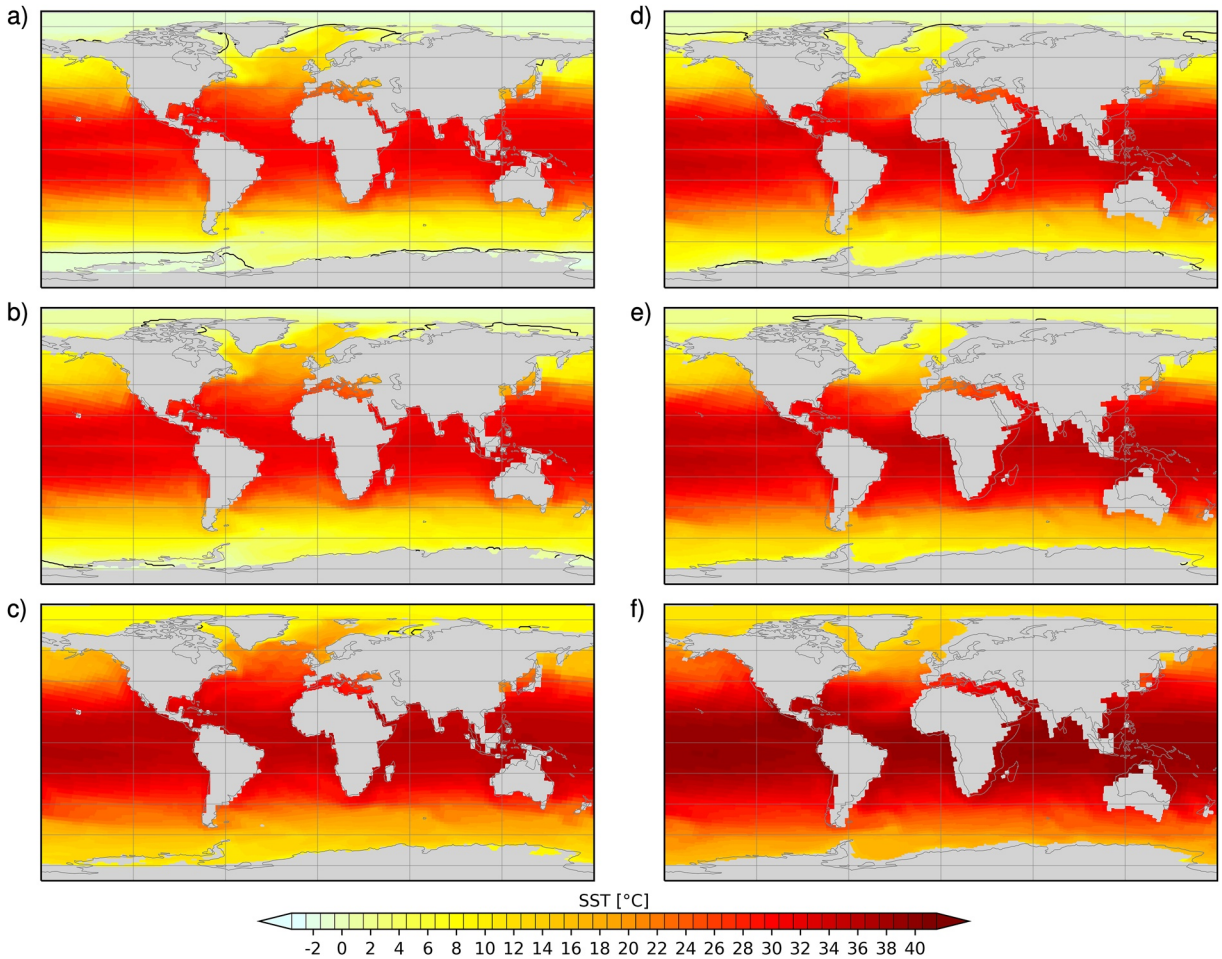

Figure 3. Annual mean absolute sea surface temperature (SST, shading) and position of the sea ice border illustrated via the 15%-isoline (black contour) for simulations with enhanced vertical mixing. Shown are Pliocene (a, b, c) and Miocene (d, e, f) simulations for 5 times (a, d; $Plio400_{Mix5}$, $Mio450_{Mix5}$), 10 times (b, e; $Plio400_{Mix10}$, $Mio450_{Mix10}$), and 25 times (c, f; $Plio400_{Mix25}$, $Mio450_{Mix25}$) enhanced mixing. Note that the Isthmus of Panama is closed in (a, b, c) as indicated in panel (b) of Figure 1. Gray shading illustrates the position of the continents in the Pliocene and Miocene model setups, respectively.

3.2. Impact on SST and Sea Ice

Sea ice is strongly affected by vertical mixing as compared to radiative forcing caused by CO_2, which is seen in maps of SST and from the position of the sea ice border (Figure 3). For both Pliocene and Miocene, increasing vertical mixing leads to ocean conditions without appreciable amounts of sea ice in the annual mean at comparatively low CO_2 (Figure 3; also confer Figure S5 in Supporting Information S1 for Pliocene simulations with 450 ppmv). This effect is stronger in the SH, where a nearly ice-free sea surface is already achieved at 10 times the standard mixing parameters (cf. Figures 3b and 3e to 3a and 3d). The effect is also stronger in the Miocene setup (450 ppmv in comparison to 400 ppmv in the Pliocene reference setup), where already in the simulation with 5 times increased vertical mixing a quasi-ice-free surface is present in the Southern Ocean (Figure 3d). For Pliocene paleogeography and low (400 ppmv) CO_2, the Arctic Ocean is quasi-free of sea ice in the simulation with 25 times increased vertical mixing (Figure 3c). Only in few regions, sea ice compactness remains above 15%. These are the Barents Sea, the Hudson Bay, and the East Siberian Sea. In contrast, only for the small enhancement of vertical mixing (5 times; Figure 3a) there is appreciable Arctic Sea ice present in the annual mean. Aforementioned results are not largely influenced if CO_2 is increased in the Pliocene reference setup to 450 ppmv. Only the state of the sea ice edge in the central Arctic Ocean shows appreciable response to increasing Pliocene CO_2 by 50 ppmv in setups with enhanced vertical mixing (cf. Figure S5 in Supporting Information S1 to Figure 3).

Sensitivity experiments related to the atmospheric CO_2 concentration at standard vertical mixing (Figure 4) on the other hand show a weaker response of the sea ice edge. Even at comparably high CO_2 (560 ppmv in the Pliocene

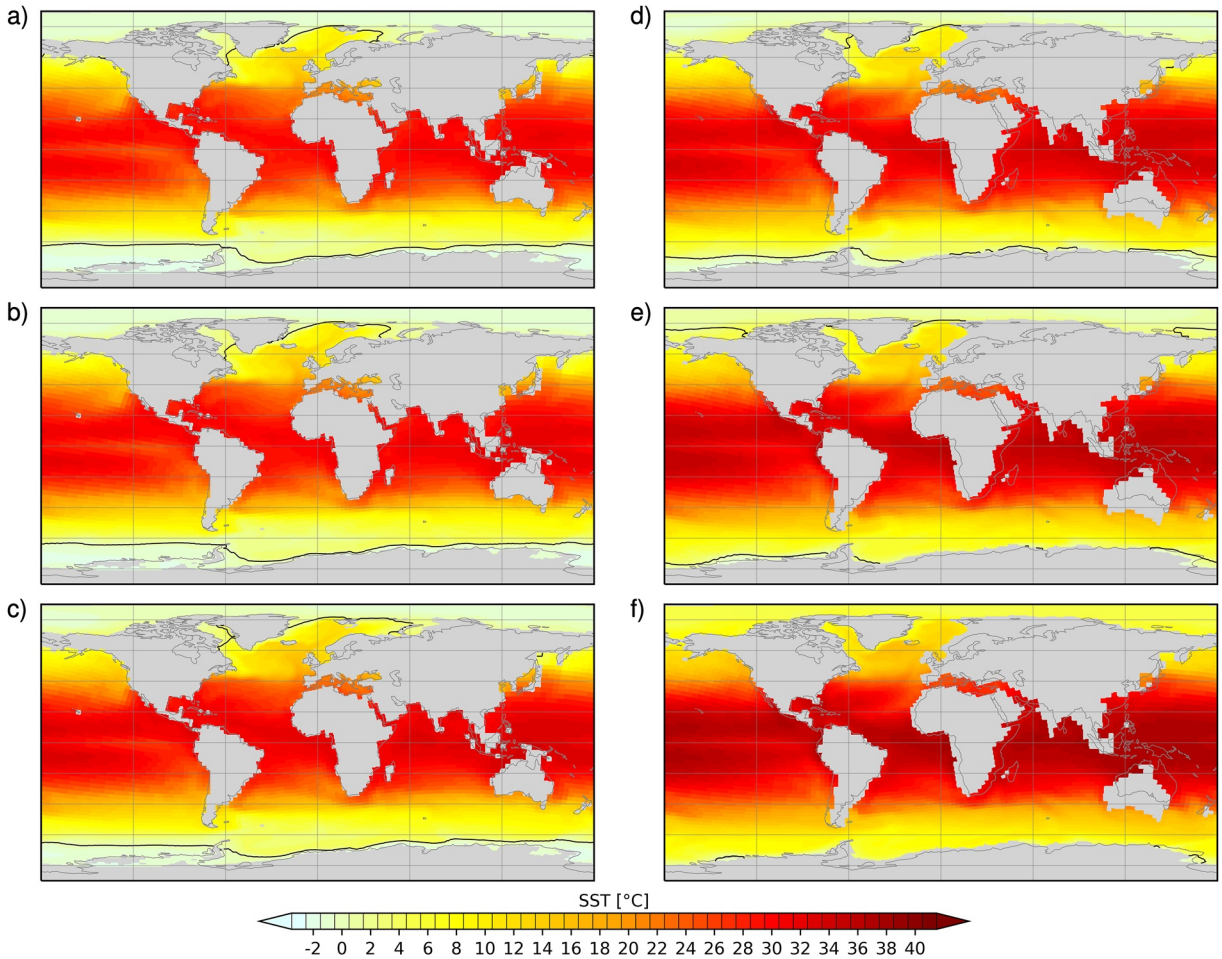

Figure 4. Annual mean absolute sea surface temperature (SST, shading) and position of the sea ice border illustrated via the 15%-isoline (black contour) for simulations with standard vertical mixing parameters. Shown are Pliocene (a, b, c) and Miocene (d, e, f) simulations. Carbon dioxide concentrations increase from up to down: Pliocene 400 ppmv (a; Plio400), 450 ppmv (b; Plio450), and 560 ppmv (c; Plio560); Miocene 450 ppmv (d; Mio450), 600 ppmv (e; Mio600), and 840 ppmv (f; Mio840). Note that the Isthmus of Panama is closed in (a, b, c) as indicated in panel (b) of Figure 1. Gray shading illustrates the position of the continents in the Pliocene and Miocene model setups, respectively.

and 600 ppmv in the Miocene) we find that sea ice is still present across the Arctic Ocean (Figures 4c and 4e). Seasonally ice-free conditions in the Miocene are only present for the extreme CO_2 concentration (840 ppmv, Figure 4f). Sea ice conditions in the Pliocene are at high CO_2 and standard vertical mixing comparable to the climate states based on low CO_2 and slightly enhanced mixing (5 times), compare Figures 3a and 4c. For the Miocene, there is a hemispheric bias with regard to the radiative-forced or mixing-forced experiment. A climate state without any sea ice in the Southern Ocean cannot be achieved by means of 450, 600, and 840 ppmv—yet, even a 5 times increase in ocean mixing parameters creates SH sea ice conditions as in a simulation with 840 ppmv and standard vertical mixing, while 10 times enhanced vertical mixing effectively removes annual sea ice (cf. Figures 3d, 3e to 4d–4f). In the NH, by increasing CO_2 we are in principle able to generate a nearly ice-free Arctic Ocean—yet, this state is already reached at 450 ppmv with 10 times increased vertical mixing (cf. Figures 3e and 4f). For a small enhancement of the vertical mixing (5 times), we generate sea ice conditions that are comparable to those that we find in the standard mixing setup with low CO_2 (450 ppmv) in the North Atlantic sector of the Arctic Ocean and with 600 ppmv of CO_2 in the East Siberian Sea (cf. Figures 3d and 4d, 4e). Increasing CO_2 in the Miocene generally reduces the amount of available sea ice, and Arctic Sea ice vanishes at high levels of CO_2 at 840 ppm (cf. Figure 4f). Results of our simulations highlight the impact of increased vertical mixing on sea ice in comparison to the respective effect of increased concentrations of CO_2. Results presented in Figures 3a and 4c and Table 2 illustrate that in the framework of prescribed Pliocene paleogeography, in the SH even a relatively small increase in vertical mixing by a factor of 5 nearly reproduces the effect of increasing CO_2

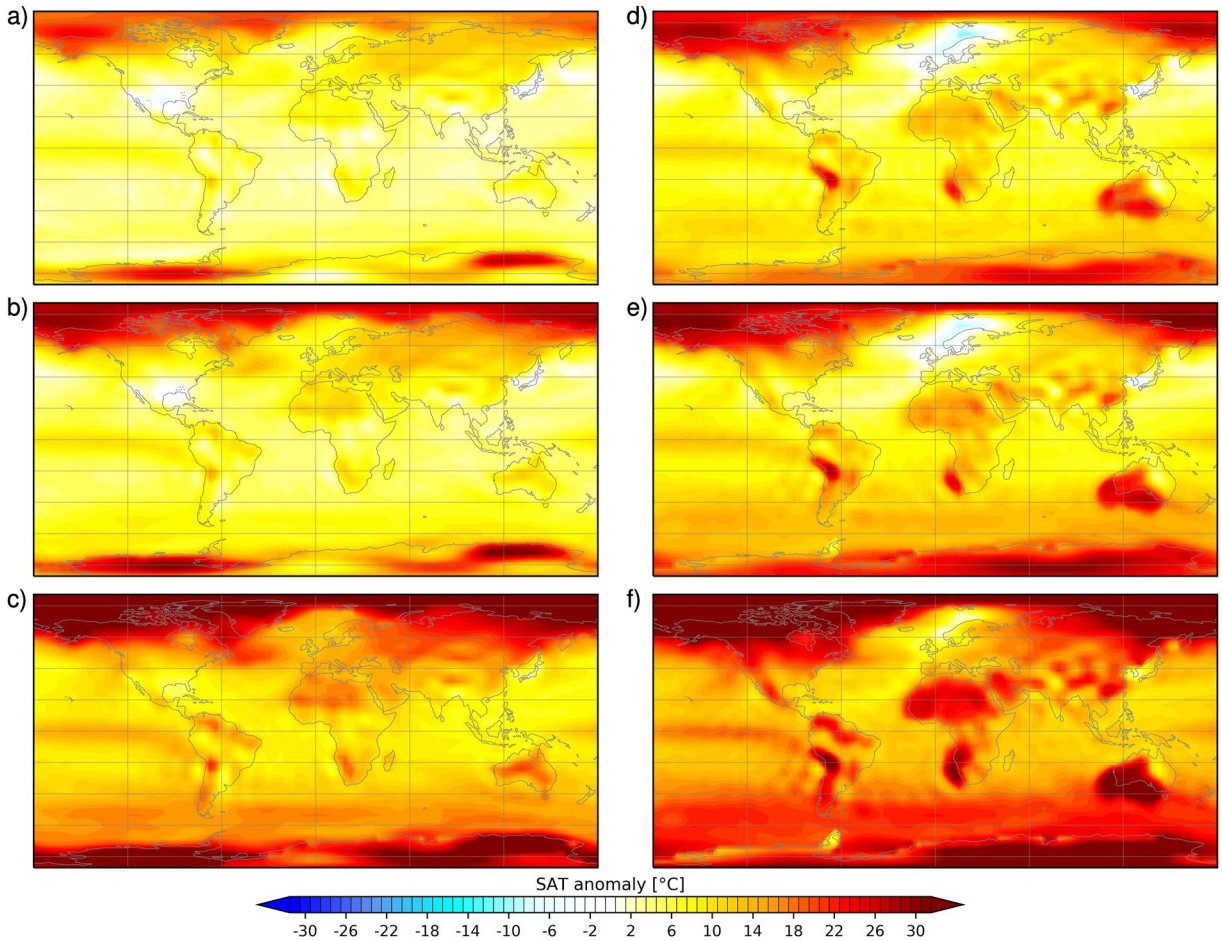

Figure 5. Anomaly of DJF surface air temperature (SAT) with respect to preindustrial (PI) for simulations with enhanced vertical mixing. Pliocene (a, b, c) and Miocene (d, e, f) simulations for 5 times (a, d; Plio400$_{Mix5}$, Mio450$_{Mix5}$), 10 times (b, e; Plio400$_{Mix10}$, Mio450$_{Mix10}$), and 25 times (c, f; Plio400$_{Mix25}$, Mio450$_{Mix25}$) enhanced mixing. Regions, where the anomaly is not significant based on a *t*-test with 95% confidence interval, are highlighted by dots. Note that there are only few regions where the anomaly is not significant.

to 560 ppmv in austral winter and exceeds the effect in austral summer. While the respective effect is weaker in the NH, 5 times increased vertical mixing still causes sea ice retreat that is similar to that induced by the most extreme CO_2 concentration considered in the Pliocene simulation ensemble (Figures 3a and 4c). SST, similarly to the meridional temperature gradient, is only moderately impacted by differences in orbital forcing and concentrations of CH_4 and N_2O in Pliocene and Miocene setups (cf. Figures S2 and S3 in Supporting Information S1). This signifies absence of an appreciable impact of the Miocene and Pliocene reference model setups on the findings presented above.

3.3. Seasonality and Polar Amplification Due to CO_2 and Vertical Mixing

Furthermore, the change of the SAT is subject to seasonal modulation especially over land for the simulations with enhanced vertical mixing (Figures 5 and 6). The respective winter season shows a pronounced high-latitude warming where the Miocene SAT increase (Figures 5d–5f) is more pronounced than in the Pliocene (Figures 5a–5c), with small exceptions where the Miocene simulation is adapted to a subaerial Barents Sea. Polar amplification is less pronounced in the CO_2 sensitivity experiments (Figures 7 and 8), but again the respective winter warming is more pronounced, with the exception of the region of the subaerial Barents Sea, in the Miocene. In the Pliocene NH, boreal winter dominates the simulated change of the meridional temperature gradient with 7.8°C (Plio560 and Plio400 in Table 2), while for boreal summer, we actually find a slight increase in the

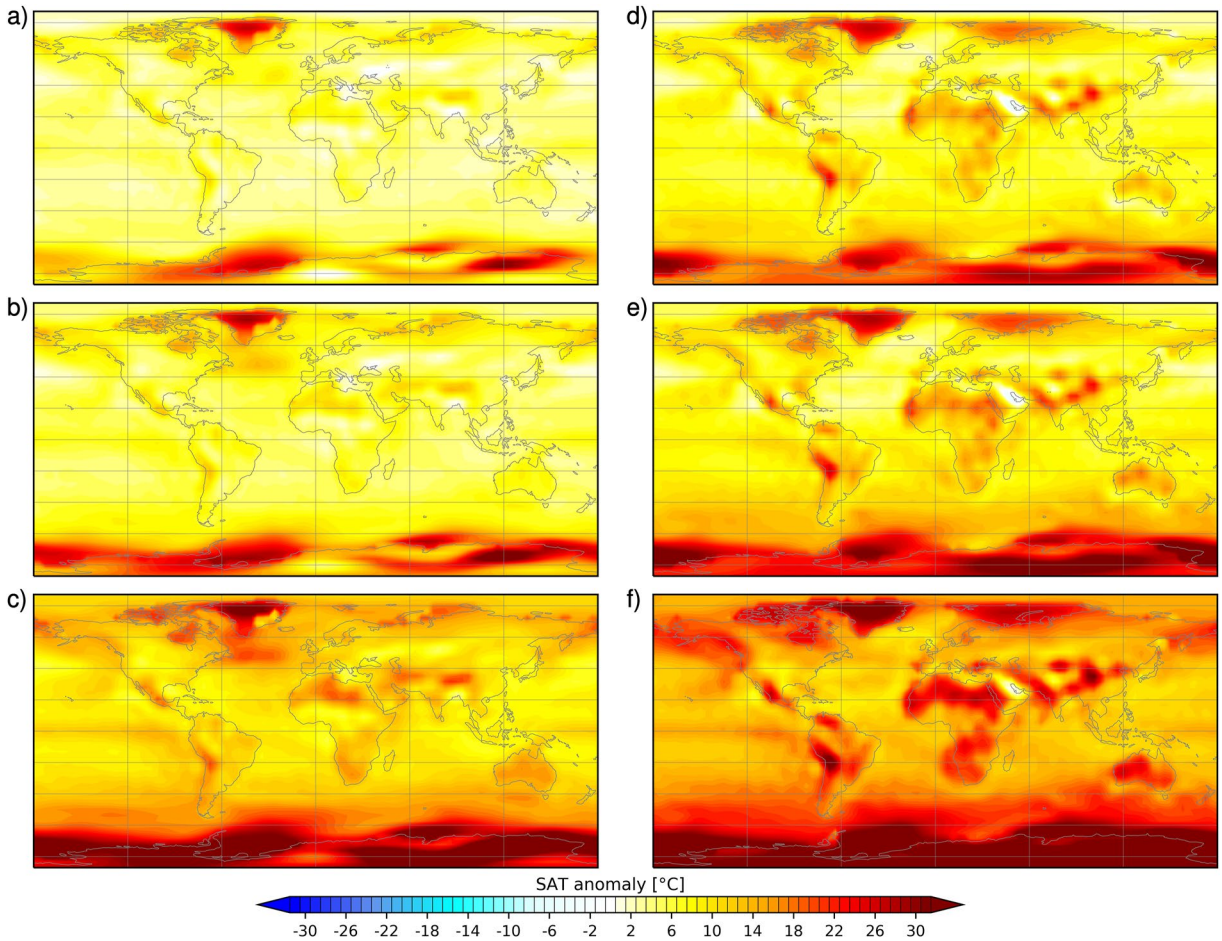

Figure 6. As Figure 5, but for boreal summer/austral winter (JJA).

meridional SAT spread by 1.5°C with CO_2 rise from 400 to 560 ppmv. A weak seasonal variation of the reduction of the meridional temperature gradient due to CO_2 is found for the SH (0.6°C for DJF, 0.7°C for JJA).

Mixing-related and CO_2-related changes in SST are illustrated in Figures 9 and 10, respectively. For the Pliocene, modulation of ocean surface temperature by CO_2 is particularly pronounced in the North Atlantic Ocean toward the Nordic and the Barents Seas, the North Pacific, as well as the Sea of Okhotsk (Figure 10). For high Pliocene CO_2 (560 ppmv), we also find that large regions of the Indian Ocean and Southern Ocean are particularly warm (Figure 10c). With Miocene paleogeography, we find similar results, but acknowledge that warming of the sea surface is in comparison to the Pliocene setup strongly enhanced, in particular at midlatitude to high latitude of the western North Atlantic Ocean, the eastern North Pacific Ocean, as well as the Southern Ocean across all longitudes. Enhanced sensitivity of Miocene climate to radiative forcing by CO_2, in comparison to Pliocene climate, is particularly evident when comparing SST anomalies with respect to PI for simulations Plio450 and Mio450 (cf. Figures 10b and 10d). Except for regional Pliocene temperature patterns in the North Atlantic realm, the temperature anomaly provoked by similar levels of radiative forcing via greenhouse gases is larger in the Miocene. This suggests that the background climate contributes to the temperature effect of CO_2 on the Pliocene and Miocene climate.

For both time slices, changes in the vertical mixing on the other hand provoke a more evenly distributed pattern of SST change with reduced temperature gradient (Figure 9), a result that is robust to differences in the orbital, CH_4, and N_2O forcing between Pliocene and Miocene modeling frameworks and a change of 50 ppmv in the Pliocene (cf. Figure S6 in Supporting Information S1 to Figure 9). Warming of ocean regions between 40°S and 40°N, of the northeast of the Atlantic Ocean, as well as of the Pliocene North Pacific Ocean, are comparably mild. We note that for the Miocene model setup, pronounced warming due to changes in vertical mixing appears in the SH.

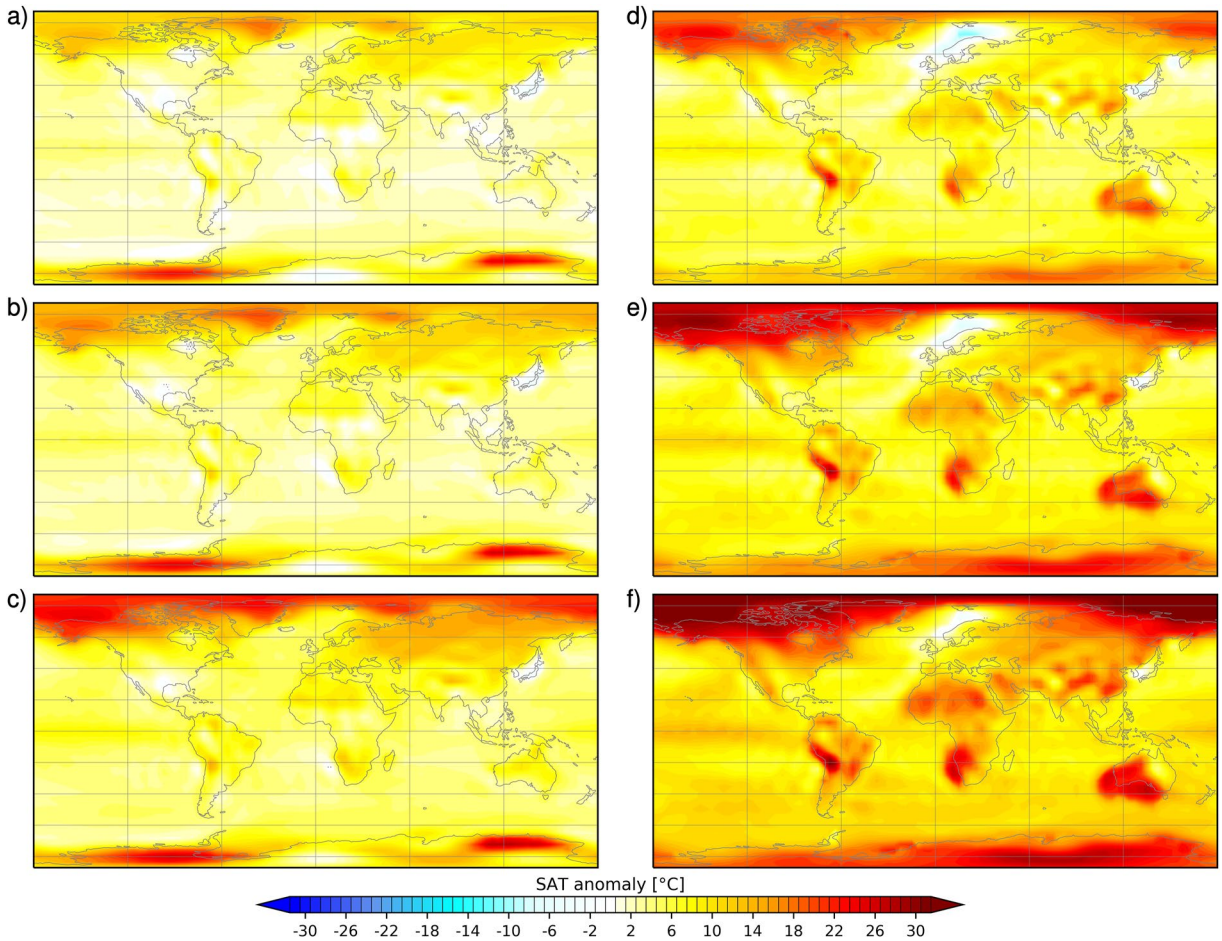

Figure 7. Anomaly of boreal winter/austral summer (DJF) surface air temperature (SAT) with respect to preindustrial (PI) for simulations with standard vertical mixing parameters. Shown are Pliocene (a, b, c) and Miocene (d, e, f) simulations. Carbon dioxide concentrations for the Pliocene are 400 ppmv (a; Plio400), 450 ppmv (b; Plio450), and 560 ppmv (c; Plio560); for the Miocene 450 ppmv (d; Mio450), 600 ppmv (e; Mio600), and 840 ppmv (f; Mio840). Regions, where the anomaly is not significant based on a *t*-test with 95% confidence interval, are highlighted by dots. Note that there are only few regions where the anomaly is not significant.

In all simulations with enhanced vertical mixing, the Southern Ocean is a hotspot of temperature increase, while the regions north of 40°N and in particular the Arctic Ocean experience warming of a similar degree only regionally, and only for the setup with 25 times increased vertical mixing. Examples for pronounced regional warming include the North Pacific Ocean north of 40°N toward the Bering Sea, regions of the North Atlantic Ocean, as well as the tropical Pacific Ocean. In comparison to the mixing effect in the NH, extreme warming in the SH is in comparison much more evenly distributed. This interhemispheric warming bias is linked to the finding that sea ice reacts particularly sensitive to increased vertical mixing in the Southern Ocean.

In parallel to the result that the impact of CO_2 on changes of surface temperature appears to be generally enhanced for Miocene paleogeography, we note a similar state-dependency for the warming effect of vertical mixing from a comparison of simulations with Pliocene geography and 400 ppmv and simulations with Miocene geography and 450 ppmv (Figure 9). This inference is robust also if we make a similar comparison for climate states with identical greenhouse forcing of 450 ppmv both in Pliocene and Miocene (Figures S5 and S6 in Supporting Information S1). It is evident that, overall, enhanced vertical mixing is more efficient in the Miocene setup, a characteristic that is related to differences in ocean circulation. This effect will be explored further below. The surplus warming effect for Miocene geography and climate state is particularly pronounced in the Southern Ocean, the low latitudes of the Indian Ocean, and the low latitude to midlatitude of the Pacific Ocean. For a large enhancement of vertical mixing (25 times), also the Arctic Ocean's surface gets warmer in the Miocene than in the Pliocene (Figure 9). In contrast, we find a pronounced pattern of warming in the North Atlantic Ocean north of 40°N, where the effect of vertical mixing is generally more pronounced in the Pliocene, confirming inference

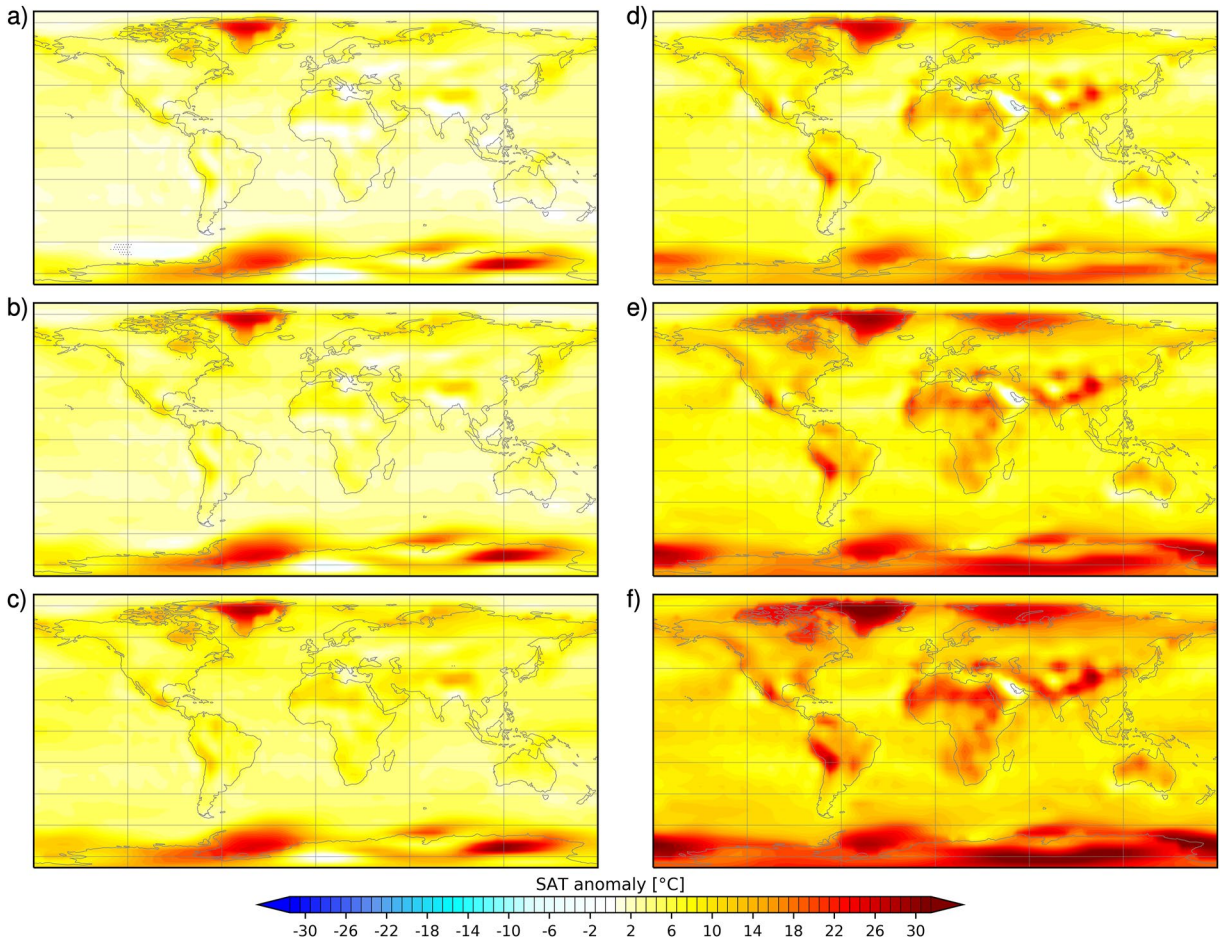

Figure 8. As Figure 7, but for boreal summer/austral winter (JJA).

from Figures 9b and 9e. Strikingly, the pattern of particularly elevated SST in the Pliocene North Atlantic Ocean overlaps with pronounced temperature anomalies reconstructed in that region for the Pliocene (e.g., Dowsett, Foley, et al., 2013; Dowsett, Robinson, et al., 2013; Haywood et al., 2020; McClymont et al., 2020).

We find that the SST mismatch between the reconstructed and simulated SST in the Pliocene reference setup (Plio400) is strongly mitigated north of 60°N in all simulations with enhanced vertical mixing. There, a best fit is derived for a simulation where the mixing parameters are 10-fold the standard values. This result is related to the finding that model simulations with enhanced vertical mixing better represent temperature reconstructions that are based on cores ODP 907, ODP 909, and ODP 911 (not shown).

Our findings on simulated surface temperature highlight two pathways for enhanced vertical mixing impacting climate. On the one hand, enhanced vertical mixing generates surface temperature anomalies that are particularly pronounced toward high latitudes. On the other hand, its impact appears to differ in dependence of the geographic setup employed in the model—Pliocene versus Miocene. Toward gaining an understanding of these mechanisms, we analyze simulated ocean meridional heat transport in the ocean—on the one hand, the global transport, integrated across all basins, as implied by atmosphere-ocean heat exchange (line plots in Figure 11), and on the other hand, the Atlantic Ocean basin component only, based on net heat transport by advection (scatter plots in Figure 11).

The PI simulation reproduces well-known first-order characteristics of global and Atlantic Ocean meridional heat transport reported in the literature (e.g., Forget & Ferreira, 2019), whereas details of transport patterns of other simulations depend on the kind of perturbation (geography, carbon dioxide, vertical mixing) that we apply. For modern geography and preindustrial greenhouse gas concentrations in simulation PI, there is a clear maximum of

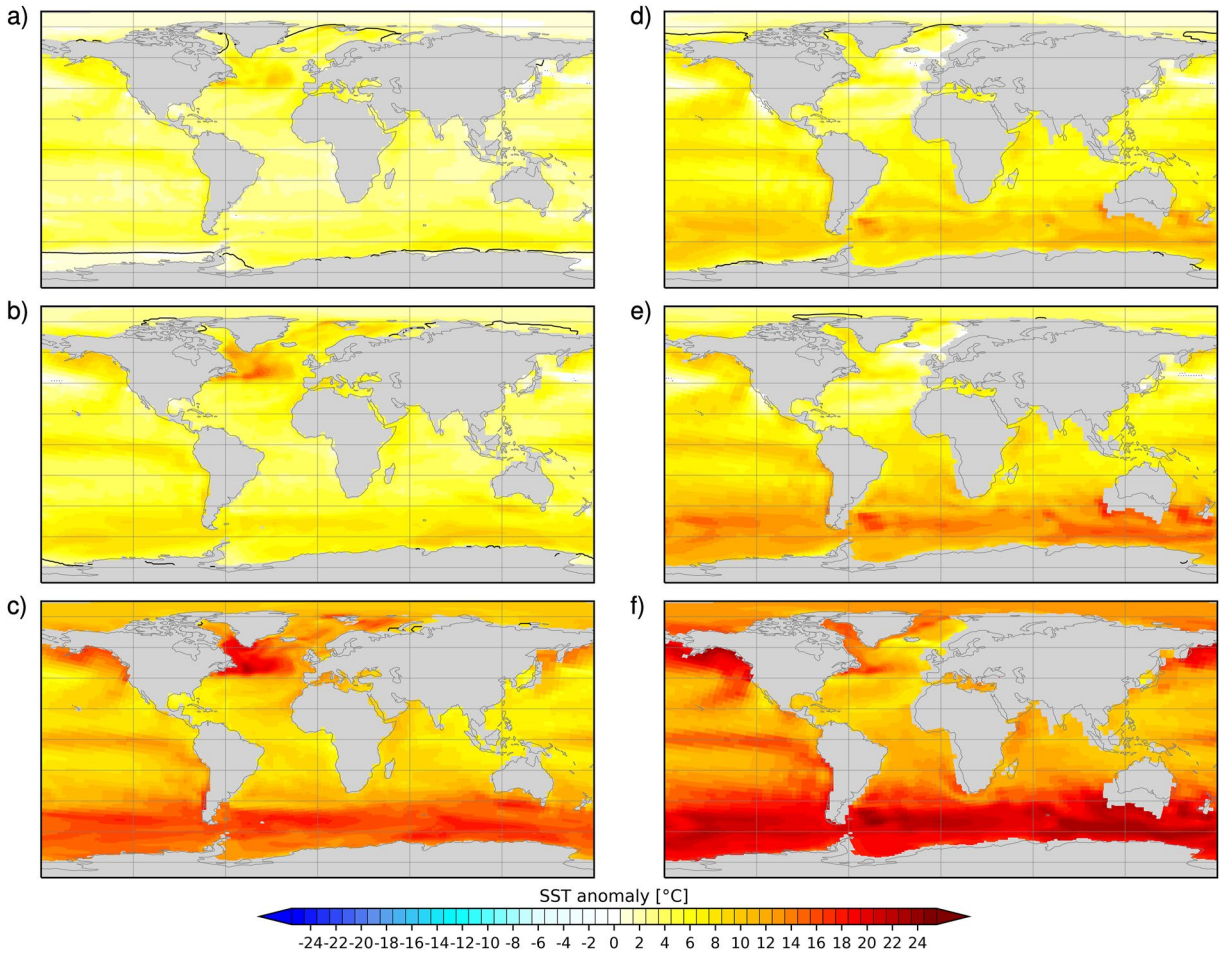

Figure 9. Annual mean sea surface temperature (SST) anomaly with respect to preindustrial (PI) and position of the sea ice border (15%-isoline: black contour) for simulations with enhanced vertical mixing. Shown are Pliocene (a, b, c) and Miocene (d, e, f) simulations for 5 times (a, d; $Plio400_{Mix5}$, $Mio450_{Mix5}$), 10 times (b, e; $Plio400_{Mix10}$, $Mio450_{Mix10}$), and 25 times (c, f; $Plio400_{Mix25}$, $Mio450_{Mix25}$) enhanced mixing. Regions, where the anomaly is not significant based on a *t*-test with 95% confidence interval, are highlighted by dots. Note that there are only few regions where the anomaly is not significant. Gray shading illustrates a superposition of the continents in the Pliocene/preindustrial and Miocene/preindustrial model setups, respectively.

global northward heat transport at about 15°N, and a similar, but weaker, maximum of southward heat transport at about 15°S (Figure 11a). Global meridional heat transport reduces toward zero near the poles and has local maxima at midlatitudes. The advection component of Atlantic Ocean meridional heat transport is mainly directed toward the north across both hemispheres; it is zero (or slightly negative) at about 60°N.

If we first focus on the impact of perturbations of greenhouse gases on the simulation of global meridional ocean heat transport in a setup of modern geography, we find that increasing carbon dioxide from preindustrial concentrations to 400, 560, and 600 ppmv (simulations E400, E560, and E600 by Stepanek et al., 2020) has only a minor effect on global meridional ocean heat transport. With increasing carbon dioxide, there is a slight increase in northward heat transport in the NH, whereas there is a slight decrease in southward heat transport in the SH. This illustrates that from the viewpoint of meridional heat transport carbon dioxide is mainly impacting the exchange of heat along and across hemispheres.

A similar response of SH heat transport is evident for simulations where carbon dioxide is altered in a Pliocene geography setup (Figure 11c), whereas in these Pliocene simulations northward heat transport is largely unaltered in the NH. For a Miocene geography (Figure 11b), on the other hand, an increase in carbon dioxide reduces poleward global ocean heat transport in the NH and causes minor increase in southward heat transport at low latitude and midlatitude in the SH. Characteristics of Miocene simulations differ from those based on a Pliocene setup in that northward global heat transports are weaker than their PI counterparts in all simulations with standard

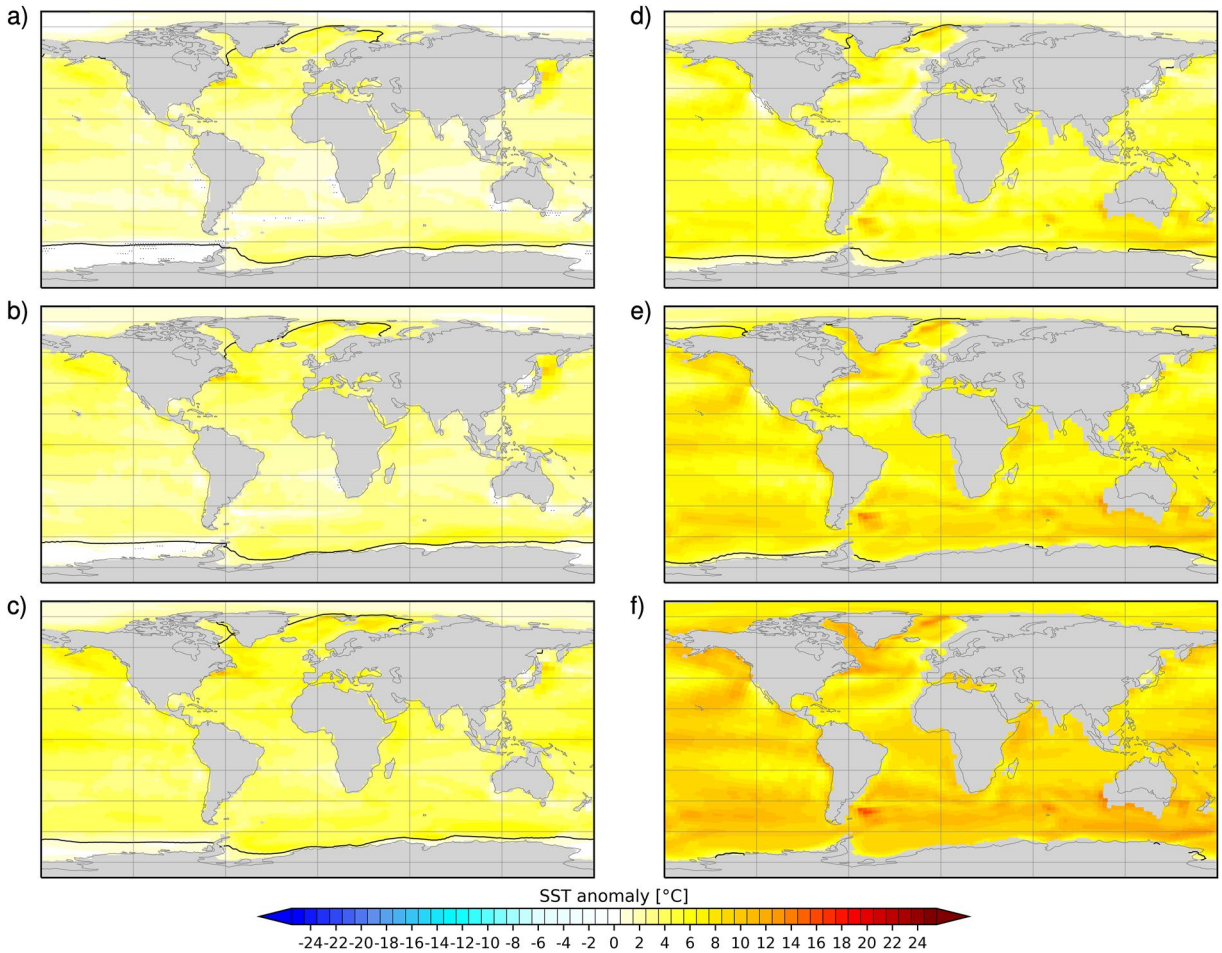

Figure 10. Annual mean sea surface temperature (SST) anomaly with respect to preindustrial (PI) and position of the sea ice border (15%-isoline: black contour) for simulations with standard vertical mixing parameters. Shown are Pliocene (a, b, c) and Miocene (d, e, f) simulations. Carbon dioxide concentrations for the Pliocene are 400 ppmv (a; Plio400), 450 ppmv (b; Plio450), and 560 ppmv (c; Plio560); for the Miocene 450 ppmv (d; Mio450), 600 ppmv (e; Mio600), and 840 ppmv (f; Mio840). Regions, where the anomaly is not significant based on a *t*-test with 95% confidence interval, are highlighted by dots. Note that there are only few regions where the anomaly is not significant. Gray shading illustrates a superposition of the continents in the Pliocene/preindustrial and Miocene/preindustrial model setups, respectively.

mixing parameters. This effect is related to differences in low-latitude geography—in particular, presence of the Panama Seaway in the Miocene setup, that reduces the salinity gradient between Atlantic and Pacific Ocean basins and impacts on both meridional overturning circulation and meridional heat transport in the ocean (Maier-Reimer et al., 1990).

When considering the impact of enhanced vertical mixing in the ocean (Figures 11b–11d) we find that meridional ocean heat transport is strongly modulated by a respective change in model parameters. In particular, the effect of enhanced vertical mixing is at an amplitude that is clearly exceeding that of modifications in geography or increased carbon dioxide. For both Pliocene and Miocene, poleward global heat transport is enhanced in both hemispheres if vertical mixing is increased. Low-latitude peaks of heat transport strengthen, broaden, and are shifted toward the poles, while local heat transport maxima in midlatitudes vanish. This indicates that enhanced vertical mixing favors a strongly enhanced "meridional heat pump" in the ocean, counteracting impacts of geography: in the Miocene setup with an open Panama Seaway, enhancing vertical mixing by a factor of 5 to 10 partly mitigates the drop of global northward heat transport that is evident in comparison to the PI state. Twenty-five times enhanced vertical mixing is able to overcompensate the reduction introduced by carbon dioxide and geography. The analysis in Figure 11d demonstrates that during the Pliocene endmembers of poleward heat transport are located in the NH, while they are present in the SH during the Miocene. Consequently, there is a geography-controlled hemispheric preference of mixing-induced heat transport anomalies.

10.1029/2020PA003953

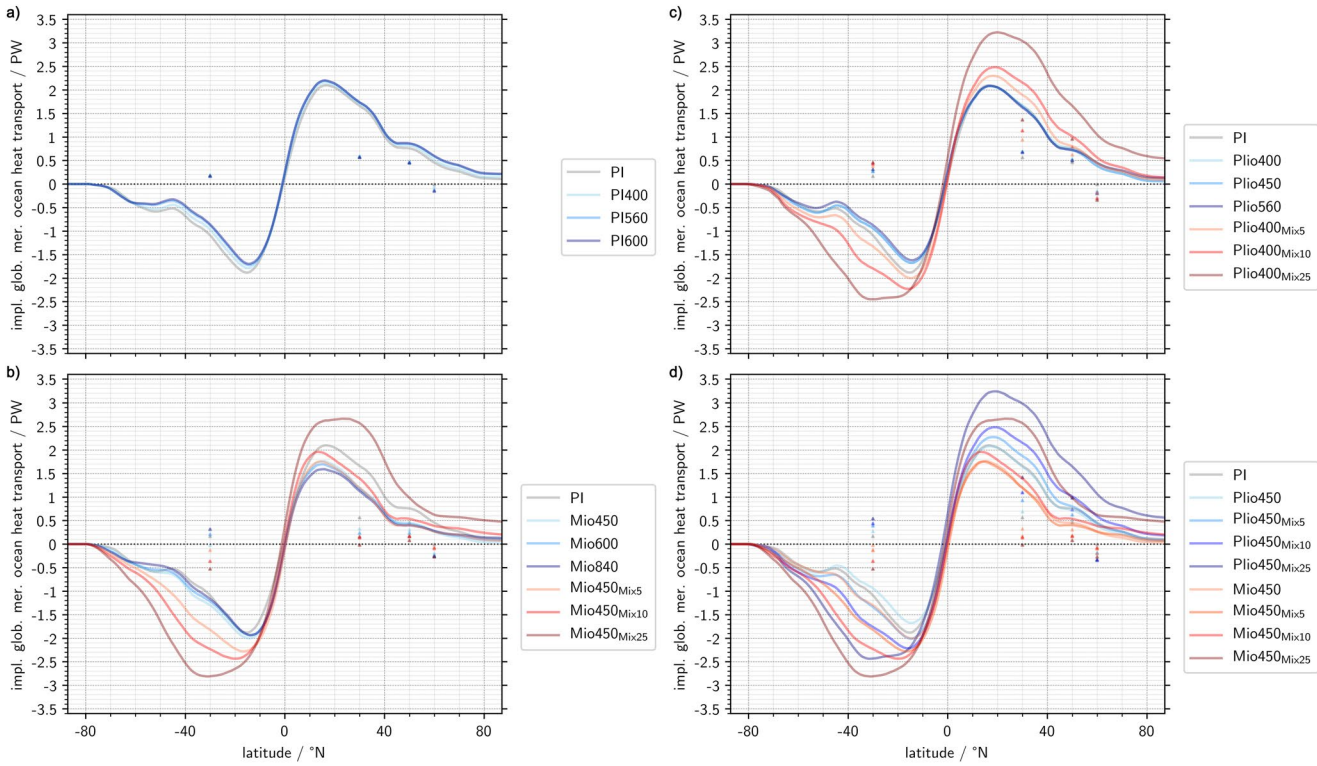

Figure 11. Meridional heat transport in the ocean for various simulations employing modern (preindustrial (PI), PI400 (E400 in Stepanek et al., 2020), PI560 (E560 in Stepanek et al., 2020), PI600 (E600 in Stepanek et al., 2020); a), Pliocene (Plio; b), and Miocene (Mio; c) geography setups. Simulations employing various concentrations of carbon dioxide and mixing parameters for different geographic setups (a)–(c) and a constant concentration of carbon dioxide (450 ppmv) for Pliocene and Miocene (d). Shown are global heat transports (lines) and net heat transports in the Atlantic Ocean only (triangles). Global meridional heat transport as implied from the global budget of heat exchange between ocean and atmosphere: heat fluxes across the atmosphere-ocean interface are integrated zonally and cumulatively summed up in south-north direction starting at Antarctica. This analysis assumes a state of equilibrium between ocean and atmosphere; disequilibrium in simulations with strongly enhanced (25 times) vertical mixing is evident as the implied meridional heat transport does not converge toward zero at the North Pole. Net heat transport in the basin of the Atlantic Ocean is explicitly computed by the ocean model based on velocity and thermodynamic properties of sea water—consequently, these results are independent of the assumption of vanishing heat exchange between ocean and atmosphere. Levels of carbon dioxide indicated by numbers after the time period. Simulations, where vertical mixing is increased by 5, 10, and 25 times relative to the reference setup, are indicated by subscripts Mix5, Mix10, and Mix25, respectively. Positive values indicate heat transport toward the north. Preindustrial (PI) shown for reference in (a)–(d).

In the Atlantic Ocean basin, we find that state-dependency (Pliocene versus Miocene geography) of the impact of enhanced vertical mixing is pronounced. While increased vertical mixing enhances northward ocean heat transport in the midlatitude Atlantic of the Pliocene, it generally reduces northward heat transport in the Miocene, where it nearly diminishes northward heat transport for 25 times enhanced vertical mixing. In the SH, combining Miocene geography with enhanced vertical mixing causes a switch from northward directed to southward directed heat transport, thereby altering a first-order characteristic of modern ocean heat transport in the Atlantic Ocean basin.

Above-described changes in simulated meridional ocean heat transport are accompanied by strong aberrations of global meridional overturning circulation (Figures 12 and 13). A robust feature of simulations of Pliocene and Miocene climate with standard mixing parameters is clockwise (from the viewpoint of Europe/Africa) circulation of the North Atlantic Deepwater branch of ocean circulation between 60°S and 60°N of the upper ocean, down to about 2,000–3,000 m of depth. With increased vertical mixing, this circulation pattern is altered from the modern-type state. A strong counter-clockwise circulation, that feeds into the deep-circulation branch of Antarctic Bottom Water, appears at low latitude to midlatitude of the SH. The volume flow of both North Atlantic Deepwater and Antarctic Bottom Water increases with enhanced vertical mixing, but the intense circulation in the south pushes the North Atlantic Deepwater branch toward the NH. For very strong mixing, the latter is confined to latitudes north of 20°S in the Pliocene, and exclusively to the NH in the Miocene.

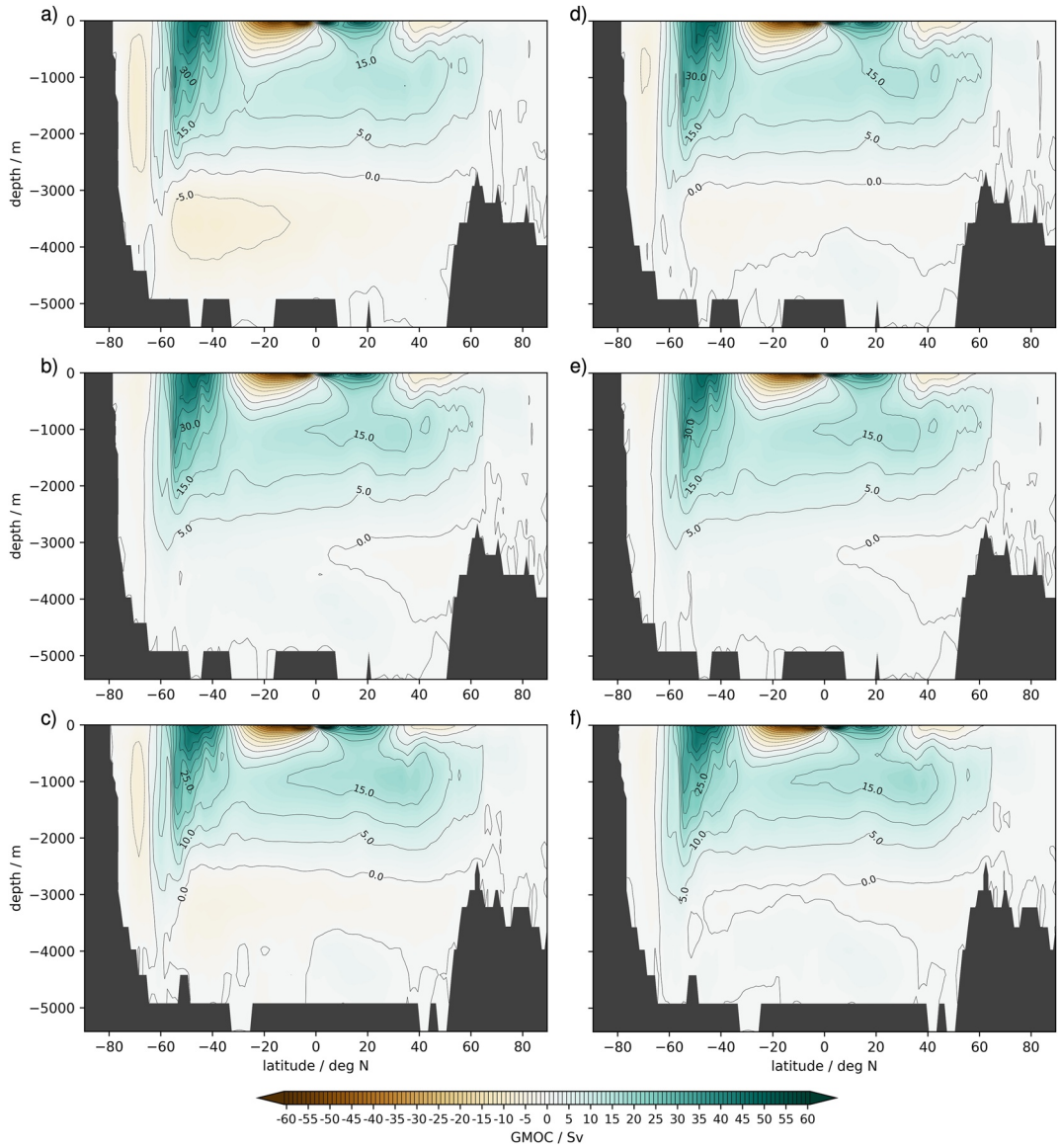

Figure 12. Stream function of the global meridional overturning circulation (GMOC) in simulations with standard mixing parameters. Shown are preindustrial (PI; a), PI560 (E560 in Stepanek et al., 2020) (b), Plio450 (c), PI400 (E400 in Stepanek et al., 2020) (d), PI600 (E600 in Stepanek et al., 2020) (e), and Plio560 (f). Zonal average bathymetry indicated via shading; clockwise circulation indicated via positive values.

These findings illustrate that temperature differences at high latitudes, and differences in vertical mixing's effectiveness in warming the climate of the Pliocene and Miocene setups, are linked to a complex reorganization of meridional ocean heat transport across different ocean basins. This effect is also pronounced in the Atlantic Ocean basin, where, in the Miocene, northward heat transport is breaking down north of 30°N, whereas the total heat transport is more dominated by other transport pathways. While for Pliocene geography enhanced vertical mixing is strengthening the role of the Atlantic Ocean to provide heat predominantly to high latitudes of the NH, in a Miocene simulation vertical mixing rather alters this characteristic of Atlantic Ocean circulation, instead contributing more to a warming of the SH. This is in agreement with our analysis of SST anomalies (Figure 9) showing largest anomalies due to vertical mixing to occur south of 30°S.

Our simulated surface temperature distribution with enhanced mixing bears similarities with Cenzoic climate change in one important aspect (e.g., Bradshaw et al., 2012; Dowsett, Foley, et al., 2013; Dowsett, Robinson,

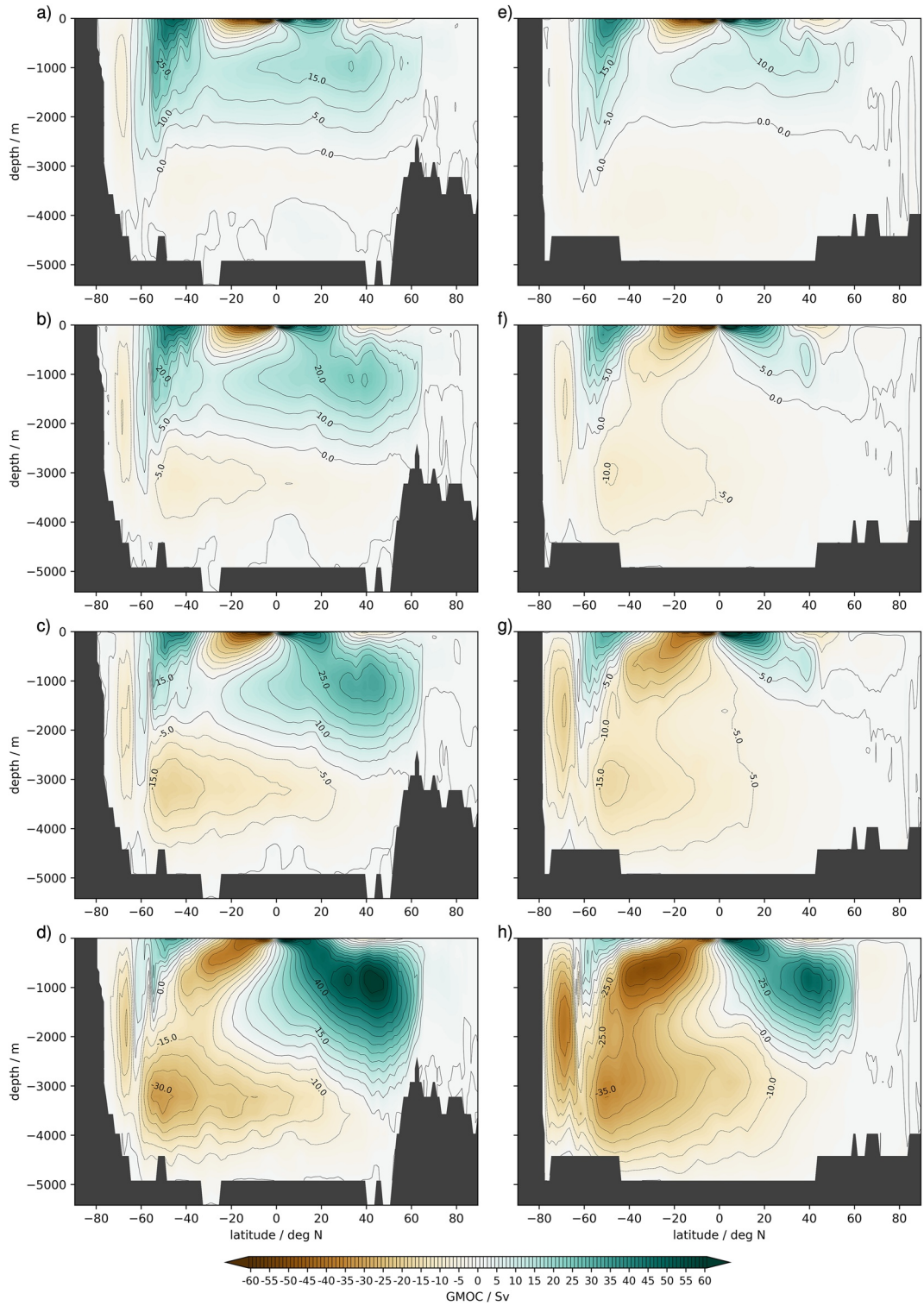

Figure 13. Stream function of the global meridional overturning circulation (GMOC) in simulations with enhanced mixing parameters. Pliocene left, Miocene right. Shown are Plio400 (a), Plio400$_{Mix5}$ (b), Plio400$_{Mix10}$ (c), Plio400$_{Mix25}$ (d), Mio450 (e), Mio400$_{Mix5}$ (f), Mio400$_{Mix10}$ (g), Mio400$_{Mix25}$ (h). Zonal average bathymetry indicated via black shading; clockwise circulation indicated via positive values.

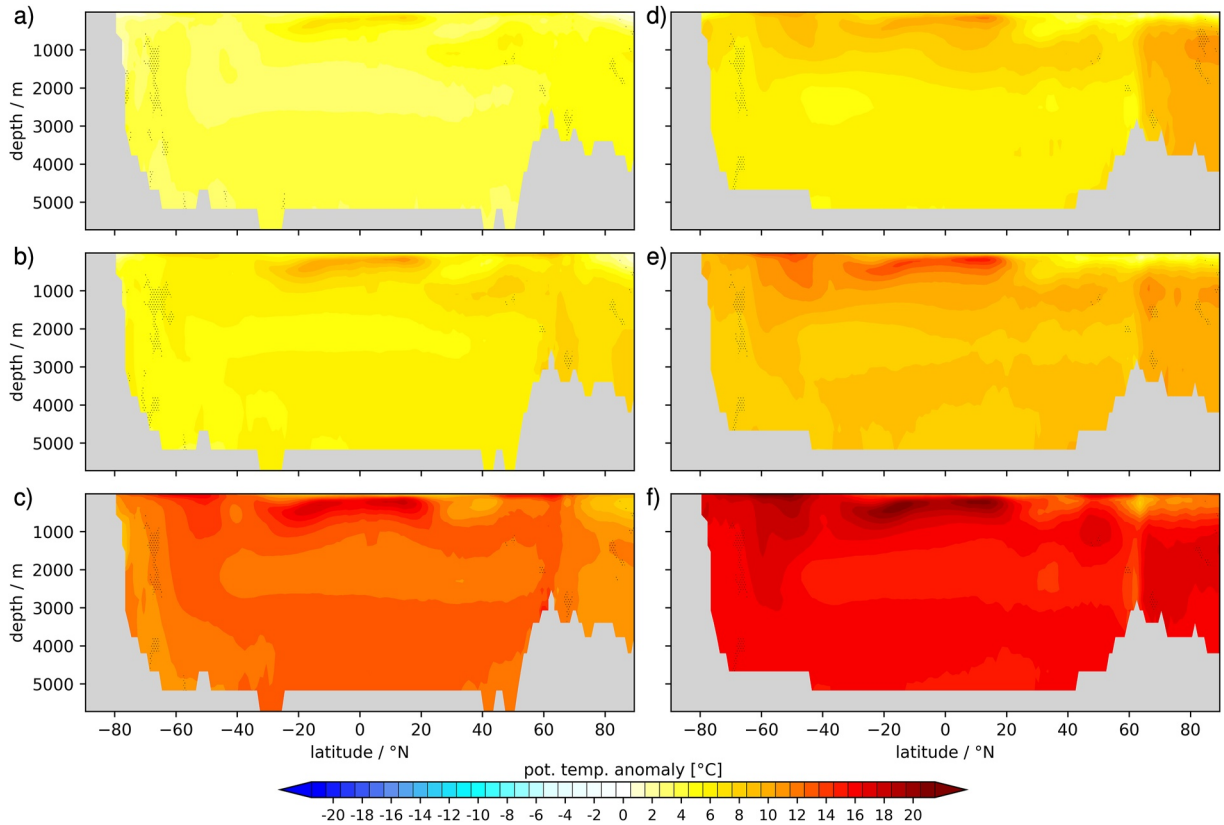

Figure 14. Zonal mean annual mean potential sea water temperature anomaly with respect to preindustrial (PI) for simulations with enhanced vertical mixing. Shown are Pliocene (a, b, c) and Miocene (d, e, f) simulations for 5 times (a, d; $Plio400_{Mix5}$, $Mio450_{Mix5}$), 10 times (b, e; $Plio400_{Mix10}$, $Mio450_{Mix10}$), and 25 times (c, f; $Plio400_{Mix25}$, $Mio450_{Mix25}$) enhanced mixing. Regions, where the anomaly is not significant based on a *t*-test with 95% confidence interval, are highlighted by dots. Gray shading illustrates the position of zonal mean bathymetry in the Pliocene and Miocene model setups, respectively.

et al., 2013; Pound et al., 2012; Utescher & Mosbrugger, 2007; Utescher et al., 2017; Wolfe, 1994): both simulated and reconstructed temperature patterns emphasize a pronounced high-latitude and moderate low-latitude warming. The modeled warming is more pronounced in winter than in summer (Figures 5 and 6) as seasonal paleoclimate data suggests (Utescher & Mosbrugger, 2007). It is conceivable that a combination of more effective ocean mixing and higher atmospheric CO_2 is responsible for much warmer than present high latitudes and a reduced summer-to-winter range of temperature (Sloan & Barron, 1990; Sloan et al., 2001; Spicer et al., 2004; Valdes et al., 1996). We note that a lower seasonality can contribute to an annual mean temperature increase due to the nonlinearity in outgoing radiation (Lohmann, 2020).

3.4. Temperature-Response of the Water Column

Furthermore, we analyze the vertical temperature distribution in the ocean that is particularly altered if vertical mixing is modified (Figure 14). Overall, changing CO_2 is not able to generate a similar warming of the various ocean layers for both Pliocene and Miocene (Figure 15). Differences in orbit, CH_4, and N_2O between Pliocene and Miocene setups have again a minor impact on these results (cf. Figure S4 in Supporting Information S1). Increasing concentrations of CO_2 enable a moderate Pliocene warming in the South Atlantic Ocean (across the water column), the upper Arctic Ocean, as well as the low latitude to midlatitude oceans at intermediate depth (at about 1,000–2,000 m). However, even a moderate increase of vertical mixing (5 times; cf. Figures 15a–15c to 14a) exceeds the effect of applying the highest concentration of CO_2. This highlights the effectivity of vertical mixing to create a pathway for surplus heat, that is available from radiative forcing, from the ocean surface toward the deep ocean. Employing higher vertical mixing coefficients causes dramatic changes in particular in the upper 1,000 m of the low-latitude oceans, the deep Arctic Ocean and, for 25 times enhanced vertical mixing, the midlatitudes of the Southern Ocean, as well as the deep ocean below 3,000 m across all latitudes. Warming patterns in

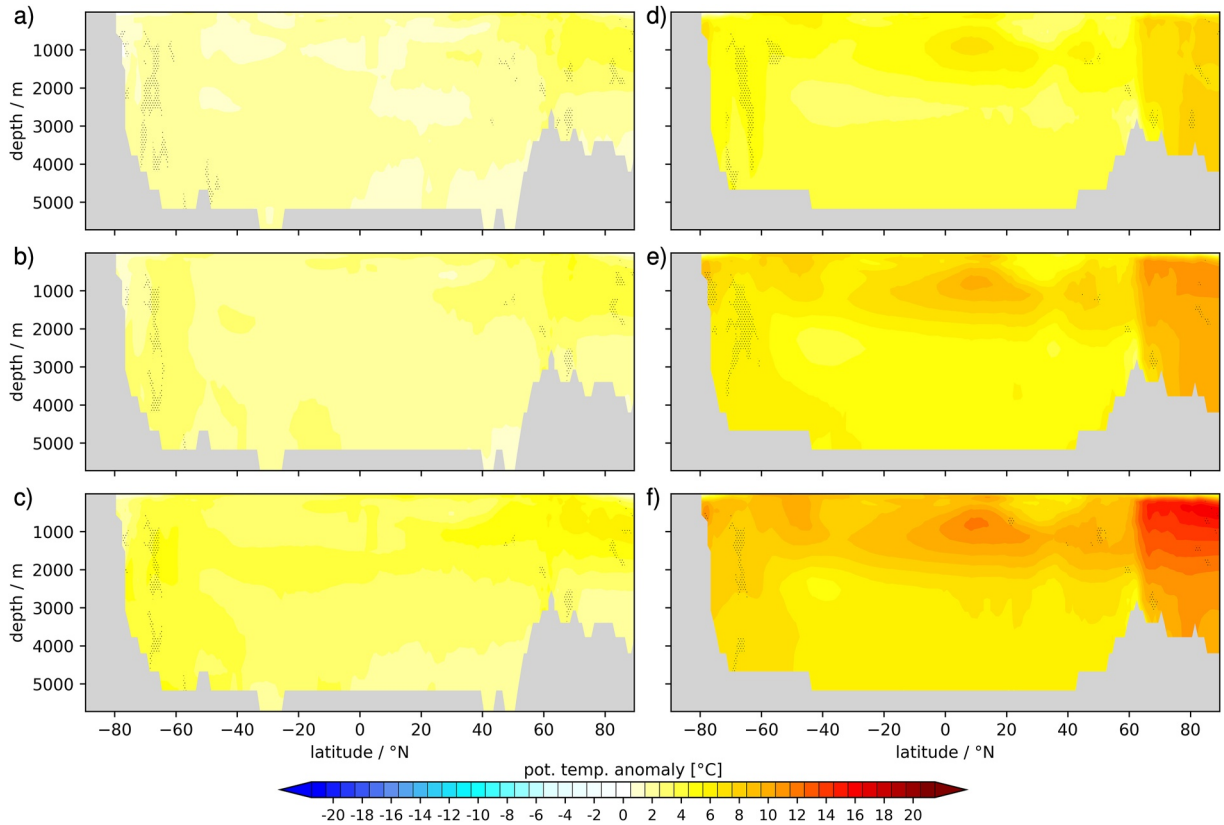

Figure 15. Zonal mean annual mean potential sea water temperature anomaly with respect to preindustrial (PI) for simulations with standard vertical mixing parameters. Shown are Pliocene (a, b, c) and Miocene (d, e, f) simulations. Carbon dioxide concentrations for the Pliocene are 400 ppmv (a; Plio400), 450 ppmv (b; Plio450), and 560 ppmv (c; Plio560); for the Miocene 450 ppmv (d; Mio450), 600 ppmv (e; Mio600), and 840 ppmv (f; Mio840). Gray shading illustrates the position of zonal mean bathymetry in the Pliocene and Miocene model setups, respectively.

Pliocene and Miocene are similar in most regions (except for the Arctic and Southern Oceans), but the amplitude is stronger in the Miocene (Figure 14). Changing CO_2 in the Pliocene from 400 to 450 ppmv has a comparably minor impact on these findings (cf. Figure S7 in Supporting Information S1 and Figure 14).

The effect of increased CO_2 on ocean temperatures is in the Pliocene simulation ensemble comparably mild, with a tendency to warm the upper ocean more than the deep ocean (Figures 15a–15c). Vertical mixing in the Miocene simulation ensemble is on the other hand able to much more effectively warm the deep ocean of the high latitudes than it is for the Pliocene (Figure 14). The Pliocene model setup with enhanced vertical mixing differs—besides paleogeography—also with regard to CO_2, as simulations are forced with a lower concentration (400 ppmv in the Pliocene in comparison to 450 ppmv in the Miocene mixing simulations). As the warming effect by 50 ppmv (from 400 to 450 ppmv) in the Pliocene is only moderate (cf. Figures 15a and 15b), this hints to a potential modulation of the effectivity of vertical mixing in the ocean by paleogeography and background climate of the Miocene. This statement is confirmed by Figure S7 in Supporting Information S1 that provides a quantification of the impact of paleogeography and background climate on the efficiency of enhanced vertical mixing in Pliocene and Miocene model setups with identical CO_2 (450 ppmv) and 5, 10, and 25 times enhanced vertical mixing. Similar to results from Figures S5 and S6 in Supporting Information S1, it is evident that vertical mixing is more effective in transporting heat into the deep ocean for the Miocene. In that geographical setup warming is particularly enhanced in the upper to middepths of the Southern Ocean and in ocean regions between 60°S and 20°N (Figure 14). On the other hand, north of 40°N, we find a distinctive dipole pattern between the Miocene deep ocean and the upper several hundred meters of the water column. In this region, the Miocene near-surface ocean is less effectively warmed by increased vertical mixing than the underlying water column (Figures 14d–14f). In contrast, in the Pliocene, this dipole pattern is violated at latitudes between about 50°N and 70°N (Figures 14a–14c). This effect is particularly pronounced for the simulations with 10 and 25 times enhanced vertical mixing. Taken

together, these findings confirm inferences derived from results presented in Figure 9 and Figures S5 and S6 in Supporting Information S1. Enhanced vertical mixing is particularly effective in warming the sea surface in the Pliocene North Atlantic Ocean. Our results highlight a region of particular warmth of the Pliocene sea surface of the North Atlantic Ocean (Figures 9a–9c) that overlaps with reconstructions of pronouncedly elevated Pliocene SSTs. For that region, a link between surface temperatures and strength of the Atlantic Ocean Meridional Circulation has been proposed (Drijfhout et al., 2012; Rahmstorf et al., 2015). Indeed, the intensity of anomalous surface warmth appears in our simulations to be linked to the strength of the meridional overturning circulation (the global stream functions are shown in Figures 13b–13d)—the stronger the poleward meridional circulation in the NH, the more pronounced is the simulated warming. In other regions, on the other hand, enhanced vertical mixing is more effective in providing heat to the ocean interior for the Miocene climate state.

These findings highlight that, independent of the employed paleogeography (Miocene or Pliocene), for the chosen settings of CO_2 concentrations and vertical mixing coefficients, CO_2 impacts in particular the temperatures of the upper ocean down to a depth of about 2,000 m. An exception to this rule is the Southern Ocean, where, in particular for high concentrations of CO_2 (above 450 ppmv), deep ocean temperatures are also sensitive to warming by means of CO_2 (Figure 15). Modification in the parameterization of vertical mixing on the other hand influences (and does so to a larger extent than CO_2) both the upper (down to 2,000 m, depending on employed paleogeography and mixing parameter settings) and deep ocean across all latitudes, while the intermediate ocean (between a depth of about 1,500 and 3,000 m, again depending on the model setup) is impacted relatively mildly by vertical mixing (Figure 14). Vertical mixing thus is, not surprisingly, a very effective means of heating the upper and deep ocean, while CO_2 can only generate warm sea water in particular in the uppermost 2,000 m of the ocean. The difference in preference of heating due to CO_2 and vertical mixing is subject to a latitudinal bias and particularly pronounced in low latitudes. In high latitudes, the difference in effectivity of warming, due to adjustments of CO_2 on the one hand, and due to vertical mixing on the other hand, is weaker. There, temperature anomalies are more similar across the water column in particular for the Miocene model configuration (cf. Figures 14 and 15).

3.5. Equilibrium Climate Sensitivity in Different Climate States

Finally, we analyze the dependency of global average annual average near-surface air temperature in simulations with and without enhanced vertical mixing on concentrations of CO_2 (Figure 16). We perform this analysis in consideration of the impact of different parameters of vertical mixing and geographic model setups. In addition to simulations with Pliocene and Miocene paleogeography, and to the PI reference period presented in detail in this work (Table 1), we also consider in Figure 16 simulations with a modern geography and elevated levels of CO_2—400, 560, and 600 ppmv. These are identified as simulations PI400, PI560, and PI600, respectively, and have been described and analyzed more broadly by Stepanek et al. (2020) where they are referred to as E400, E560, and E600.

The slope of temperature versus CO_2 for different model configurations (PI, as well as Pliocene and Miocene with and without enhanced vertical mixing) provides an estimate of the equilibrium climate sensitivity (ECS) of the model climate. In the model setup with standard vertical mixing, the ECS is slightly higher in the Pliocene model setup than for a modern geography, but this result is within the margin of error (Stepanek et al., 2020). For the simulations with a Miocene geography, the ECS is found to be slightly higher (0.7 K) than for the present-day configuration. Simulations with enhanced vertical mixing on the other hand do not lead to an obvious change of the slope, temperature versus CO_2 concentration, but rather cause a pronounced temperature offset. At similar levels of CO_2, a Pliocene climate based on 10 times enhanced vertical mixing is getting warmer than a Miocene climate based on the standard mixing parameters and 450 ppm of CO_2; a Pliocene climate based on 25 times enhanced vertical mixing is, with regard to global average surface air temperature, about halfway between Miocene climates with vertical mixing parameters that are enhanced by factors of 10 and 25, respectively. The impact of vertical mixing is once more shown to outpace the impact of geography and CO_2, highlighting the effectivity by which vertical mixing is capable of impacting on the global climate.

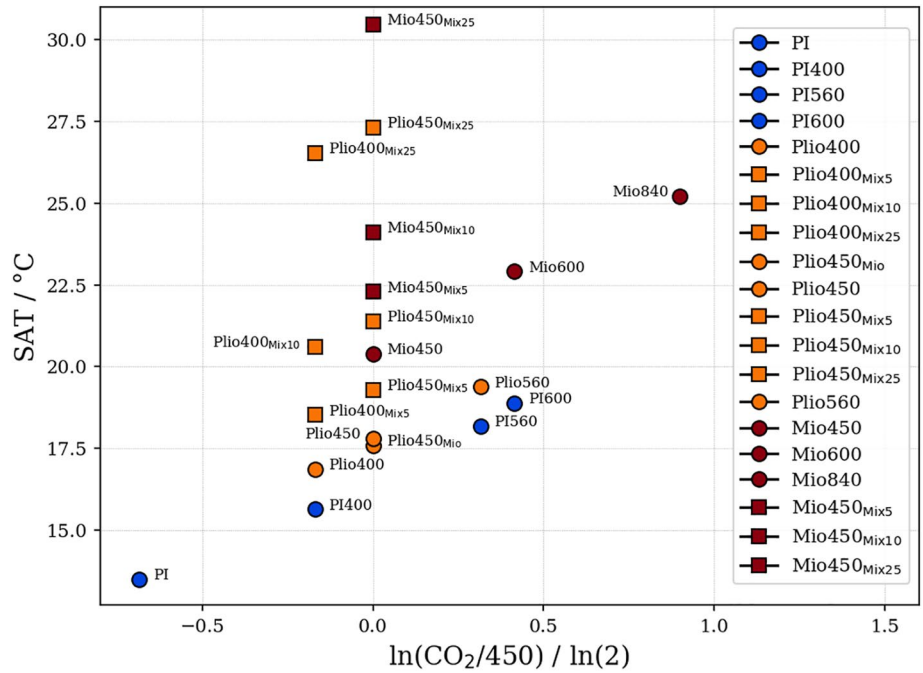

Figure 16. Dependency of annual mean global average surface air temperature (SAT) on carbon dioxide (CO_2) concentration for various modeling frameworks with modern (preindustrial (PI)), Pliocene (Plio), and Miocene (Mio) geography, and for various settings of vertical mixing parameters. Differences in color signify differences in geographic settings. Circles represent simulations based on standard vertical mixing parameters; squares show results that have been computed by means of enhanced vertical mixing. CO_2 level indicated by numbers, mixing enhancement factor specified by the number after the subscript "Mix". Simulation PI is forced with 280 ppmv of CO_2. Simulation $Plio450_{Mio}$ is slightly colder than simulation Plio450 due to reduced concentrations of methane and nitrous oxide in the Miocene modeling framework. See text for details and refer to Table 1 for an overview of the characteristics of each simulation.

4. Quantification of Warming Contributors

Results of the previous chapter have shown that carbon dioxide and changes in model parameters of vertical mixing have a large impact on meridional temperature gradient (Figure 2), sea surface temperature and near-surface air temperature (Figures 3–10), as well as on the temperature distribution in the water column of the global ocean (Figures 14 and 15). Based on Figure 16, we have been able to identify dependency between SAT on the one hand and CO_2 and vertical mixing parameters on the other hand.

To identify the mechanisms that cause the surface temperature differences, we fit a zero and one-dimensional energy balance model (EBM) to the results, following the approach of Heinemann et al. (2009) and Lunt et al. (2012). This model assumes a gray atmosphere and sets the incoming shortwave radiation at the left-hand side of the model equation equal to the outgoing longwave radiation at the right-hand side. Incoming shortwave radiation is a function of planetary albedo. Outgoing longwave radiation is a function of effective longwave emissivity of the climate system and of surface temperature. Consequently, this model can be used to separate contributions of emissivity and albedo to a specific change in surface temperature between different simulations. The one-dimensional EBM (Heinemann et al., 2009) includes the divergence of heat transport and resolves the latitudinal dependency of effective longwave emissivity and planetary albedo. We evaluate the results in comparison to SAT, water vapor content, and surface albedo computed by the GCM (Figure 17 and Table 3). By means of the zero-dimensional EBM, we split the temperature anomaly between various simulations into contributions from planetary albedo and effective longwave emissivity based on the physical model of a gray body (Figure 18 and Table 3). To this end, planetary albedo and effective emissivity are computed from radiation quantities of our GCM following Heinemann et al. (2009). The implied surface temperature in the one-dimensional and zero-dimensional EBM is diagnosed from planetary albedo, effective emissivity (zero-dimensional case), as well as

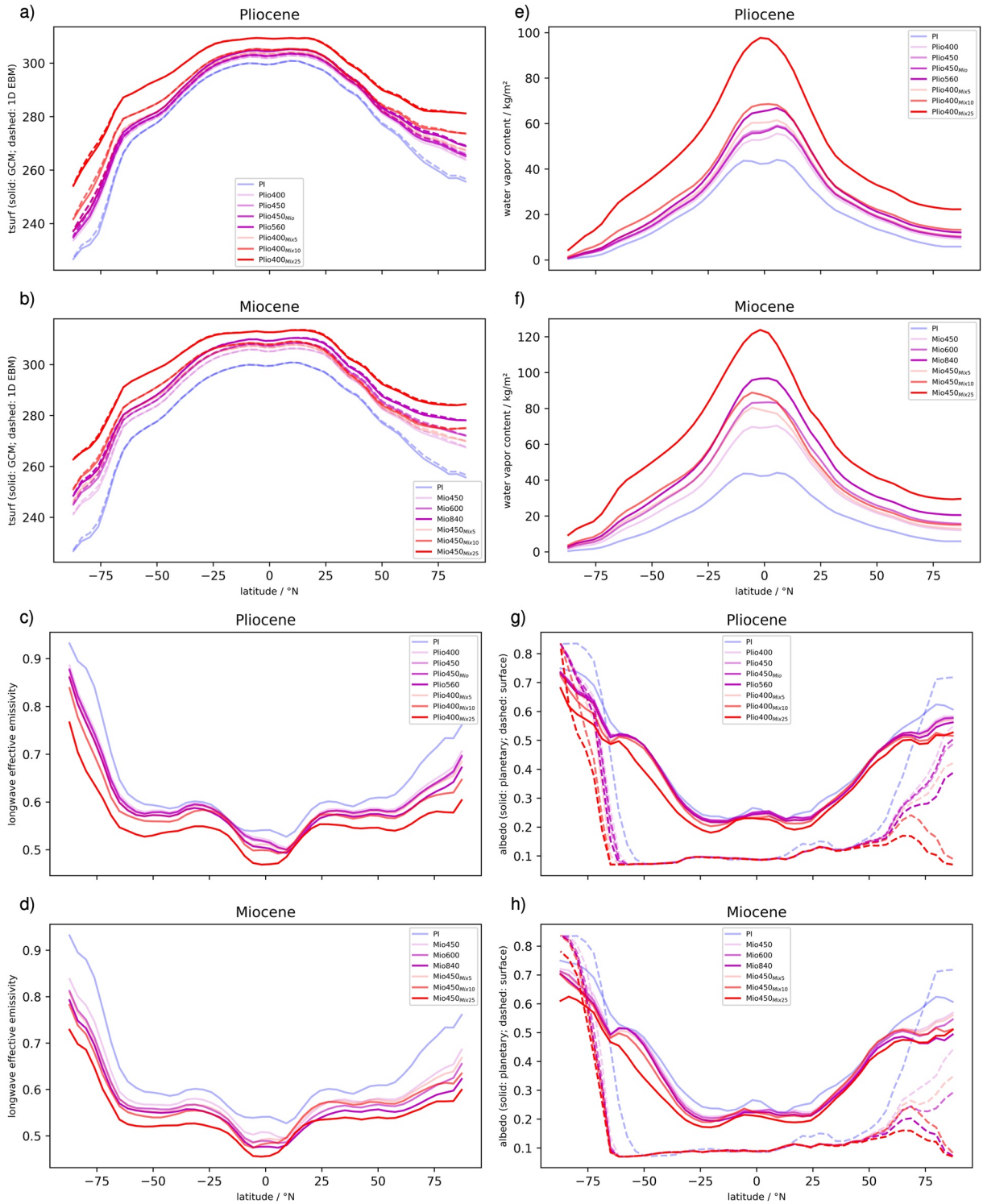

Figure 17. Meridional profile of contributors (c, d, e, f, g, h) to temperature change in simulations of the Pliocene and Miocene (a, b) with standard and enhanced vertical mixing. Zonal mean profiles of the surface temperature (K) as diagnosed from the GCM (solid lines) and the one-dimensional energy balance model (1D-EBM, dashed lines) for Pliocene (a) and Miocene (b); vertically integrated water vapor content of the air column in the GCM for Pliocene (e) and Miocene (f); effective longwave emissivity diagnosed from the 1D-EBM for Pliocene (c) and Miocene (d); surface albedo, simulated by the GCM (dashed), and planetary albedo, diagnosed from the 1D-EBM (solid), for Pliocene (g) and Miocene (h).

Table 3
Global Average Climate Metrics Computed From the Climate Model (GCM) and Diagnosed From Zero-Dimensional (0D-EBM) and One-Dimensional (1D-EBM) Energy Balance Models for Various Simulations of Pliocene and Miocene Climate With Both Standard and Enhanced Vertical Mixing Parameters

Simulation	$T_{S,GCM}$	$T_{S,0D}$	$T_{S,1D}$	α_{GCM}	α_{0D}	ε_{0D}	$RLW_{S,u}$	ccov	vap	imb
PI	287.48	289.30	287.73	0.17	0.32	0.59	−394.34	0.62	25.15	1.73
Plio400	290.68	292.32	290.90	0.14	0.31	0.57	−410.82	0.60	30.89	1.89
$Plio400_{Mix5}$	292.27	293.88	292.46	0.13	0.30	0.56	−419.31	0.59	34.17	2.11
$Plio400_{Mix10}$	294.29	295.85	294.47	0.12	0.30	0.55	−430.29	0.58	38.51	2.32
$Plio400_{Mix25}$	300.05	301.56	300.20	0.11	0.27	0.53	−463.70	0.54	56.73	2.82
Plio450	291.58	293.20	291.79	0.14	0.31	0.56	−415.73	0.60	32.85	1.91
$Plio450_{Mio}$	291.38	293.00	291.59	0.14	0.31	0.57	−414.64	0.60	32.45	1.91
Mio450	294.09	295.50	294.31	0.13	0.30	0.56	−430.46	0.57	39.43	1.10
$Mio450_{Mix5}$	295.92	297.27	296.13	0.13	0.29	0.55	−440.69	0.56	44.17	1.21
$Mio450_{Mix10}$	297.69	299.04	297.89	0.12	0.28	0.54	−450.80	0.55	49.22	1.48
$Mio450_{Mix25}$	303.87	305.22	304.06	0.12	0.26	0.52	−488.15	0.51	72.42	2.11
Mio600	296.51	297.91	296.74	0.13	0.29	0.54	−444.45	0.56	46.70	1.25
Mio840	298.73	300.13	298.96	0.12	0.28	0.53	−457.58	0.55	54.00	1.40

Note. Shown are surface skin temperature of the GCM ($T_{S,GCM}$, K), surface temperature diagnosed from the 0D-EBM ($T_{S,0D}$, K) and 1d-EBM ($T_{S,1D}$, K), surface albedo of the GCM (α_{GCM}), planetary albedo (α_{0D}), and effective longwave emissivity (ε_{0D}) diagnosed from the 0D-EBM, as well as the GCM climate variables upward longwave radiation at the Earth's surface ($RLW_{S,u}$, W/m^2; upward negative), total cloud cover (ccov, fractional), vertically integrated water vapor content of the atmosphere (vap, kg/m^2), and top of the atmosphere radiative imbalance (imb, W/m^2).

from incoming shortwave radiation and longwave and shortwave net fluxes at the top of the atmosphere (one-dimensional case).

We solve the one-dimensional EBM for SAT and find that there is good agreement (to a few tenths of a Kelvin) with the global average SAT of the GCM (Table 3). Discrepancies between simulated GCM and diagnosed one-dimensional EBM SAT are largely limited to high latitudes (Figures 17a and 17b). The increase in zonal mean temperatures, that is strongly biased toward high latitudes, is accompanied by substantially increased water vapor content in the atmosphere (Figures 17e and 17f). As quantified by the Clausius-Clapeyron equation, the ability of air to store water vapor is increased at higher temperatures. The strong nonlinearity of this effect is highlighted in our simulations in the tropics and for simulations with higher mixing parameters and higher CO_2 concentrations. The strong peak of water vapor at low latitudes is accompanied by a pronounced minimum of effective emissivity (Figures 17c and 17d). Amplified warming at high latitudes for simulations with increased CO_2 and enhanced vertical mixing is related to a dampening of emissivity. The effect is pronounced in particular at high NH latitudes. Planetary albedo is reduced for warmer climates (related to both CO_2 and enhanced vertical mixing), again with a strong bias toward high latitudes (Figures 17g and 17h). The change of surface albedo as simulated by the GCM is extreme at high latitudes for high CO_2 values and enhanced vertical mixing, where in some simulations the albedo reaches a clear minimum in the NH (Figures 17g and 17h). Overall, there is a clear inverse relation between increased global average SAT due to CO_2 and enhanced mixing on the one hand, and reduced surface albedo, planetary albedo, effective emissivity, and cloud cover on the other hand. Similarly, increased SAT goes in hand with strongly increased water vapor content of the atmosphere. In comparison to PI, we find up to a doubling of water vapor content in the atmosphere in the Miocene simulation with high CO_2, and nearly a tripling in the Miocene simulation with enhanced vertical mixing. The overall upward flux of longwave radiation from the surface increases with the global average SAT (Table 3). All these results show that enhanced CO_2 and vertical mixing strongly amplify differences in the radiative balance with regard to PI from conditions apparent in the reference Pliocene and Miocene climate states (Plio400 and Mio450).

While surface temperature, as diagnosed from the zero-dimensional EBM, is offset in relation to that predicted by the GCM (by 1–2 K), the EBM's simplicity allows us to quantify the global contribution of both planetary albedo and effective emissivity to the overall warming in the various simulations (Figure 18). For the reference states

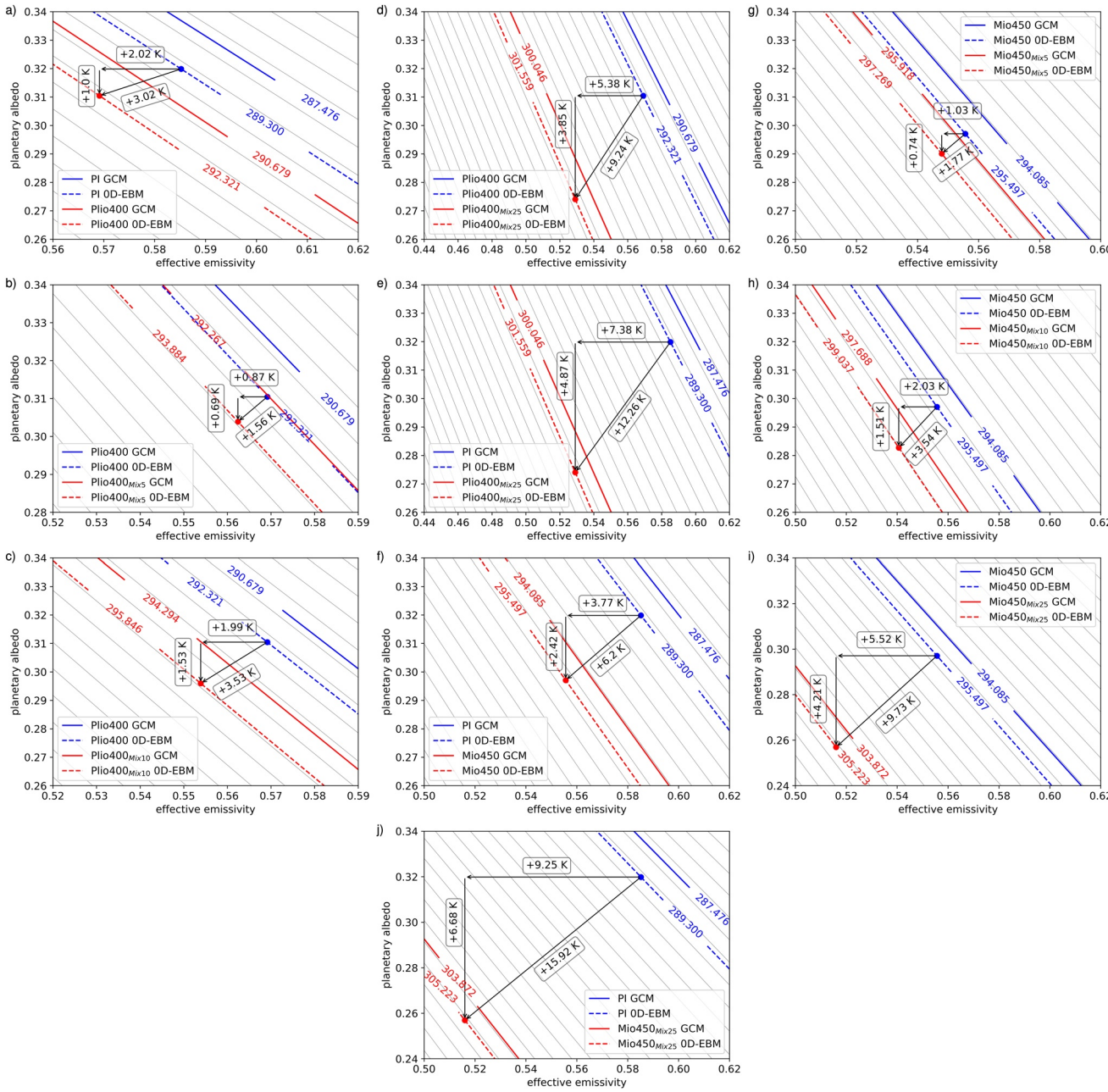

Figure 18. Quantification of contributions of planetary albedo and effective longwave emissivity to surface temperature differences between specific simulation pairs. We show results for surface temperature anomalies of Pliocene (a, b, c, d, e) and Miocene (f, g, h, i, j) simulations at the example of the reference climate states of Pliocene (Plio400, a) and Miocene (Mio450, b) as well as simulations with enhanced vertical mixing for Pliocene (b, c, d, e) and Miocene (g, h, i, j). Simulated (GCM) isotherms shown by thick continuous lines, diagnosed (0D-EBM) isotherms shown by thick dashed lines. In each of the plots, the cooler of the two simulations is shown in blue, whereas the warmer simulation is indicated in red. Isotherms in the phase space of planetary albedo and effective longwave emissivity are illustrated by thin black lines with a spacing of 1 K. Arrows quantify the individual contributions of effective shortwave emissivity (horizontal arrows) and planetary albedo (vertical arrows) to the diagnosed total temperature change (hypotenuse of the right-angled triangle).

of Pliocene (Plio400) and Miocene (Mio450), i.e., for simulations where temperature anomalies with respect to PI are driven by a combination of geographic boundary conditions and CO_2, we find a relatively clear separation of warming contributors. There, warming with respect to PI is dominated by the contribution from the effective emissivity (Figures 18a and 18f). About two-thirds (2.02 and 3.77 K, respectively) of the overall temperature anomaly with respect to PI (3.02 and 6.2 K, respectively) are due to emissivity (e.g., 67% for the simulation pair PI and Plio400), whereas the remainder is caused by reduced planetary albedo. There are variations to this

ratio across the simulation ensemble. For temperature anomalies between simulations that are purely driven by differences in CO_2, the ratio is biased toward lower contributions from planetary albedo (e.g., 26% in the case of simulations Mio450 and Mio600, not shown). Simulations, where the temperature difference is driven by enhanced vertical mixing alone, are on the other hand characterized by warming effects that are more equally contributed by planetary albedo and effective emissivity (e.g., a contribution by planetary albedo of 44% for simulation pairs Plio400/Plio400$_{Mix5}$ and of 42% for Mio450/Mio450$_{Mix5}$, Figures 18b and 18g). The drivers behind different contributions of planetary albedo and effective emissivity to the overall temperature change in the model appear complex. The fact that the overall strength of the climate anomaly differs in between simulations hampers a direct comparison of individual climate variables' effects. Yet, there are some hints (Figure S9 in Supporting Information S1) that the finding may be related to different reaction of clouds, water vapor, and surface albedo to the imposed climate forcing. Simulations driven by a strong increase in vertical mixing show a comparably strong drop in low latitude to midlatitude cloud cover. In particular in the latitude band 25°S to 60°S, cloud cover change appears linked to a pronounced reduction of planetary albedo. Surface albedo is, especially for the Pliocene, more strongly reducing at high latitudes if there is enhanced vertical mixing. There, planetary albedo changes correspondingly are more pronounced in simulations forced by mixing. Yet, it must be acknowledged that also emissivity change is biased toward high latitudes in mixing driven simulations as water vapor increase is particularly strong there. Latitude-dependency of the overall potence of planetary albedo or effective emissivity in shaping the global temperature signal is key.

Furthermore, we analyze the anomalous heat flux between ocean and atmosphere (Figure 19) highlighting changes in the spatial distribution of regions where the ocean acts as a net-energy sink versus net-energy source to the atmosphere. Regional shifts of atmosphere-ocean heat balance are linked to large-scale changes of the annual mean mixed layer depth (Figure S8 in Supporting Information S1) and poleward ocean heat transport by thermohaline or wind-driven circulation, albeit not linearly. It should be noted that the global ocean is not fully in equilibrium, and the degree of disequilibrium at the top of the atmosphere is larger in simulations with enhanced vertical mixing—up to 2.82 W/m^2 in Pliocene and 2.11 W/m^2 in Miocene mixing simulations, compared to around 1–2 W/m^2 in simulations with standard vertical mixing (Table 3). This is related to the ocean's more robust intake of heat from the atmosphere in model setups with enhanced mixing (Figure 19). Yet, there are lines of evidence highlighting that in simulations with enhanced vertical mixing the spatial distribution of ocean regions, that act as net sources and sinks of energy, depends on the background climate state (Pliocene versus Miocene). In the Pliocene model setup, enhanced vertical mixing leads to large parts of the North Atlantic Ocean to become net sources of heat to the atmosphere, whereas at low latitudes the ocean net heat sink is increased. For the Miocene, on the other hand, the picture is less clear (Figure 19). There, the effect of enhanced vertical mixing is more toward generating a bipolar pattern between Atlantic and Pacific Ocean basins. While the Miocene Atlantic Ocean takes up more heat from the atmosphere as a result of enhanced vertical mixing, in particular for midlatitude to high latitude, the North Pacific and the Southern Ocean become more dominant sources of heat to the atmosphere. Modified atmosphere-ocean heat exchange is a result of reorganized meridional circulation patterns and the related redirection of ocean heat transport as well as reduced vertical stratification in the ocean. This finding is linked to the evidence that deep-water formation regions are predominantly present in the Pliocene North Atlantic Ocean at enhanced vertical mixing. In contrast, for Miocene setups with enhanced vertical mixing, the mixed layer thickness increases particularly in the SH and in the North Pacific Ocean (Figure S8 in Supporting Information S1). This finding is consistent with Thomas et al. (2014) indicating that amplifying mixing values in their model strengthen sinking at both the northern and southern end of the Pacific.

5. Discussion and Conclusions

We performed sensitivity experiments with respect to atmospheric CO_2 and vertical mixing for mid-Miocene (Hossain et al., 2020; Stärz et al., 2017) and mid-Pliocene (Samakinwa et al., 2020; Stepanek et al., 2020) model set ups. We study these time intervals to explore the effect of atmospheric CO_2 and ocean mixing on surface and deep ocean temperatures. We find that the warming effects due to atmospheric CO_2 and increased vertical mixing have different contributions from surface albedo and effective emissivity. Our methodology of attributing components of simulated warming to different physical mechanisms in the climate system follows the work by Heinemann et al. (2009) and Lunt et al. (2012), who studied warming components of the Paleocene/Eocene and

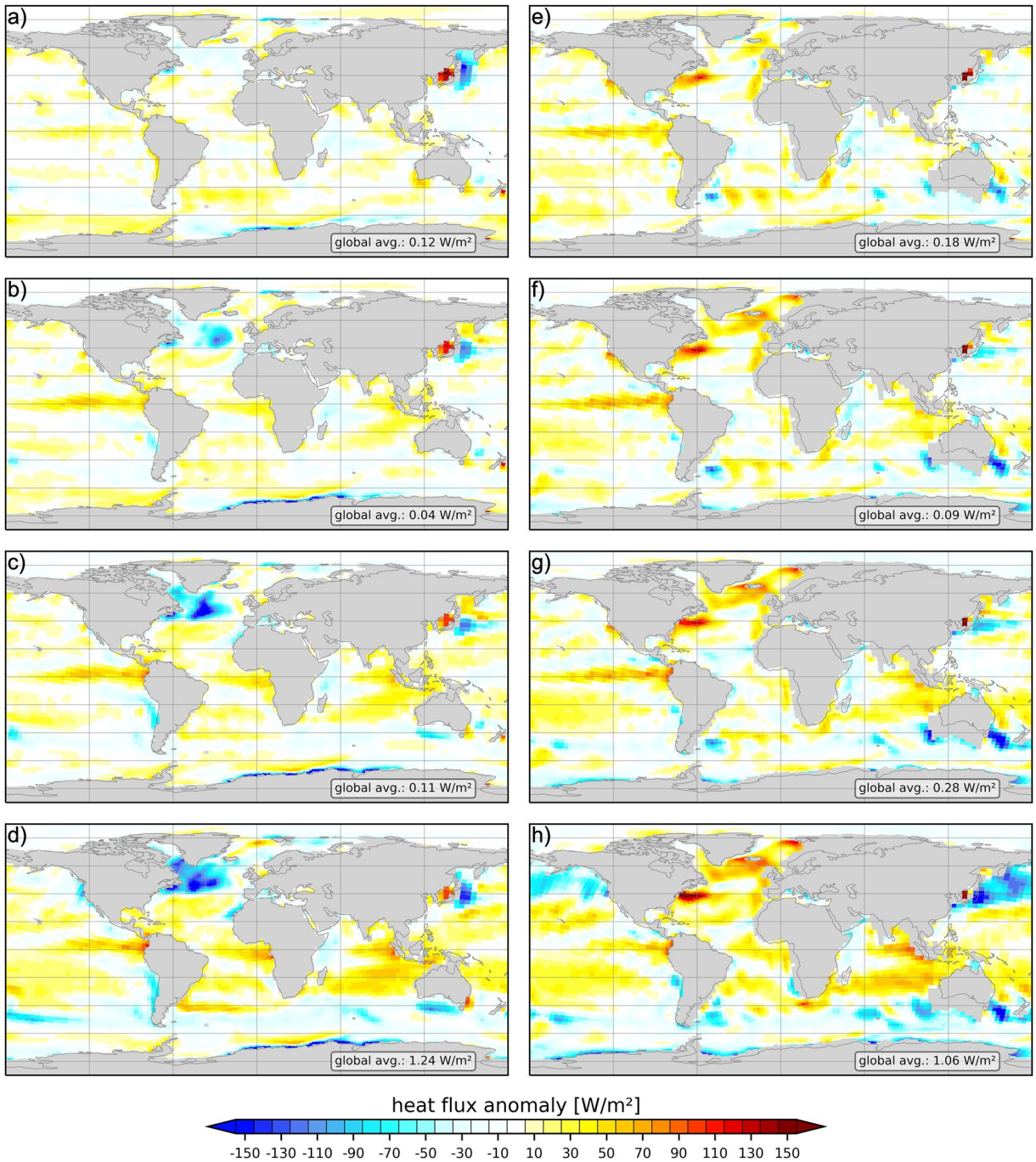

Figure 19. Anomaly of annual average heat flux between ocean and atmosphere with respect to preindustrial (PI). Shown are simulations for Pliocene (a, b, c, d) with 400 ppmv of carbon dioxide and Miocene (e, f, g, h) with 450 ppmv of carbon dioxide. From top to bottom, the panel shows simulations with increasing vertical mixing: standard vertical mixing parameters (a, e; Plio400, Mio450), 5 times enhanced vertical mixing (b, f; $Plio400_{Mix5}$, $Mio450_{Mix5}$), 10 times enhanced vertical mixing (c, g; $Plio400_{Mix10}$, $Mio450_{Mix10}$), and 25 times enhanced vertical mixing (d, h; $Plio400_{Mix25}$, $Mio450_{Mix25}$). Positive values indicate increased heat flux from the atmosphere to the ocean in comparison to PI. In the lower right of each panel, global average anomalies are displayed.

of the Pliocene, respectively. For CO_2, the predominant effect is due to a smaller effective emissivity, in contrast to the mixing experiments where the albedo and emissivity share about equal contributions.

The Miocene is a period of sustained global warmth, and it is useful to discuss the model runs in light of available data. Reconstructions suggest that SSTs were up to 10°C warmer than present at high southern latitudes (Shevenell et al., 2004) and that deep ocean temperatures were 5–10°C warmer than today (Lear et al., 2000, 2015).

Even in the colder late Miocene (11.6-5.33 Ma), SSTs still range between 10 and 15°C warmer at high latitudes, 5–10°C warmer in the midlatitudes, and 2–4°C warmer in the tropics compared to today (Herbert et al., 2016; La Riviere et al., 2012). Temperatures in the deep ocean were ∼4°C warmer than present (La Riviere et al., 2012).

The Miocene experiment with the standard mixing coefficient and an atmospheric CO_2 concentration of 600 ppm provides a ∼9°C warmer global-mean temperature relative to PI, and captures some basic large-scale temperature characteristics of the MMCO with respect to SST and deep-water temperature. In case of increased vertical mixing, surface temperature anomalies and deep-sea temperatures show a significant warming of up to 5–10°C and an Arctic temperature anomaly of >12°C. In the vertical mixing experiments, the surface albedo and emissivity are decreased, and tropical heat uptake by the ocean is enhanced. Most pronounced changes are detected at high latitudes. When the sea ice disappears, the summer heating can reach the surface water and can store heat energy in the subsurface. The high CO_2 sensitivity experiment with 840 ppmv during the mid-Miocene produces a sea ice-free Arctic Ocean. In our experiments, we see that the Arctic warming is strongest for high CO_2, consistent with the finding in the context of the Eocene that the degree of polar amplification increases as a function of CO_2 concentrations (e.g., Huber & Caballero, 2011; Zhu et al., 2019).

In the Pliocene simulations, the influence of vertical mixing and CO_2 is less important, especially for the deeper levels in the ocean. The heat uptake and changes in the mixed layer depth are different for the Miocene and Pliocene simulations, indicating that the climate background plays an important role. Due to changes in the mixed layer depth in the Southern Ocean, even a relatively small increase in vertical mixing causes sea ice retreat similar to that induced by the most extreme CO_2 concentration considered in the Pliocene.

There is an influence of gateways and ocean geometry for the deep-water hydrography and circulation during the Miocene. During the late Miocene, deep water in the North Atlantic Ocean is reconstructed to be ∼4°C warmer than in the Pleistocene (Lear et al., 2003). Previously, we interpreted this as an already established meridional overturning circulation despite an open Central American Seaway at this time (Lohmann et al., 2015). However, as an alternative hypothesis, and in the light of our results, such drastic temperature increase may be linked to an enhanced heat uptake in the North Atlantic during that time. Gateway configurations like the Greenland-Iceland-Scotland Ridge have a smaller imprint on the deep ocean temperature changes (e.g., Stärz et al., 2017). However, the geometry of the ocean basin could also affect mixing, and thus, the carbon cycle (de Boer & Hogg, 2014; Munk & Wunsch, 1998). In our experiments, we find a different pattern of heat uptake for the Miocene and Pliocene conditions, that are related to strong reorganization of meridional heat transport and global meridional overturning circulation in the ocean. Enhanced vertical mixing acts as an intensifier for the meridional heat pump. Furthermore, the extent of changes in the heat transport is in simulations with enhanced vertical mixing controlled by the geographic setup, Pliocene versus Miocene. For the Pliocene, we see an additional tropical heat uptake and a release in the northern North Atlantic. For the Miocene the Atlantic acts more as an energy sink, even in the North Atlantic, and additional heat release is evident in the northern North Pacific (this effect is strongest for large mixing coefficients). This is due to a pronounced deep-water formation in this area with increased mixed layer. Interestingly, this is consistent with the combined data-model study of Thomas et al. (2014) indicating enhanced circulation rates in the Pacific Ocean with resulting Nd isotope distributions.

On glacial-interglacial time scales, changes in ocean heat uptake have been reconstructed using measurements of noble gases in modern or ancient air (Bereiter et al., 2018; Ritz et al., 2011). Changes in the abundance of gases in the atmosphere respond to whole ocean warming through the temperature dependence of gas solubility in seawater. It is interesting to explore if proxy approaches can be used to reconstruct the ocean mixing. When the ocean warms, the solubility of carbon drops, and the amount of gas lost by the ocean may be quantified by complementary changes in the marine carbon cycle and paleoceanographic tracers.

So far we have not discussed the potential processes for Pliocene or Miocene mixing rate changes. Suggested possibilities range from tidal dissipation resulting from the changes in continental geography (de Boer & Hogg, 2014; Green, 2010; Green & Huber, 2013; Wilmes et al., 2019), increases in tropical wind forcing (Fedorov et al., 2010; Korty et al., 2008; Nilsson, 1995; Sriver et al., 2010; Wijesekera & Gregg, 1996), to higher than modern values of the geothermal heat flux (Emile-Geay & Madec, 2009). The enhanced mixing in warmer climates due to tropical cyclones has been studied extensively (e.g., Emanuel, 2001; Fedorov et al., 2010; Jansen & Ferrari, 2009; Korty et al., 2017; Sriver, 2013; Sriver & Huber, 2010; Sriver et al., 2010; Vincent et al., 2013). Their effect can influence regions of the Earth that are distant from the tropics, as, e.g., through dissipative equatorial waves (Sriver

et al., 2013). Scott and Marotzke (2002) showed that the mixing in the thermocline (where stratification is strongest) has a much larger effect than abyssal mixing which is largely stirring already blended cold water together. With SST increase, the intensity of tropical cyclones can increase which would be highly transient, intense, spatially localized, and positioned in the upper ocean (Emanuel, 2001, and references therein). Boos et al. (2004) advanced the finding of Scott and Marotzke (2002) by showing that any increase in potential intensity that is sporadic in time can affect the ocean if it is strong enough. This is important because actual measurements indicate that observed diapycnal mixing is slightly weaker than in models (e.g., Jing et al., 2016), but that episodic blasts of higher mixing may raise the effective "average" mixing above the low values.

Another possibility of changes in vertical mixing is due to tides (e.g., Green et al., 2017; Haigh et al., 2019). It is possible that some combination of all of these processes contributed to enhanced abyssal mixing. Using a tide model, it has been demonstrated that the rate of energy dissipation is strongly affected by the ocean continental geometry and sea floor topography (Haigh et al., 2019; Lambeck & Runcorn, 1977). The upper ocean mixing processes are largely limited to the upper tens of meters which are only partly understood (Smyth & Moum, 2012) and are highly parameterized in large-scale ocean models. The Kelvin-Helmholtz instability is critical for ocean mixing and remains a first-order problem in oceanography (Smyth & Moum, 2012). Indeed, the uncertainty in tidal dissipation is high. Paleotides depend on the geometry and the presence/absence of continental shelf seas affecting the resonance between the oceans and paleotides (e.g., Egbert et al., 2004; Green, 2010; Schmittner et al., 2015; Wilmes & Green, 2014). Such resonance can reduce the damping of the M2 tide and produce tidal amplification (Egbert et al., 2004; Green, 2010). The vertical mixing is a critical parameter on the large-scale circulation. Vallis (2000) emphasized the effects of geometry and diffusion, and Saenko et al. (2012) emphasized more specifically the combined effect of tidally and eddy-driven diapycnal mixing, indicating how sensitive these critical processes are for climate and climate change scenarios (Brierley et al., 2010).

Wang et al. (2019) elaborate that mixing induced by nonbreaking surface waves can considerably improve the ocean temperatures at the subsurface, bringing heat to deeper levels in ocean models. Parameterizations of such important processes are under construction to be applied for paleoclimate research. Other mixing processes by vertical plankton movement have been proposed to affect global ocean circulation to a degree comparable to winds and tides (Wilhelmus & Dabiri, 2014). The effect is, however, unknown and estimated to be low (Visser, 2007) because the biologically induced turbulence is limited to the scale of the individual animals involved. However, recent studies (Houghton et al., 2018; Tarling & Thorpe, 2017; Wang & Ardekani, 2015) emphasize that a collective vertical migration of swimmers (e.g., undergoing the diurnal cycle) generates eddies even in the presence of a strong density stratification relative to typical values observed in the ocean. The extent of biogenic mixing depends on the swimming mode of organisms during their migration, where the mixing efficiency induced by vertical swimming can be 2 orders of magnitude larger than that induced by horizontal swimming (Wang & Ardekani, 2015). However, we would like to emphasize that our work only presents a sensitivity study. Our simulations are not able to realistically represent the vertical mixing. Our aim is to approach the possible solutions for the Pliocene and Miocene under changed sensitive ocean parameters.

For the current warming, the deep-ocean heat uptake occurs mainly in the North Atlantic and the Southern Ocean (Gregory, 2000; Raper et al., 2002), a process that strongly depends on the description of the isopycnal mixing (e.g., Wiebe & Weaver, 1999). As the climate sensitivity depends on the mixing, the link between ocean temperature and CO_2 can depend on climate states. It has been speculated that the thermocline shoaled during the Pliocene, making the surface water more sensitive to CO_2 (Ford et al., 2015; La Riviere et al., 2012). Consistent with this inference, atmospheric thermal gradients were reduced throughout the Miocene and strongly steepened in the Pliocene (Utescher et al., 2017). As a consequence, one shall evaluate the change in climate sensitivity depending on the thermocline dynamics. It has been shown that climate sensitivity might have to be recalibrated for the past (Lohmann, 2020). Our results suggest that a retuning of models to simulate warm climates of the geological past should not be ruled out. We propose to test our mixing hypothesis with seasonal paleoclimate data, since increased mixing is expected to result in a deeper ocean mixed layer and dampened seasonality. Constraints could come from more paleoclimate reconstructions of vertical ocean temperature, SSTs, sea ice, and tracer distribution in the ocean. Of course, enhanced vertical mixing may not be sufficient to fully explain thermocline changes or reduced seasonality in past warm climates. Consequently, future research should test the mixing hypotheses further, potentially identifying fingerprints in the climate that are unique to vertical mixing.

Data Availability Statement

The code of version COSMOS-landveg r2413 (2009) is available upon request from the MPI (https://www.mpi-met.mpg.de/en/science/models/availability-licenses). Data of the final results are available through PANGAEA (Lohmann et al., 2021).

Acknowledgments
This work was institutionally funded at AWI via the research program PACES-II of the Helmholtz Association. All simulations were performed at the AWI Computing Center. Gregor Knorr and Christian Stepanek acknowledge funding by the Helmholtz Climate Initiative REKLIM. Thanks go to Michael Stärz and Madlene Pfeiffer for earlier sensitivity experiments and setups. Thanks go to Wilfried Jokat, numerous colleagues as well as persons in DeepMIP and PlioMIP for their efforts toward provision of robust paleogeography and model forcing. We are grateful to three anonymous referees and the editor who provided valuable comments improving the manuscript. We thank the Max Planck Institute for Meteorology (MPI) in Hamburg, Germany for providing the model code. Open access funding enabled and organized by Projekt DEAL.

References

Abbot, D. S., & Tziperman, E. (2008). A high-latitude convective cloud feedback and equable climates. *Quarterly Journal of the Royal Meteorological Society*, *134*(630), 165–185. https://doi.org/10.1002/qj.211

Barker, S., & Knorr, G. (2007). Antarctic climate signature in the Greenland ice core record. *Proceedings of the National Academy of Sciences of the United States of America*, *104*, 17278–17282. https://doi.org/10.1073/pnas.0708494104

Barron, E. J. (1987). Eocene equator-to-pole surface ocean temperatures: A significant climate problem? *Paleoceanography*, *2*, 729–739. https://doi.org/10.1029/PA002i006p00729

Bereiter, B., Shackleton, S., Baggenstos, D., Kawamura, K., & Severinghaus, J. (2018). Mean global ocean temperatures during the last glacial transition. *Nature*, *553*, 39–44. https://doi.org/10.1038/nature25152

Berner, R. A. (1992). Palaeo-CO_2 and climate. *Nature*, *358*, 114. https://doi.org/10.1038/358114a0

Bice, K., Scotese, C., Seidov, D., & Barron, E. (2000). Quantifying the role of geographic change in Cenozoic Ocean heat transport using uncoupled atmosphere and ocean models. *Palaeogeography, Palaeoclimatology, Palaeoecology*, *161*, 295–310. https://doi.org/10.1016/S0031-0182(00)00072-9

Boos, W. R., Scott, J. R., & Emanuel, K. A. (2004). Transient diapycnal mixing and the meridional overturning circulation. *Journal of Physical Oceanography*, *34*(1), 334–341. https://doi.org/10.1175/1520-0485(2004)034<0334:tdmatm>2.0.co;2

Braconnot, P., & Kageyama, M. (2015). Shortwave forcing and feedbacks in last glacial maximum and mid-Holocene PMIP3 simulations. *Philosphical Transactions of the Royal Society A*, *373*, 20140424. https://doi.org/10.1098/rsta.2014.0424

Bradshaw, C., Lunt, D., Flecker, R., Salzmann, U., Pound, M., Haywood, A., & Eronen, J. (2012). The relative roles of CO_2 and palaeogeography in determining late Miocene climate: Results from a terrestrial model-data comparison. *Climate of the Past*, *8*(2), 715–786. https://doi.org/10.5194/cp-8-1257-2012

Brierley, C. M., Collins, M., & Thorpe, A. J. (2010). The impact of perturbations to ocean-model parameters on climate and climate change in a coupled model. *Climate Dynamics*, *34*, 325–343. https://doi.org/10.1007/s00382-008-0486-3

Brierley, C. M., & Fedorov, A. V. (2016). Comparing the impacts of Miocene-Pliocene changes in inter-ocean gateways on climate: Central American seaway, Bering Strait, and Indonesia. *Earth and Planetary Science Letters*, *444*, 116–130. https://doi.org/10.1016/j.epsl.2016.03.010

Brovkin, V., Raddatz, T., Reick, C. H., Claussen, M., & Gayler, V. (2009). Global biogeophysical interactions between forest and climate. *Geophysical Research Letters*, *36*, L07405. https://doi.org/10.1029/2009GL037543

Burls, N. J., Bradshaw, C. D., De Boer, A. M., Herold, N., Huber, M., Pound, M., et al. (2021). Simulating Miocene warmth: Insights from an opportunistic multi-model ensemble (MioMIP1). *Paleoceanography and Paleoclimatology*, *36*, e2020PA004054. https://doi.org/10.1029/2020PA004054

Burls, N. J., & Fedorov, A. V. (2014). Simulating Pliocene warmth and a permanent El Niño-like state: The role of cloud albedo. *Paleoceanography*, *29*, 893–910. https://doi.org/10.1002/2014PA002644

Butt, F. A., Drange, H., Elverhøi, A., Otterå, O. H., & Solheim, A. (2002). Modelling late Cenozoic isostatic elevation changes in the Barents Sea and their implications for oceanic and climatic regimes: Preliminary results. *Quaternary Science Reviews*, *21*, 1643–1660. https://doi.org/10.1016/S0277-3791(02)00018-5

Butzin, M., Lohmann, G., & Bickert, T. (2011). Miocene ocean circulation inferred from marine carbon cycle modeling combined with benthic isotope records. *Paleoceanography*, *26*, PA1203. https://doi.org/10.1029/2009PA001901

Coxall, H. K., Wilson, P. A., Pälike, H., Lear, C. H., & Backman, J. (2005). Rapid stepwise onset of Antarctic glaciation and deeper calcite compensation in the Pacific Ocean. *Nature*, *433*, 53–57. https://doi.org/10.1038/nature03135

Cristini, L., Grosfeld, K., Butzin, M., & Lohmann, G. (2012). Influence of the opening of the drake passage on the Cenozoic Antarctic ice sheet: A modeling approach. *Palaeogeography, Palaeoclimatology, Palaeoecology*, *339–341*, 66–73. https://doi.org/10.1016/j.palaeo.2012.04.023

Cronin, T. W., & Tziperman, E. (2015). Low clouds suppress Arctic air formation and amplify high-latitude continental winter warming. *Proceedings of the National Academy of Sciences of the United States of America*, *112*(37), 11490–11495. https://doi.org/10.1073/pnas.1510937112

Crowley, T. J. (2000). Carbon dioxide and Phanerozoic climate: An overview. In B. T. Huber, K. G. MacLeod, & S. L. Wing (Eds.), *Warm climates in Earth history* (pp. 425–444). Cambridge University Press.

de Boer, A. M., & Hogg, A. M. (2014). Control of the glacial carbon budget by topographically induced mixing. *Geophysical Research Letters*, *41*, 4277–4284. https://doi.org/10.1002/2014GL059963

DeConto, R. M., & Pollard, D. (2003). A coupled climate-ice sheet modeling approach to the early Cenozoic history of the Antarctic ice sheet. *Palaeogeography, Palaeoclimatology, Palaeoecology*, *198*, 39–52. https://doi.org/10.1016/S0031-0182(03)00393-6

de Nooijer, W., Zhang, Q., Li, Q., Zhang, Q., Li, X., Zhang, Z., et al. (2020). Evaluation of Arctic warming in mid-Pliocene climate simulations. *Climate of the Past*, *16*, 2325–2341. https://doi.org/10.5194/cp-16-2325-2020

Donnadieu, Y., Godderis, Y., Pierrehumbert, R., Dromart, G., Fluteau, F., & Jacob, R. (2006). A GEOCLIM simulation of climatic and biogeochemical consequences of Pangea breakup. *Geochemistry, Geophysics, Geosystems*, *7*, Q11019. https://doi.org/10.1029/2006GC001278

Dowsett, H., Barron, J., & Poore, R. (1996). Middle Pliocene Sea surface temperatures: A global reconstruction. *Marine Micropaleontology*, *27*, 13–25. https://doi.org/10.1016/0377-8398(95)00050-X

Dowsett, H., Dolan, A., Rowley, D., Mocha, R., Forte, A. M., Mitrovica, J. X., et al. (2016). The PRISM4 (mid-Piacenzian) palaeoenvironmental reconstruction. *Climate of the. Past*, *12*, 1519–1538. https://doi.org/10.5194/cp-12-1519-2016

Dowsett, H. J., & Caballero Gill, R. P. (2010). Pliocene climate. *Stratigraphy*, *7*, 105–110.

Dowsett, H. J., Foley, K. M., Stoll, D. K., Chandler, M. A., Sohl, L. E., Bentsen, M., et al. (2013). Sea surface temperature of the mid-Piacenzian ocean: A data-model comparison. *Scientific Reports*, *3*, 2013. https://doi.org/10.1038/srep02013

Dowsett, H. J., Robinson, M. M., Stoll, D. K., Foley, K. M., Johnson, A. L. A., Williams, M., & Riesselman, C. R. (2013). The PRISM (Pliocene palaeoclimate) reconstruction: Time for a paradigm shift. *Philosophical Transactions of the Royal Society A*, *371*, 20120524. https://doi.org/10.1098/rsta.2012.0524

Drijfhout, S., van Oldenborgh, G. J., & Cimatoribus, A. (2012). Is a decline of AMOC causing the warming Hole above the north Atlantic in observed and modeled warming patterns? *Journal of Climate*, *25*(24), 8373–83791. https://doi.org/10.1175/jcli-d-12-00490.1

Egbert, G. D., Ray, R. D., & Bills, B. G. (2004). Numerical modeling of the global semidiurnal tide in the present day and in the last glacial maximum. *Journal of Geophysical Research*, *109*, C03003. https://doi.org/10.1029/2003JC001973

Ehlers, B.-M., & Jokat, W. (2013). Paleo-bathymetry of the northern North Atlantic and consequences for the opening of the Fram strait. *Marine Geophysical Researches*, *34*, 25–43. https://doi.org/10.1007/s11001-013-9165-9

Emanuel, K. (2001). Contribution of tropical cyclones to meridional heat transport by the oceans. *Journal of Geophysical Research*, *106*(D14), 14771–14781. https://doi.org/10.1029/2000JD900641

Emile-Geay, J., & Madec, G. (2009). Geothermal heating, diapycnal mixing and the abyssal circulation. *Ocean Science*, *5*, 203–217. https://doi.org/10.5194/os-5-203-2009

Fedorov, A., Brierley, C., & Emanuel, K. (2010). Tropical cyclones and permanent El Niño in the early Pliocene epoch. *Nature*, *463*, 1066–1070. https://doi.org/10.1038/nature08831

Fedorov, A. V., Brierley, C. M., Lawrence, K. T., Liu, Z., Dekens, P. S., & Ravelo, A. C. (2013). Patterns and mechanisms of early Pliocene warmth. *Nature*, *496*(7443), 43–49. https://doi.org/10.1038/nature12003

Fedorov, A. V., Burls, N. J., Lawrence, K. T., & Peterson, L. C. (2015). Tightly linked zonal and meridional sea surface temperature gradients over the past five million years. *Nature Geoscience*, *8*(12), 975–980. https://doi.org/10.1038/ngeo2577

Ferrari, R., & Wunsch, C. (2009). Ocean circulation kinetic energy: Reservoirs, sources, and sinks. *Annual Review of Fluid Mechanics*, *41*, 253–282. https://doi.org/10.1146/annurev.fluid.40.111406.102139

Ford, H. L., Ravelo, A. C., Dekens, P. S., LaRiviere, J. P., & Wara, M. W. (2015). The evolution of the equatorial thermocline and the early Pliocene El Padre mean state. *Geophysical Research Letters*, *42*, 4878–4887. https://doi.org/10.1002/2015GL064215

Forest, C. E., Stone, P. H., Sokolov, A. P., Allen, M. R., & Webster, M. D. (2002). Quantifying uncertainties in climate system properties with the use of recent climate observations. *Science*, *295*(5552), 113–117. https://doi.org/10.1126/science.1064419

Forget, G., & Ferreira, D. (2019). Global ocean heat transport dominated by heat export from the tropical pacific. *Nature Geoscience*, *12*, 351–354. https://doi.org/10.1038/s41561-019-0333-7

Gierz, P., Lohmann, G., & Wei, W. (2015). Response of Atlantic overturning to future warming in a coupled atmosphere-ocean-ice sheet mode. *Geophysical Research Letters*, *42*, 6811–6818. https://doi.org/10.1002/2015GL065276

Goldner, A., Herold, N., & Huber, M. (2014). The challenge of simulating the warmth of the mid-Miocene climatic optimum in CESM1. *Climate of the Past*, *10*, 523–536. https://doi.org/10.5194/cp-10-523-2014

Green, J. A. M. (2010). Ocean tides and resonance. *Ocean Dynamics*, *60*, 1243–1253. https://doi.org/10.1007/s10236-010-0331-1

Green, J. A. M., & Huber, M. (2013). Tidal dissipation in the early Eocene and implications for ocean mixing. *Geophysical Research Letters*, *40*, 2707–2713. https://doi.org/10.1002/grl.50510

Green, J. A. M., Huber, M., Waltham, D., Buzan, J., & Wells, M. (2017). Explicitly modelled deep-time tidal dissipation and its implication for Lunar history. *Earth and Planetary Science Letters*, *461*, 46–53. https://doi.org/10.1016/j.epsl.2016.12.038

Greenwood, D., & Wing, S. (1995). Eocene continental climates and latitudinal temperature gradients. *Geology*, *23*, 1044–1048. https://doi.org/10.1130/0091-7613(1995)023<1044:eccalt>2.3.co;2

Gregory, J. M. (2000). Vertical heat transports in the ocean and their effect on time-dependent climate change. *Climate Dynamics*, *16*, 501–515. https://doi.org/10.1007/s003820000059

Griffies, S. M., Gnanadesikan, A., Dixon, K. W., Dunne, J. P., Gerdes, R., Harrison, M. J., et al. (2005). Formulation of an ocean model for global climate simulations. *Ocean Science*, *1*, 45–79. https://doi.org/10.5194/os-1-45-2005

Hagemann, S. (2002). *An improved land surface parameter dataset for global and regional climate models* (Vol. 336). Report/Max-Planck-Institut für Meteorologie. Retrieved from http://hdl.handle.net/11858/00-001M-0000-002B-539B-6

Hagemann, S., Botzet, M., Dümenil, L., & Machenhauer, B. (1999). *Derivation of global GCM boundary conditions from 1km land use satellite data* (Vol. 289). Report/Max-Planck-Institut für Meteorologie. Retrieved from http://hdl.handle.net/21.11116/0000-0000-F816-0

Hagemann, S., & Dümenil, L. (1997). A parameterization of the lateral waterflow for the global scale. *Climate Dynamics*, *14*, 17–31. https://doi.org/10.1007/s003820050205

Hagemann, S., & Gates, L. D. (2003). Improving a subgrid runoff parameterization scheme for climate models by the use of high resolution data derived from satellite observations. *Climate Dynamics*, *21*, 349–359. https://doi.org/10.1007/s00382-003-0349-x

Haigh, I. D., Pickering, M. D., Green, J. A. M., Arbic, B. K., Arns, A., Dangendorf, S., et al. (2019). The tides they are a-changin': A comprehensive review of past and future nonastronomical changes in tides, their driving mechanisms and future implications. *Reviews of Geophysics*, *57*, e2018RG000636. https://doi.org/10.1029/2018RG000636

Hay, W. W., DeConto, R. M., & Wold, C. N. (1997). Climate: Is the past the key to the future? *Geologische Rundschau*, *86*, 471–491. https://doi.org/10.1007/s005310050155

Haywood, A. M., Dowsett, H. J., Dolan, A. M., Chandler, M. A., Hunter, S. J., Lunt, D. J., et al. (2016). The Pliocene Model Intercomparison Project (PlioMIP) phase 2: Scientific objectives and experimental design. *Climate of the Past*, *12*(3), 663–675. https://doi.org/10.5194/cp-12-663-2016

Haywood, A. M., Hill, D. J., Dolan, A. M., Otto-Bliesner, B., Bragg, F., Chan, W.-L., et al. (2013). Large-scale features of Pliocene climate: Results from the Pliocene Model Intercomparison Project. *Climate of the Past*, *9*, 191–209. https://doi.org/10.5194/cp-9-191-2013

Haywood, A. M., Tindall, J. C., Dowsett, H. J., Dolan, A. M., Foley, K. M., Hunter, S. J., et al. (2020). The Pliocene Model Intercomparison Project phase 2: Large-scale climate features and climate sensitivity. *Climate of the Past*, *16*, 2095–2123. https://doi.org/10.5194/cp-16-2095-2020

Haywood, A. M., Valdes, P. J., Aze, T., Barlow, N., Burke, A., Dolan, A. M., et al. (2019). What can palaeoclimate modelling do for you? *Earth Systems and Environment*, *3*, 1–18. https://doi.org/10.1007/s41748-019-00093-1

Heede, U. K., Fedorov, A. V., & Burls, N. J. (2020). Time scales and mechanisms for the tropical Pacific response to global warming: A tug of war between the ocean thermostat and weaker walker. *Journal of Climate*, *33*, 6101–6118. https://doi.org/10.1175/jcli-d-19-0690.1

Heinemann, M., Jungclaus, J. H., & Marotzke, J. (2009). Warm Paleocene/Eocene climate as simulated in ECHAM5/MPIOM. *Climate of the Past*, *5*, 785–802. https://doi.org/10.5194/cp-5-785-2009

Herbert, T. D., Lawrence, K. T., Tzanova, A., Peterson, L. C., Caballero-Gill, R., & Kelly, C. S. (2016). Late Miocene global cooling and the rise of modern ecosystems. *Nature Geoscience*, *9*, 843–847. https://doi.org/10.1038/ngeo2813

Herold, N., Seton, M., Müller, R. D., You, Y., & Huber, M. (2008). Middle Miocene tectonic boundary conditions for use in climate models. *Geochemistry, Geophysics, Geosystems*, *9*, Q10009. https://doi.org/10.1029/2008GC002046

Hibler, W. D. (1979). A dynamic thermodynamic sea ice model. *Journal of Physical Oceanography*, *9*, 815–846. https://doi.org/10.1175/1520-0485(1979)009<0815:adtsim>2.0.co;2

Hossain, A., Knorr, G., Lohmann, G., Stärz, M., & Jokat, W. (2020). Simulated thermohaline fingerprints in response to different greenland-scotland ridge and fram strait subsidence histories. *Paleoceanography and Paleoclimatology*, *35*, e2019PA00384. https://doi.org/10.1029/2019PA003842

Houghton, I. A., Koseff, J. R., Monismith, S. G., & Dabiri, J. O. (2018). Vertically migrating swimmers generate aggregation-scale eddies in a stratified column. *Nature*, *556*, 497–500. https://doi.org/10.1038/s41586-018-0044-z

Hu, A., Meehl, G., Otto-Bliesner, B., Waelbroeck, C., Han, W., Loutre, M.-F., et al. (2010). Influence of Bering Strait flow and North Atlantic circulation on glacial sea-level changes. *Nature Geosci*, *3*, 118–121. https://doi.org/10.1038/ngeo729

Hu, A., Meehl, G. A., Han, W., Otto-Bliesner, B., Abe-Ouchi, A., & Rosenbloom, N. (2015). Effects of the Bering Strait closure on AMOC and global climate under different background climates. *Progress in Oceanography*, *132*, 174–196. https://doi.org/10.1016/j.pocean.2014.02.004

Huang, X., Staerz, M., Knorr, G., Gohl, K., & Lohmann, G. (2017). Impact of Weddell Sea shelf progradation on Antarctic bottom water formation during the Miocene. *Paleoceanography*, *32*, 304–317. https://doi.org/10.1002/2016PA002987

Huber, B. T., MacLeod, K. G., & Wing, S. L. (Eds.) (2000). *Warm climates in Earth history*. Cambridge University Press.

Huber, M., & Caballero, R. (2011). The early Eocene equable climate problem revisited. *Climate of the Past*, *7*, 603–633. https://doi.org/10.5194/cp-7-603-2011

Huber, M., & Nof, D. (2006). The ocean circulation in the Southern Hemisphere and its climatic impacts in the Eocene. *Palaeogeography, Palaeoclimatology, Palaeoecology*, *231*, 9–28. https://doi.org/10.1016/j.palaeo.2005.07.037

Huber, M., & Sloan, L. C. (2001). Heat transport, deep waters, and thermal gradients: Coupled simulation of an Eocene greenhouse climate. *Geophysical Research Letters*, *28*(18), 3481–3484. https://doi.org/10.1029/2001GL012943

IPCC. (2013). Climate change. In T. F. Stocker, D. Qin, G.-K. Plattner, M. Tignor, S. K. Allen, J. Boschung, et al. (Eds.), *The physical science basis. Contribution of working group I to the Fifth Assessment Report of the Intergovernmental Panel on Climate Change*. Cambridge University Press.

Jansen, M., & Ferrari, R. (2009). Impact of the latitudinal distribution of tropical cyclones on ocean heat transport. *Geophysical Research Letters*, *36*, L06604. https://doi.org/10.1029/2008GL036796

Jing, Z., Wu, L., Ma, X., & Chang, P. (2016). Overlooked role of mesoscale winds in powering ocean diapycnal mixing. *Scientific Reports*, *6*, 37180. https://doi.org/10.1038/srep37180

Jungclaus, J. H., Lorenz, S. J., Timmreck, C., Reick, C. H., Brovkin, V., Six, K., et al. (2010). Climate and carbon-cycle variability over the last millennium. *Climate of the Past*, *6*, 723–737. https://doi.org/10.5194/cp-6-723-2010

Kagan, B. A., & Sündermann, J. (1996). Dissipation of tidal energy, paleotides, and evolution of the Earth-Moon system. *Advances in Geophysics*, *38*, 179–266. https://doi.org/10.1016/S0065-2687(08)60021-7

Klages, J. P., Salzmann, U., Bickert, T., Hillenbrand, C.-D., Gohl, K., Kuhn, G., et al. (2020). Temperate rainforests near the south pole during peak cretaceous warmth. *Nature*, *580*, 81–86. https://doi.org/10.1038/s41586-020-2148-5

Kleidon, A. (2012). How does the Earth system generate and maintain thermodynamic disequilibrium and what does it imply for the future of the planet? *Philosophical Transactions of the Royal Society A*, *370*, 1012–1040. https://doi.org/10.1098/rsta.2011.0316

Klotz, S., Fauquettec, S., Combourieu-Nebout, N., Uhl, D., Suc, J.-P., & Mosbrugger, V. (2006). Seasonality intensification and long-term winter cooling as a part of the late Pliocene climate development. *Earth and Planetary Science Letters*, *241*(1–2), 174–187. https://doi.org/10.1016/j.epsl.2005.10.005

Knorr, G., Butzin, M., Micheels, A., & Lohmann, G. (2011). A warm Miocene climate at low atmospheric CO_2 levels. *Geophysical Research Letters*, *38*, L20701. https://doi.org/10.1029/2011GL048873

Knorr, G., & Lohmann, G. (2014). A warming climate during the Antarctic ice sheet growth at the middle Miocene transition. *Nature Geoscience*, *7*, 376–381. https://doi.org/10.1038/ngeo2119

Knutti, R., & Sedláček, J. (2012). Robustness and uncertainties in the new CMIP5 climate model projections. *Nature Climate Change*, *3*, 369–373. https://doi.org/10.1038/nclimate1716

Korty, R. L., Emanuel, A. K. A., & Scott, J. R. (2008). Tropical cyclone-induced upper-ocean mixing and climate: Application to equable climates. *Journal of Climate*, *21*, 638–654. https://doi.org/10.1175/2007JCLI1659.1

Korty, R. L., Emanuel, K. A., Huber, M., & Zamora, R. A. (2017). Tropical cyclones downscaled from simulations with very high carbon dioxide levels. *Journal of Climate*, *30*(2), 649–667. https://doi.org/10.1175/jcli-d-16-0256.1

Kürschner, W., Kvacek, Z., & Dilcher, D. (2008). The impact of Miocene atmospheric carbon dioxide fluctuations on climate and the evolution of terrestrial ecosystems. *Proceedings of the National Academy of Sciences of the United States of America*, *105*, 449–453. https://doi.org/10.1073/pnas.0708588105

Lambeck, K., & Runcorn, S. K. (1977). Tidal dissipation in the oceans: Astronomical, geophysical and oceanographic consequences. *Philosophical Transactions of the Royal Society of London-Series A: Mathematical and Physical Sciences*, *287*, 545–594. https://doi.org/10.1098/rsta.1977.0159

La Riviere, J. P., Ravelo, A. C., Crimmins, A., Dekens, P. S., Ford, H. L., Lyle, M., & Wara, M. W. (2012). Late Miocene decoupling of oceanic warmth and atmospheric carbon dioxide forcing. *Nature*, *486*, 97–100. https://doi.org/10.1038/nature11200

Lear, C. H., Coxall, H. K., Foster, G. L., Lunt, D. J., Mawbey, E. M., Rosenthal, Y., et al. (2015). Neogene ice volume and ocean temperatures: Insights from infaunal foraminiferal Mg/Ca paleothermometry. *Paleoceanography*, *30*, 1437–1454. https://doi.org/10.1002/2015PA002833

Lear, C. H., Elderfield, H., & Wilson, P. A. (2000). Cenozoic deep-sea temperatures and global ice volumes from Mg/Ca in benthic foraminiferal calcite. *Science*, *287*(5451), 269–272. https://doi.org/10.1126/science.287.5451.269

Lear, C. H., Rosenthal, Y., & Wright, J. D. (2003). The closing of a seaway: Ocean water masses and global climate change. *Earth and Planetary Science Letters*, *210*, 425–436. https://doi.org/10.1016/S0012-821X(03)00164-X

Lohmann, G. (2020). Temperatures from energy balance models: The effective heat capacity matters. *Earth System Dynamics*, *11*, 1195–1208. https://doi.org/10.5194/esd-11-1195-2020

Lohmann, G., Butzin, M., & Bickert, T. (2015). Effect of vegetation on the late Miocene Ocean circulation. *Journal of Marine Science and Engineering*, *3*(4), 1311–1333. https://doi.org/10.3390/jmse3041311

Lohmann, G., Butzin, M., Eissner, N., Shi, X., & Stepanek, C. (2020). Abrupt climate and weather changes across timescales. *Paleoceanography and Paleoclimatology*, *35*, e2019PA003782. https://doi.org/10.1029/2019PA003782

Lohmann, G., Haak, H., & Jungclaus, J. H. (2008). Estimating trends of Atlantic meridional overturning circulation from long-term hydrographic data and model simulations. *Ocean Dynamics*, *58*(2), 127–138. https://doi.org/10.1007/s10236-008-0136-7

Lohmann, G., Knorr, G., Hossain, A., & Stepanek, C. (2021). *Climate model output illustrating effects of carbon dioxide and ocean mixing on Miocene and Pliocene climate*. PANGAEA. Retrieved from https://doi.pangaea.de/10.1594/PANGAEA.927137

Lohmann, G., Pfeiffer, M., Laepple, T., Leduc, G., & Kim, J.-H. (2013). A model-data comparison of the Holocene global sea surface temperature evolution. *Climate of the Past*, *9*, 1807–1839. https://doi.org/10.5194/cp-9-1807-2013

Lorenz, E. (1960). Generation of available potential energy and the intensity of the global circulation. In *Dynamics of climate* (pp. 86–92). Pergamon Press. https://doi.org/10.1016/b978-1-4831-9890-3.50021-9

Lunt, D. J., Dunkley Jones, T., Heinemann, M., Huber, M., LeGrande, A., Winguth, A., et al. (2012). A model-data comparison for a multi-model ensemble of early Eocene atmosphere-ocean simulations: EoMIP (2012). *Climate of the Past*, *8*, 1717–1736. https://doi.org/10.5194/cp-8-1717-2012

Lyle, M. (1997). Could early cenozoic thermohaline circulation have warmed the poles? *Paleoceanography*, *12*(2), 161–167. https://doi.org/10.1029/96PA03330

Maier-Reimer, E., Mikolajewicz, U., & Crowley, T. (1990). Ocean general circulation model sensitivity experiment with an open central American Isthmus. *Paleoceanography*, *5*(3), 349–366. https://doi.org/10.1029/PA005i003p00349

Marincovich, L., Jr. (2000). Central American paleogeography controlled Pliocene Arctic Ocean molluscan migrations. *Geology*, *28*, 551–554. https://doi.org/10.1130/0091-7613(2000)028<0551:capcpa>2.3.co;2

Marincovich, L., Jr., & Gladenkov, A. Y. (1999). Evidence for an early opening of the Bering Strait. *Nature*, *397*, 149–151. https://doi.org/10.1038/16446

Marincovich, L., Jr., & Gladenkov, A. Y. (2001). New paleontological information about the first opening of Bering Strait. *Quaternary Science Reviews*, *20*, 329–335. https://doi.org/10.1016/S0277-3791(00)00113-X

Markwick, P. J. (1994). "Equability", continentality and Tertiary "climate": The crocodilian perspective. *Geology*, *22*(7), 613–616. https://doi.org/10.1130/0091-7613(1994)022<0613:ecatct>2.3.co;2

Marsland, S. J., Haak, H., Jungclaus, J. H., Latif, M., & Röske, F. (2003). The Max-Planck-Institute global ocean/sea ice model with orthogonal curvilinear coordinates. *Ocean Modelling*, *5*, 91–127. https://doi.org/10.1016/S1463-5003(02)00015-X

Matthiessen, J., Knies, J., Vogt, C., & Stein, R. (2009). Pliocene palaeoceanography of the Arctic Ocean and Subarctic Seas. *Philosophical Transactions of the Royal Society A: Mathematical, Physical & Engineering Sciences*, *367*, 21–48. https://doi.org/10.1098/rsta.2008.0203

McClymont, E. L., Ford, H. L., Ho, S. L., Tindall, J. C., Haywood, A. M., Alonso-Garcia, M., et al. (2020). Lessons from a high-CO_2 world: An ocean view from ~3 million years ago. *Climate of the Past*, *16*, 1599–1615. https://doi.org/10.5194/cp-16-1599-2020

Micheels, A., Bruch, A. A., Eronen, J., Fortelius, M., Harzhauser, M., Utescher, T., & Mosbrugger, V. (2011). Analysis of heat transport mechanisms from a late Miocene model experiment with a fully-coupled atmosphere-ocean general circulation model. *Palaeogeography, Palaeoclimatology, Palaeoecology*, *304*, 337–350. https://doi.org/10.1016/j.palaeo.2010.09.021

Micheels, A., Bruch, A. A., Uhl, D., Utescher, T., & Mosbrugger, V. (2007). A late Miocene climate model simulation with ECHAM4/ML and its quantitative validation with terrestrial proxy data. *Palaeogeography, Palaeoclimatology, Palaeoecology*, *253*, 251–270. https://doi.org/10.1016/j.palaeo.2007.03.042

Mikolajewicz, U., Maier-Reimer, E., Crowley, T. J., & Kim, K.-Y. (1993). Effect of drake and panamanian gateways on the circulation of an ocean model. *Paleoceanography*, *8*(4), 409–426. https://doi.org/10.1029/93PA00893

Molnar, P. (2008). Closing of the central American seaway and the ice age: A critical review. *Paleoceanography*, *23*, PA2201. https://doi.org/10.1029/2007PA001574

Mosbrugger, V., Utescher, T., & Dilcher, D. L. (2005). Cenozoic continental climatic evolution of Central Europe. *Proceedings of the National Academy of Sciences of the United States of America*, *102*, 14964–14969. https://doi.org/10.1073/pnas.0505267102

Mudelsee, M., Bickert, T., Lear, C. H., & Lohmann, G. (2014). Cenozoic climate changes: A review based on time series analysis of marine benthic $\delta^{18}O$ records. *Reviews of Geophysics*, *52*, 333–374. https://doi.org/10.1002/2013RG000440

Munk, W., & Wunsch, C. (1998). Abyssal recipes II: Energetics of tidal and wind mixing. *Deep-Sea Research*, *45*, 1977–2010. https://doi.org/10.1016/S0967-0637(98)00070-3

Niezgodzki, I., Knorr, G., Lohmann, G., Tyszka, J., & Markwick, P. J. (2017). Late Cretaceous climate simulations with different CO_2 levels and subarctic gateway configurations: A model-data comparison. *Paleoceanography*, *32*, 980–998. https://doi.org/10.1002/2016PA003055

Niezgodzki, I., Tyszka, J., Knorr, G., & Lohmann, G. (2019). Was the Arctic Ocean ice free during the latest Cretaceous? The role of CO_2 and gateway configurations. *Global and Planetary Change*, *177*, 201–212. https://doi.org/10.1016/j.gloplacha.2019.03.011

Nilsson, J. (1995). Energy flux from traveling hurricanes to the oceanic internal wave field. *Journal of Physical Oceanography*, *25*, 558–573. https://doi.org/10.1175/1520-0485(1995)025<0558:effttht>2.0.co;2

Nilsson, J., Broström, G., & Walin, G. (2003). The thermohaline circulation and vertical mixing: Does weaker density stratification give stronger overturning? *Journal of Physical Oceanography*, *33*, 2781–2795. https://doi.org/10.1175/1520-0485(2003)033<2781:ttcavm>2.0.co;2

Nong, G., Najjar, R., Seidov, D., & Peterson, W. (2000). Simulation of ocean temperature change due to the opening of the Drake Passage. *Geophysical Research Letters*, *27*(17), 2689–2692. https://doi.org/10.1029/1999GL011072

Otto-Bliesner, B. L., Braconnot, P., Harrison, S. P., Lunt, D. J., Abe-Ouchi, A., Albani, S., et al. (2017). The PMIP4 contribution to CMIP6—Part 2: Two interglacials, scientific objective and experimental design for Holocene and last interglacial simulations. *Geoscientific Model Development*, *10*, 3979–4003. https://doi.org/10.5194/gmd-10-3979-2017

Otto-Bliesner, B. L., Jahn, A., Feng, R., Brady, E. C., Hu, A., & Löfverström, M. (2017). Amplified North Atlantic warming in the late Pliocene by changes in Arctic gateways. *Geophysical Research Letters*, *4*, 957–964. https://doi.org/10.1002/2016GL071805

Otto-Bliesner, B. L., & Upchurch, G. R. (1997). Vegetation-induced warming of high-latitude regions during the late cretaceous period. *Nature*, *385*, 804–807. https://doi.org/10.1038/385804a0

Pacanowski, R. C., & Philander, S. G. H. (1981). Parameterization of vertical mixing in numerical models of tropical oceans. *Journal of Physical Oceanography*, *11*, 83–89. https://doi.org/10.1175/1520-0485(1981)011<1443:povmin>2.0.co;2

Pagani, M., Arthur, M. A., & Freeman, K. H. (1999). Miocene evolution of atmospheric carbon dioxide. *Paleoceanography*, *14*(3), 273–292. https://doi.org/10.1029/1999PA900006

Pearson, P. N., & Palmer, M. R. (2000). Atmospheric carbon dioxide concentrations over the past 60 million years. *Nature*, *406*, 695–699. https://doi.org/10.1038/35021000

Pfeiffer, M., & Lohmann, G. (2016). Greenland ice sheet influence on last interglacial climate: Global sensitivity studies performed with an atmosphere-ocean general circulation model. *Climate of the Past*, *12*, 1313–1338. https://doi.org/10.5194/cp-12-1313-2016

Pithan, F., & Mauritsen, T. (2014). Arctic amplification dominated by temperature feedbacks in contemporary climate models. *Nature Geoscience*, *7*, 181–184. https://doi.org/10.1038/ngeo2071

Pound, M. J., Haywood, A. M., Salzmann, U., & Riding, J. B. (2012). Global vegetation dynamics and latitudinal temperature gradients during the mid to late Miocene (15.97–5.33 Ma). *Earth-Science Reviews*, *112*(1–2), 1–22. https://doi.org/10.1016/j.earscirev.2012.02.005

Prange, M., Lohmann, G., & Paul, A. (2003). Influence of vertical mixing on the thermohaline hysteresis: Analyses of an OGCM. *Journal of Physical Oceanography*, *33*(8), 1707–1721. https://doi.org/10.1175/2389.1

Raddatz, T. J., Reick, C. H., Knorr, W., Kattge, J., Roeckner, E., Schnur, R., et al. (2007). Will the tropical land biosphere dominate the climate-carbon cycle feedback during the twenty first century? *Climate Dynamics*, *29*, 565–574. https://doi.org/10.1007/s00382-007-0247-8

Rahmstorf, S., Box, J., Feulner, G., Mann, M. E., Robinson, A., Rutherford, S., & Schaffernicht, E. J. (2015). Exceptional twentieth-century slowdown in Atlantic Ocean overturning circulation. *Nature Climate Change*, *5*, 475–480. https://doi.org/10.1038/nclimate2554

Raper, S. C. B., Gregory, J., & Stouffer, R. S. (2002). The role of climate sensitivity and ocean heat uptake on AOGCM transient temperature response. *Journal of Climate*, *15*, 124–130. https://doi.org/10.1175/1520-0442(2002)015<0124:trocsa>2.0.co;2

Raymo, M. E. (1991). Geochemical evidence supporting T.C. Chamberlin's theory of glaciation. *Geology*, *19*, 344–347. https://doi.org/10.1130/0091-7613(1991)019<0344:gestcc>2.3.co;2

Raymo, M. E. (1994). The initiation of Northern Hemisphere glaciation. *Annual Review of Earth and Planetary Sciences*, *22*, 353–383. https://doi.org/10.1146/annurev.ea.22.050194.002033

Ritz, S. P., Stocker, T. F., & Severinghaus, J. P. (2011). Noble gases as proxies of mean ocean temperature: Sensitivity studies using a climate model of reduced complexity. *Quaternary Science Reviews*, *30*, 3728–3741. https://doi.org/10.1016/j.quascirev.2011.09.021

Roeckner, E., Bäuml, G., Bonaventura, L., Brokopf, R., Esch, M., Giorgetta, M., et al. (2003). *The atmospheric general circulation model ECHAM5. Part I: Model description* (Vol. 349). Report/Max-Planck-Institut für Meteorologie. Retrieved from http://hdl.handle.net/11858/00-001M-0000-0012-0144-5

Roeckner, E., Brokopf, R., Esch, M., Giorgetta, M., Hagemann, S., Kornblueh, L., et al. (2006). Sensitivity of simulated climate to horizontal and vertical resolution in the ECHAM5 atmosphere model. *Journal of Climate*, *19*, 3771–3791. https://doi.org/10.1175/JCLI3824.1

Rögl, F. (1999). Mediterranean and paratethys. Facts and hypotheses of an oligocene to miocene paleogeography (short overview). *Geologica Carpathica*, *50*, 339–349.

Royer, D. L. (2008). Linkages between CO_2, climate, and evolution in deep time. *Proceedings of the National Academy of Sciences of the United States of America*, *105*, 407–408. https://doi.org/10.1073/pnas.0710915105

Ruddiman, W. F. (2010). A paleoclimate enigma? *Science*, *328*, 838–839. https://doi.org/10.1126/science.1188292

Saenko, O. A., Zhai, X., Merryfield, W. J., & Lee, W. G. (2012). The combined effect of tidally and eddy-driven diapycnal mixing on the large-scale ocean circulation. *Journal of Physical Oceanography*, *42*, 526–538. https://doi.org/10.1175/jpo-d-11-0122.1

Salzmann, U., Dolan, A. M., Haywood, A. M., Chan, W.-L., Voss, J., Hill, D. J., et al. (2013). Challenges in quantifying Pliocene terrestrial warming revealed by data-model discord. *Nature Climate Change*, *3*, 969–974. https://doi.org/10.1038/nclimate2008

Salzmann, U., Haywood, A. M., Lunt, D. J., Valdes, P. J., & Hill, D. J. (2008). A new global biome reconstruction and data-model comparison for the middle pliocene. *Global Ecology and Biogeography*, *17*, 432–447. https://doi.org/10.1111/j.1466-8238.2008.00381.x

Samakinwa, E., Stepanek, C., & Lohmann, G. (2020). Sensitivity of mid-Pliocene climate to changes in orbital forcing and PlioMIP's boundary conditions. *Climate of the Past*, *16*, 1643–1665. https://doi.org/10.5194/cp-16-1643-2020

Schmittner, A., Green, J. A. M., & Wilmes, S. B. (2015). Glacial ocean overturning intensified by tidal mixing in a global circulation model. *Geophysical Research Letters*, *42*, 4014–4022. https://doi.org/10.1002/2015GL063561

Scott, J. R., & Marotzke, J. (2002). The location of diapycnal mixing and the meridional overturning circulation. *Journal of Physical Oceanography*, *32*, 3328–3345. https://doi.org/10.1175/1520-0485(2002)032<3578:tlodma>2.0.co;2

Shellito, C., Sloan, L., & Huber, M. (2003). Climate model sensitivity to atmospheric CO_2 levels in the early-Middle Paleogene. *Palaeogeography, Palaeoclimatology, Palaeoecology*, *193*, 113–123. https://doi.org/10.1016/S0031-0182(02)00718-6

Shevenell, A. E., Kennett, J. P., & Lea, D. W. (2004). Middle Miocene Southern Ocean cooling and Antarctic cryosphere expansion. *Science*, *305*(5691), 1766–1770. https://doi.org/10.1126/science.1100061

Shevenell, A. E., Kennett, J. P., & Lea, D. W. (2008). Middle Miocene ice sheet dynamics, deep-sea temperatures, and carbon cycling: A Southern Ocean perspective. *Geochemistry, Geophysics, Geosystems*, *9*, Q02006. https://doi.org/10.1029/2007GC001736

Sijp, W., England, M., & Toggweiler, J. R. (2009). Effect of ocean gateway changes under greenhouse warmth. *Journal of Climate*, *22*, 6639–6652. https://doi.org/10.1175/2009JCLI3003.1

Skinner, L. C., Fallon, S., Waelbroeck, C., Michel, E., & Barker, S. (2010). Ventilation of the deep Southern Ocean and deglacial CO_2 rise. *Science*, *328*, 1147–1151. https://doi.org/10.1126/science.1183627

Sloan, L. C., & Barron, E. J. (1990). "Equable" climates during Earth history. *Geology*, *18*, 489–492. https://doi.org/10.1130/0091-7613(1990)018<0489:ecdeh>2.3.co;2

Sloan, L. C., Huber, M., Crowley, T. J., Sewall, J. O., & Baum, S. (2001). Effect of sea surface temperature configuration on model simulations of equable climate in the early Eocene. *Palaeogeography, Palaeoclimatology, Palaeoecology*, *167*, 321–335. https://doi.org/10.1016/S0031-0182(00)00245-5

Sloan, L. C., & Rea, D. K. (1996). Atmospheric carbon dioxide and early Eocene climate: A general circulation modeling sensitivity study. *Palaeogeography, Palaeoclimatology, Palaeoecology*, *119*, 275–292. https://doi.org/10.1016/0031-0182(95)00012-7

Smyth, W. D., & Moum, J. N. (2012). Ocean mixing by Kelvin-Helmholtz instability. *Oceanography*, *25*(2), 140–149. https://doi.org/10.5670/oceanog.2012.49

Sosdian, S. M., Babila, T. L., Greenop, R., Foster, G. L., & Lear, C. H. (2020). Ocean carbon storage across the middle Miocene: A new interpretation for the Monterey event. *Nature Communications*, *11*, 134. https://doi.org/10.1038/s41467-019-13792-0

Spicer, R. A., Herman, A. B., & Kennedy, E. M. (2004). The foliar physiognomic record of climatic conditions during dormancy: CLAMP and the cold month mean temperature. *The Journal of Geology*, *112*, 685–702. https://doi.org/10.1086/424579

Sriver, R. L. (2013). Observational evidence supports the role of tropical cyclones in regulating climate. *Proceedings of the National Academy of Sciences of the United States of America*, *110*(38), 15173–15174. https://doi.org/10.1073/pnas.1314721110

Sriver, R. L., Goes, M., Mann, M. E., & Keller, K. (2010). Climate response to tropical cyclone-induced ocean mixing in an Earth system model of intermediate complexity. *Journal of Geophysical Research*, *115*, C10042. https://doi.org/10.1029/2010JC006106

Sriver, R. L., & Huber, M. (2010). Modeled sensitivity of upper thermocline properties to tropical cyclone winds and possible feedbacks on the Hadley circulation. *Geophysical Research Letters*, *37*, L08704. https://doi.org/10.1029/2010GL042836

Sriver, R. L., Huber, M., & Chafik, L. (2013). Excitation of equatorial Kelvin and Yanai waves by tropical cyclones in an ocean general circulation model. *Earth Systems Dynamics*, *4*, 1–10. https://doi.org/10.5194/esd-4-1-2013

Stap, L. B., Sutter, J., Knorr, G., Stärz, M., & Lohmann, G. (2019). Transient variability of the Miocene Antarctic ice sheet smaller than equilibrium differences. *Geophysical Research Letters*, *46*, 4288–4298. https://doi.org/10.1029/2019GL082163

Stärz, M., Jokat, W., Knorr, G., & Lohmann, G. (2017). Threshold in north Atlantic-Arctic Ocean circulation controlled by the subsidence of the Greenland-Scotland Ridge. *Nature Communications*, *8*, 15681. https://doi.org/10.1038/ncomms15681

Stein, R., Fahl, K., Gierz, P., Niessen, F., & Lohmann, G. (2017). Arctic Ocean Sea ice cover during the penultimate glacial and the last interglacial. *Nature Communications*, *8*, 373. https://doi.org/10.1038/s41467-017-00552-1

Stein, R., Fahl, K., Schreck, M., Knorr, G., Niessen, F., Forwick, M., et al. (2016). Evidence for ice-free summers in the late Miocene central Arctic Ocean. *Nature Communications*, *7*, 11148. https://doi.org/10.1038/ncomms11148

Steinthorsdottir, M., Coxall, H. K., de Boer, A. M., Huber, M., Barbolini, N., Bradshaw, C. D., et al. (2021). The Miocene: The future of the past. *Paleoceanography and Paleoclimatology*, *36*, e2020PA004037. https://doi.org/10.1029/2020PA004037

Steinthorsdottir, M., Jardine, P. E., & Rember, W. C. (2021). Near-future pCO_2 during the hot Miocene climatic optimum. *Paleoceanography and Paleoclimatology*, *36*, e2020PA003900. https://doi.org/10.1029/2020PA003900

Stepanek, C., & Lohmann, G. (2012). Modelling mid-Pliocene climate with COSMOS. *Geoscientific Model Development*, *5*, 1221–1243. https://doi.org/10.5194/gmd-5-1221-2012

Stepanek, C., Samakinwa, E., Knorr, G., & Lohmann, G. (2020). Contribution of the coupled atmosphere-ocean-sea ice-vegetation model COSMOS to the PlioMIP2. *Climate of the Past*, *16*, 2275–2323. https://doi.org/10.5194/cp-16-2275-2020

St. Laurent, L. C., Simmons, H. L., & Jayne, S. R. (2002). Estimating tidally driven mixing in the deep ocean. *Geophysical Research Letters*, *29*(23), 21–1. https://doi.org/10.1029/2002GL015633

Stoll, H. M., Guitian, J., Hernandez-Almeida, I., Mejía, L. M., Phelps, S., Polissar, P., et al. (2019). Upregulation of phytoplankton carbon concentrating mechanisms during low CO_2 glacial periods and implications for the phytoplankton pCO_2 proxy. *Quaternary Science Reviews*, *208*, 1–20. https://doi.org/10.1016/j.quascirev.2019.01.012

Super, J. R., Thomas, E., Pagani, M., Huber, M., O'Brien, C., & Hull, P. M. (2018). North Atlantic temperature and pCO_2 coupling in the early-middle Miocene. *Geology*, *46*(6), 519–522. https://doi.org/10.1130/G40228.1

Tarling, G. A., & Thorpe, S. E. (2017). Oceanic swarms of Antarctic krill perform satiation sinking. *Proceedings of the Royal Society B*, *284*, 20172015. https://doi.org/10.1098/rspb.2017.2015

Thomas, D. J., Korty, T., Huber, M., Schubert, J. A., & Haines, B. (2014). Nd isotopic structure of the Pacific Ocean 70-30 Ma and numerical evidence for vigorous ocean circulation and ocean heat transport in a greenhouse world. *Paleoceanography*, *29*, 454–469. https://doi.org/10.1002/2013PA002535

Tierney, J. E., Haywood, A. M., Feng, R., Bhattacharya, T., & Otto-Bliesner, B. L. (2019). Pliocene warmth consistent with greenhouse gas forcing. *Geophysical Research Letters*, *26*, 9136–9144. https://doi.org/10.1029/2019GL083802

Toggweiler, J. R., & Bjornsson, H. (2000). Drake passage and palaeoclimate. *Journal of Quaternary Science*, *15*, 319–328. https://doi.org/10.1002/1099-1417(200005)15:4<319::aid-jqs545>3.0.co;2-c

Toggweiler, J. R., & Samuels, B. (1995). Effect of drake passage on the global thermohaline circulation. *Deep Sea Research Part I: Oceanographic Research Papers*, *42*, 477–500. https://doi.org/10.1016/0967-0637(95)00012-U

Tripati, A. K., Delaney, M. L., Zachos, J. C., Anderson, L. D., Kelly, D. C., & Elderfield, H. (2003). Tropical sea-surface temperature reconstruction for the early Paleogene using Mg/Ca ratios of planktonic foraminifera. *Paleoceanography*, *18*(4), 1101. https://doi.org/10.1029/2003PA000937

Upchurch, G., Kiehl, J., Shields, C., Scherer, J., & Scotese, C. (2015). Latitudinal temperature gradients and high-latitude temperatures during the latest Cretaceous: Congruence of geologic data and climate models. *Geology*, *43*, 683–686. https://doi.org/10.1130/G36802.1

Utescher, T., Dreist, A., Henrot, A.-J., Hickler, T., Liu, Y.-S., Mosbrugger, V., et al. (2017). Continental climate gradients in north America and western Eurasia before and after the closure of the central American seaway. *Earth and Planetary Science Letters*, *472*, 120–130. https://doi.org/10.1016/j.epsl.2017.05.019

Utescher, T., & Mosbrugger, V. (2007). Eocene vegetation patterns reconstructed from plant diversity—A global perspective. *Palaeogeography, Palaeoclimatology, Palaeoecology*, *247*, 243–271. https://doi.org/10.1016/j.palaeo.2006.10.022

Vahlenkamp, M., Niezgodzki, I., De Vleeschouwer, D., Bickert, T., Harper, D., Turner, S. K., et al. (2018). Astronomically paced changes in deep-water circulation in the western North Atlantic during the middle Eocene. *Earth and Planetary Science Letters*, *484*, 329–340. https://doi.org/10.1016/j.epsl.2017.12.016

Vahlenkamp, M., Niezgodzki, I., De Vleeschouwer, D., Lohmann, G., Bickert, T., & Pälike, H. (2018). Ocean and climate response to North Atlantic seaway changes at the onset of long-term Eocene cooling. *Earth and Planetary Science Letters*, *498*, 185–195. https://doi.org/10.1016/j.epsl.2018.06.031

Valdes, P. J., Sellwood, B. W., & Price, G. D. (1996). The concept of Cretaceous equability. *Palaeoclimates Data and Modelling*, *1*, 139–158.

Vallis, G. K. (2000). Large-scale circulation and production of stratification: Effects of wind, geometry, and diffusion. *Journal of Physical Oceanography*, *30*, 933–954. https://doi.org/10.1175/1520-0485(2000)030<0933:lscapo>2.0.co;2

Vincent, E. M., Madec, G., Lengaigne, M., Vialard, J., & Koch-Larrouy, A. (2013). Influence of tropical cyclones on sea surface temperature seasonal cycle and ocean heat transport. *Climate Dynamics*, *41*(7–8), 2019–2038. https://doi.org/10.1007/s00382-012-1556-0

Visser, A. W. (2007). Biomixing of the oceans? *Science*, *316*(5826), 838–839. https://doi.org/10.1126/science.1141272

Von der Heydt, A. S., & Dijkstra, H. (2006). Effect of ocean gateways on the global circulation in the late Oligocene and early Miocene. *Paleoceanography*, *21*, PA1011. https://doi.org/10.1029/2005PA001149

Walliser, E. O., Lohmann, G., Niezgodzki, I., & Schöne, B. R. (2017). Inter-annual climate variability in Europe during the Oligocene Icehouse. *Palaeogeography, Palaeoclimatology, Palaeoecology*, *475*, 140–153. https://doi.org/10.1016/j.palaeo.2017.03.020

Walliser, E. O., Lohmann, G., Niezgodzki, I., Tütken, T., & Schöne, B. R. (2016). Response of Central European SST to atmospheric pCO_2 forcing during the Oligocene—A combined proxy data and numerical climate model approach. *Palaeogeography, Palaeoclimatology, Palaeoecology*, *459*, 552–569. https://doi.org/10.1016/j.palaeo.2016.07.033

Wang, S., & Ardekani, A. M. (2015). Biogenic mixing induced by intermediate Reynolds number swimming in stratified fluid. *Scientific Reports*, *5*, 17448. https://doi.org/10.1038/srep17448

Wang, S., Wang, Q., Shu, Q., Scholz, P., Lohmann, G., & Qiao, F. (2019). Improving the upper-ocean temperature in an ocean climate model (FESOM 1.4): Shortwave penetration vs. mixing induced by non-breaking surface waves. *Journal of Advances in Modeling Earth Systems*, *11*, 545–557. https://doi.org/10.1029/2018MS001494

Wei, W., & Lohmann, G. (2012). Simulated Atlantic multidecadal oscillation during the Holocene. *Journal of Climate*, *25*, 6989–7002. https://doi.org/10.1175/JCLI-D-11-00667.1

Wiebe, E. C., & Weaver, A. J. (1999). On the sensitivity of global warming experiments to the parameterisation of sub-grid scale ocean mixing. *Climate Dynamics*, *15*, 875–893. https://doi.org/10.1007/s003820050319

Wijesekera, H. W., & Gregg, M. C. (1996). Surface layer response to weak winds, westerly bursts, and rain squalls in the western Pacific warm pool. *Journal of Geophysical Research*, *101*(C1), 977–997. https://doi.org/10.1029/95JC02553

Wilhelmus, M. M., & Dabiri, J. O. (2014). Observations of large-scale fluid transport by laser-guided plankton aggregations. *Physics of Fluids*, *26*, 101302. https://doi.org/10.1063/1.4895655

Wilmes, S., Schmittner, A., & Green, J. A. M. (2019). Glacial ice sheet extent effects on modeled tidal mixing and the global overturning circulation. *Paleoceanography and Paleoclimatology*, *34*, 1437–1454. https://doi.org/10.1029/2019PA003644

Wilmes, S. B., & Green, J. A. M. (2014). The evolution of tides and tidal dissipation over the past 21,000 years. *Journal of Geophysical Research: Oceans*, *119*, 4083–4100. https://doi.org/10.1002/2013JC009605

Wolfe, J. A. (1994). Tertiary climatic changes at middle latitudes of western North America. *Palaeogeography, Palaeoclimatology, Palaeoecology*, *108*, 195–205. https://doi.org/10.1016/0031-0182(94)90233-X

Yang, H., Lohmann, G., Shi, X., Gowan, E. J., Lu, J., Liu, J., & Wang, Q. (2020). Tropical expansion driven by poleward advancing subtropical fronts. *Journal of Geophysical Research: Atmospheres*, *125*, e2020JD033158. https://doi.org/10.1029/2020JD033158

Zachos, J. C., & Kump, L. R. (2005). Carbon cycle feedbacks and the initiation of Antarctic glaciation in the earliest Oligocene. *Global and Planetary Change*, *47*, 51–66. https://doi.org/10.1016/j.gloplacha.2005.01.001

Zhu, J., Poulsen, C. J., & Tierney, J. E. (2019). Simulation of Eocene extreme warmth and high climate sensitivity through cloud feedbacks. *Science Advances*, *5*(9), eaax1874. https://doi.org/10.1126/sciadv.aax1874